Low-Cost, Industrial Class-E Power Amplifiers with Sine-Wave Drive

Thesis by

John F. Davis

In Partial Fulfillment of the Requirements

for the Degree of

Doctor of Philosophy

California Institute of Technology

Pasadena, California

2000

(Submitted December 2, 1999)

To my family and the memory of my mother, Odessa Davis

Acknowledgements

First, I would like to thank my advisor, Professor David Rutledge, for giving me the opportunity to pursue the Ph.D. at Caltech as a member of his research group. The guidance, support, and patience he showed during this process not only made the thesis possible but also a valuable learning experience. My research at Caltech was funded by fellowships from the James Irvine Foundation, the Army Research Office, and the ETO Corporation, for which I am grateful. I also would like to thank Dr. Fred Raab of Green Mountain Radio Research for the interesting discussions and suggestions related to this body of work.

I have had the privilege of knowing and working with many talented people in the RF/MMIC group at Caltech. I am grateful for the support and close friendship of Polly Preventza. As my late night ally, our late night discussions were a blast and her encouragement to go the "extra mile" was much appreciated. Another person whose support and friendship I treasure is that of Eileen Lau. No matter where she was on the planet, those cheerful and encouraging phone calls and emails just kept coming in. Blythe Deckman, is a very sincere and kind person who you just can't help but like. I appreciate his willingness to help me at any time, especially with my computer and enjoyed the interesting luncheon conversations. I would like to thank my former office mates from the Steele building, Alina Moussessian and Mike De Lisio, for their helpful suggestions, insightful comments and being examples focus and determination. Great appreciation goes to Irene Loera, Kent Potter, Connie Rodriguez, Carol Sosnowski, Dale Yee, Jung-Chih Chiao, Victor Lubecke, Shi-Jie Li, Cheh-Ming Liu, and Lee Burrows. Thanks Lee for all the long discussions we had on such varied subject matter. I wish all the best to the newer members of the group: Scott Kee, Ichiro Aoki, Lawrence Cheung, Matt Morgan, Dai Lu, and Milan Kovacevich. I am fortunate to have had the opportunity of meeting and working with the many visitors to the RF/MMIC group, including Minoru Saga, Ken Ichiro Natsume,

Kazuhiro Uehara, Taavi Hirvonen, and Toshihisa Kamei. I'd like to thank Professor Jim Rosenberg of Harvey Mudd College, a group member by association, for all his suggestions, advice, and interesting conversation. Finally, heartfelt thanks goes to the EE department staff members I have become good friends and will always remember: Linda, Illiana, Julie, Helen, Lillian, Lyn, Tanya, Janet, Lucinda.

Navigating a graduate program, especially at an institution like Caltech, can be challenging and strenuous. Throughout my tenure as a graduate student, I've been able to "tap" a source of constant encouragement that has guided me through this process. I owe a great debt of gratitude to Dr. William Whitney (Caltech '51), Dr. Fred Shair, and Linda Rodgers. Special thanks go to two of my former Arizona State University professors, Dr. Murray Sirkis and Dr. Gay Brack, who recognized my potential and heartily encouraged my pursuit of the Ph.D.

Finally, I want to express my gratitude to my immediate family. The love, encouragement, and patience of my wife, Theresa, has been a great source of strength for me. You always have the right words and thoughts to keep me focused my goals. I could not have done this without you. My mother, Odessa Davis, is not here to see my attainment, however, without her efforts early in my life, things could have been very different. My father, Henry, is one of my biggest supporters and I am glad to have a man like him in my life to emulate. To my mom, Ann, and sisters, Michelle and Cynthia, I thank for their love, understanding, and support during this endeavor.

Persistence

Nothing in the world can take the
place of persistence.

Talent will not; nothing is more
common than unsuccessful men
with talent.

Genius will not; unrewarded
genius is almost a proverb.

Education will not; the world is
full of educated derelicts.

Persistence and determination
alone are omnipotent.

—Calvin Coolidge—

Low-Cost, Industrial Class-E Power Amplifiers with Sine-Wave Drive

Abstract

The Class-E amplifier is a switching-mode amplifier in which the transistor operates as a switch with a passive, resonant load network. Losses are minimized by having the transistor switch on when both the voltage and current are small. These amplifiers are extremely efficient with about 90% of the DC input power converted to RF output power. This thesis will present two high-power Class-E amplifiers designed for the Industrial, Scientific, and Medical (ISM) frequency of 13.56 MHz. The first is a 200-W amplifier that incorporates the inexpensive International Rectifier IRFP440 MOSFET. With a drive level of 10 W, a drain efficiency of 91% and an overall efficiency of 87% are achieved. The second is a 400-W, air-cooled design that uses a new International Rectifier low-charge MOSFET, the IRFP450LC. This device features improved switching speed and reduced gate drive requirements. A drive level of 12 W is used to attain a drain efficiency of 86% and an overall efficiency of 84%. In both amplifiers, all harmonics are more than 40 dB below the carrier. Design procedures, modelling techniques, and extensive experimental results will be presented for each. In addition, results from a thermal study of a 400-W Class-E amplifier will be discussed. Component and junction temperature data are obtained by a direct measurement technique, Infrared Thermographic Imaging or Thermography and compared with simulated results. Particular attention is paid to the MOSFET and load network capacitors.

Contents

Acknowledgements iii

Abstract vi

Chapter 1. Introduction 1

1.1. Amplifier Classes: A, B, C 2

1.1.1. Class-A Amplifier 3

1.1.2. Class-B Amplifier 4

1.1.3. Class-C Amplifier 4

1.2. Class-E Amplifier Fundamentals 6

1.3. Progress of Class-E Amplifiers 9

1.4. Class-E Amplifiers Developed at Caltech 10

1.4.1. HF-Band 10

1.4.2. VHF-Band 12

1.4.3. UHF-Band 14

1.4.4. X- and Ka-Band 14

1.5. Organization of Thesis 16

Chapter 2. 200-W, 13.56-MHz Class-E Amplifier 21

2.1. International Rectifier IRFP440 Power MOSFET 22

2.2. 200-W Amplifier Design 24

2.3. Amplifier Construction 26

2.4. Tuneup and Power Calibration 29

2.5. Experimental Results 33

2.6. Class-E Amplifier Simulation Using PSpice 40

2.7. Conclusion 49

Chapter 3. A 400-W, 13.56-MHz Air-Cooled Class-E Amplifier 51

3.1. 400-W Amplifier Design 52

3.2. Amplifier Construction 58

3.3. Tuneup and Power Calibration 61
3.4. Experimental Results 64
3.5. Amplifier Simulation 70
3.6. Conclusion 80
Chapter 4. Class-E Amplifier Thermal Study 82
4.1. Infrared Thermography 83
4.1.1. Modes of Heat Transfer 83
4.1.2. Emissivity and Blackbodies 84
4.1.3. Temperature Measurement 86
4.2. Thermal Measurement Setup 88
4.3. Experimental Results 92
4.3.1. CW Operation 93
4.3.2. Keyed Operation 98
4.3.3. Capacitor Focus 101
4.4 Conclusion 108
Chapter 5. Suggestions for Future Work 110

Chapter 1

Introduction

A power amplifier can be considered "high-efficiency" if it attains an efficiency higher than that of conventional power amplifiers (A, B, C) in similar applications. This means the active devices are employed as switches rather than current sources to reduce their power dissipation (voltage-current product). As a result, higher output power from the amplifier can be realized. From a reliability standpoint, high-efficiency means a reduction in the device junction temperature. Amplifier design is also positively impacted by this technique of amplification. For example, a reduction of DC input power to produce the same output power means smaller power supplies for wireless base station transmitters and fewer batteries for cellular phones transmitters. Lower power dissipation allows for a reduction in the size and weight of the heat sink [1].

Amplifiers that operate as Class-E, fall into this high efficiency category. Class-E amplifiers were first investigated by Gerald Ewing in 1964 and further developed and patented by Nathan and Alan Sokal in 1975 [2]-[4]. In this circuit the transistor acts like a switch, half the time completely *on* and the other half completely *off*. Transistor heat loss is minimized by designing its resonant load network so that the voltage and current waveforms overlap as little as possible. Due to the switching nature of the Class-E circuit, amplification is nonlinear and limited to single band operation by the load circuitry.

The nonlinearity feature of switching amplifiers means they are not suitable

for single-sideband (SSB) transmitters without external circuitry. Distortion of the signal spectrum caused by these nonlinearities can be remedied with use of linearization techniques such as Envelope Elimination and Restoration (EER) or Cartesian Feedback [5][6]. This has been evidenced with the development of a high-efficiency HF/VHF Kahn Technique Transmitter in [7]. Class-E amplifiers work quite well, however, in transmitters using CW, FM, and AM signal formats. For CW or continuous wave communications (i.e., on-off keying by Morse Code), the information is transmitted by either turning the carrier on and off completely [8]. In FM or FSK (Frequency-Shift-Keying), the frequency of the carrier, not amplitude, is changed by small amounts. Amplitude Modulation requires a carrier signal with a time varying amplitude and this can be accomplished by variation of the drain bias since the amplifier's output power is proportional to the DC power. Industrial applications is another area well suited for Class-E amplifiers. Heat derived from the high output power is quite useful for surgical instrument sterilization and induction heating applications such as industrial cap sealing as evidenced in [9].

While the Class-E design is primarily implemented in amplifiers, there have been other successful demonstrations with oscillator and multiplier designs [10]-[13].

In the sections that follow, various classes of amplifiers for different applications will be introduced. Additionally the background, progress of Class-E amplifier development, and activities of Caltech in this area will be discussed.

1.1 Amplifier Classes: A, B, C

One aspect of signal processing in communication systems is the amplification of weak signals. Different methods of amplification exist to make these signals more useful and are embodied in distinct categories or classes of amplifiers. Each class has qualities that make it more or less suitable for given

situations. Most conventional amplifiers fall into one of three classes: A, B, or C. The following is a brief description of each of these classes. For a review of all amplifier classifications, references [1] and [14] do an admirable job.

1.1.1 Class-A Amplifier

These amplifiers are designed around a single transistor which is biased to be always active. An active transistor will simultaneously have considerable amounts of voltage across and current through it, the product of which translates into heat dissipated in the device. This circuit disperses power even when there is no output. For this reason Class-A amplifiers, have a low efficiency of about 30%. However, this does not detract from its ability to minimally introduce distortion during the amplification process. This means that a Class-A amplifier's output will look almost exactly like its input, except larger in amplitude. Class-A amplifiers are commonly used as low-level driver amplifiers [15]. Figure 1.1 shows the circuit and device characteristics.

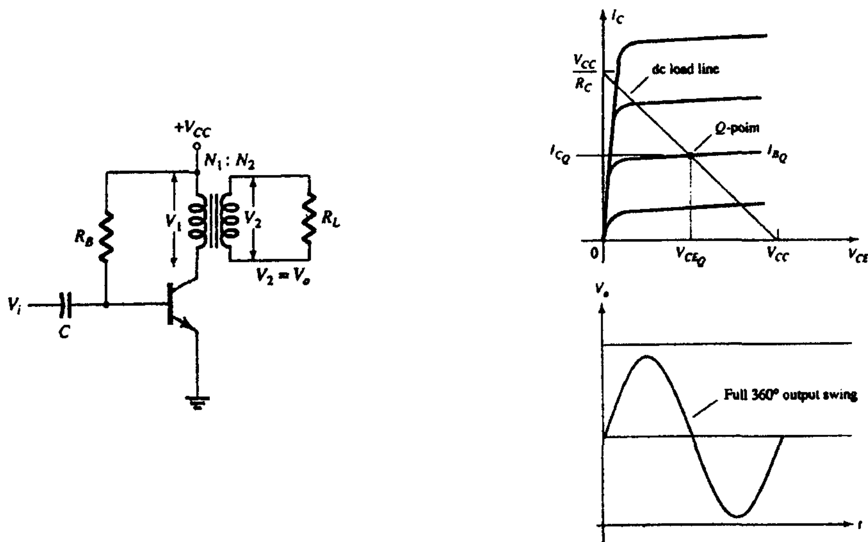

Fig. 1.1. Class-A amplifier circuit and I-V characteristics [15].

1.1.2 Class-B Amplifier

The Class-B design, shown below, centers on the use of two transistors in a push-pull configuration. This means each device, driven 180° out of phase to the other, takes turns amplifying the input signal. One transistor is active for positive half of the cycle, and the other during the negative. Efficiency is doubled to around 60%; however, small amounts of distortion exist at the signal crossover. Class-B is extensively used in medium to high-level power linear amplifiers [1].

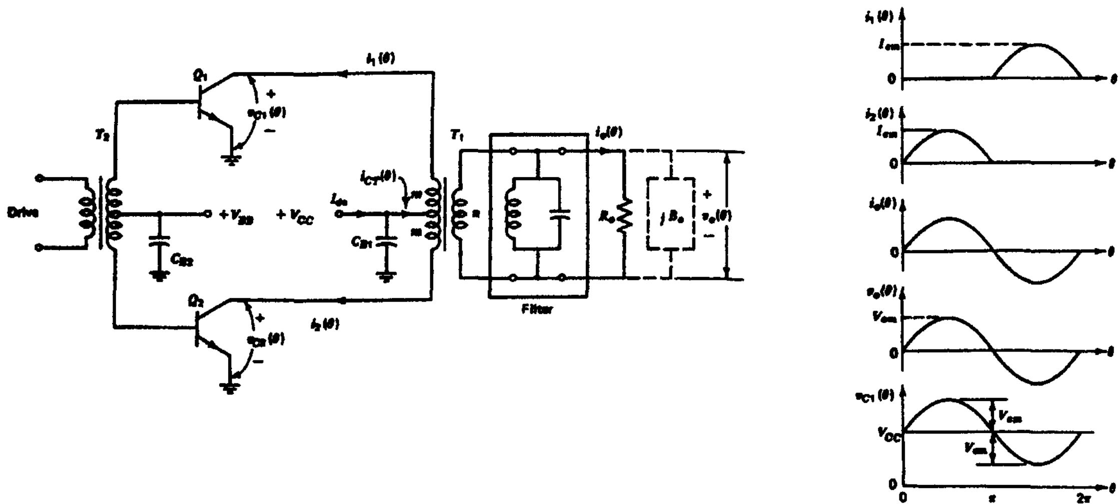

Fig. 1.2. Class-B amplifier circuit and waveforms [1].

1.1.3 Class-C Amplifier

The Class-C amplifier is a nonlinear, switching amplifier. In this circuit, the transistor operates as a switch, either completely on or completely off. In the "on" state, current flows through the device while voltage across the transistor is small. However, voltage builds across the transistor and current through it falls nearly to zero in the "off" state. As a result, overlap between voltage and current

is minimized in the transistor and translates into less power dissipation in the device and thus higher efficiency. Efficiencies of Class-C amplifiers typically range from 75-80%. A majority of the loss occurs during switching as the transistor does not go from the on to off state and vice versa instantaneously. In Figure 1.3, as the device changes state, it goes through the active region where current through it and voltage across it occur simultaneously. Thus, every time the transistor is switched, power is wasted as heat and increases at higher operational frequencies. A prime disadvantage of the Class-C design is its nonlinearity. The output may be at the same frequency as the input but may bear no resemblance due to an abundance of harmonic distortion. To reduce the harmonics, the Class-C circuit employs a tuned circuit at the output. The output amplitude depends primarily on the drain supply voltage and is insensitive to drive signal variations. Class-C amplifiers are used to amplify CW, FM and AM signals [1].

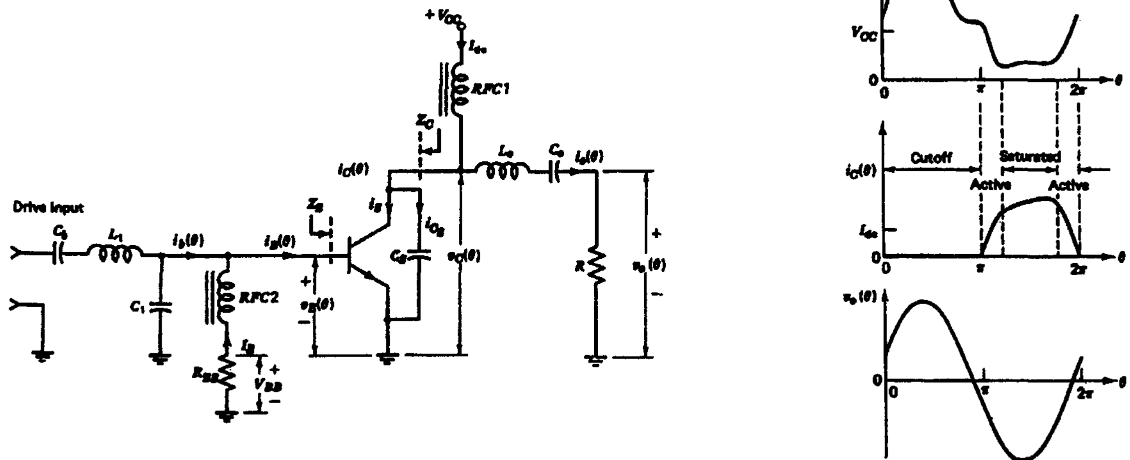

Fig. 1.3. Class-C circuit and typical waveforms [1].

1.2 Class-E Amplifier Fundamentals

The Class-E amplifier is a switching-mode amplifier, where the transistor operates as a switch. Figure 1.4 shows an idealized Class-E circuit. When the transistor is off, current flows into a resonant load network, and there is a transient voltage that rises and falls. This voltage will return to zero smoothly with zero slope, provided the load network is designed properly. When the transistor turns on, current rises smoothly until it switches off again. Losses are kept low by having the transistor switch on when both current and voltage are small. Figure 1.5 depicts the Class-E voltage and current waveforms for the switching transistor [16]. The resonant load network limits the Class-E amplifier to single-band operation.

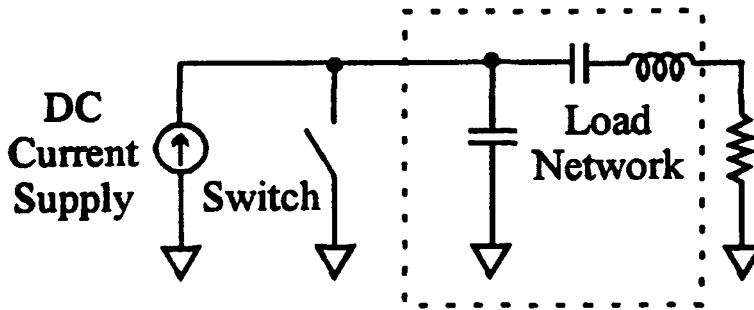

Fig. 1.4. An idealized Class-E amplifier. The switch represents the transistor that opens and closes at the RF frequency.

The high efficiency of a Class-E amplifier makes it possible to produce high output power with about 90% of the DC input power converted to RF output power. We can derive an expression between the maximum output power P_o, the maximum dissipated power P_d, and the efficiency η. Write P_o in terms of the input power P_i as

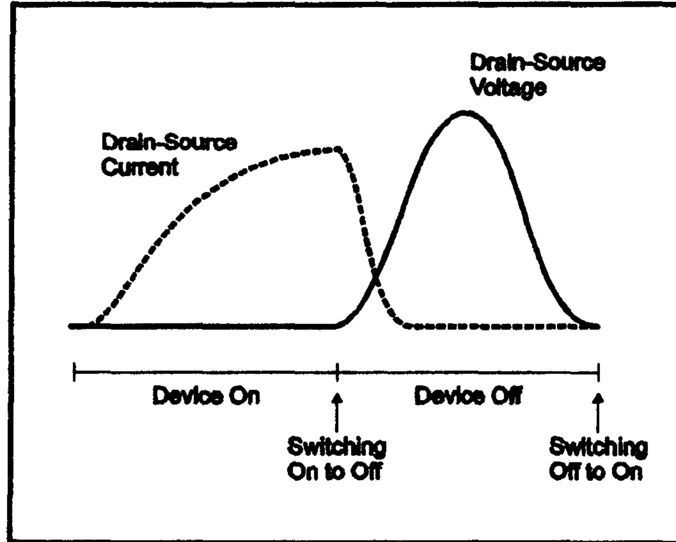

Fig. 1.5. When the transistor turns off, we have voltage and current at the same time. It is when V and I overlap that power dissipation occurs in the device [16].

$$P_o = \eta P_i \tag{1.1}$$

and the dissipated power P_d as

$$P_d = (1 - \eta)P_i. \tag{1.2}$$

Finally, divide the two formulas to get

$$\frac{P_o}{P_d} = \frac{\eta}{(1 - \eta)}. \tag{1.3}$$

Figure 1.6 shows the plot of this relation versus efficiency with the typical efficiencies for the classes of amplifiers shown. Note that you can get more power out of the same transistor if you are limited by thermal dissipation. A Class-E amplifier operating at an efficiency of 90% can produce *21 times* as much power

as a 30% efficient Class-A amplifier at the same dissipation level. This means the power output is three times greater and the dissipated power is seven times smaller.

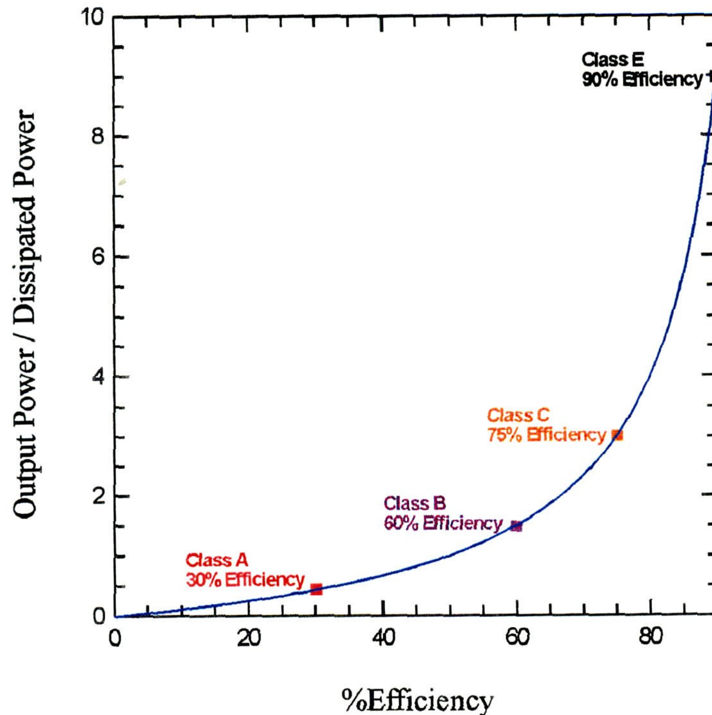

Fig. 1.6. Output power versus efficiency. High efficiency allows for much greater output power.

While RF output power is a function of the DC input power, drive signal amplitude has no impact on the output. The driver must be powerful enough to completely switch the transistor on and off so failure doesn't occur due to heat buildup.

1.3 Progress of Class-E Amplifiers

Today high-efficiency amplifiers based on the Class-E design are being developed at frequencies ranging from HF to microwaves [17]. However, at the outset of this technology's development, demonstrations occurred at HF frequencies and below. For example, Ewing [2] built a 500 kHz, 20-W Class-E amplifier with a collector efficiency of 94%. This was followed by the Sokal's [3] development of a 3.9-MHz Class-E amplifier that delivered 26 W of power and an efficiency of 96%. In that design, Motorola 2N3735 TO-5 tansisitors were used. Today, however, higher output powers are explored as power device technologies have improved. For example, Frey has demonstrated a 27.12-MHz, 500-W Class-E amplifier with an 83% drain efficiency. The device used is the Advanced Power Technology (APT) ARF448A MOSFET with a breakdown voltage of 450 V [18].

The growth of wireless communication has spurred the need to develop more efficient transmitters for cell phones and base stations. For example, Sowlati's work has been focused on developing Class-E amplifiers for mobile communications. The first design is an 835-MHz amplifier which outputs 251 mW and has a power-added efficiency (PAE) of greater than 50% with supply voltage of 2.5 V [19]. Another development is a 1.8 GHz amplifier that implements a depletion mode GaAs MESFET as the switch. This delivers 200 mW of power with 57% PAE and supply voltage of 2.4 V [20].

Class-E amplifiers designed for 0.5, 1, 2, and 5 GHz have been demonstrated by Mader [21]. With the Siemens CLY5 MESFET used as the switch in the 0.5 GHz circuit, 550 mW of output power results with a drain and power added efficiency of 83% and 80% respectively. At 5 GHz, an output power of 0.61 W was attained using a Fujitsu FLK052WG MESFET. The drain efficiency is 81% and PAE 72%. A 2×2 Class-E power combining amplifier array was developed for 5.05 GHz. It delivers 2.4 W of output power with a DC to RF conversion efficiency of 74% and PAE of 64%.

Other high frequency Class-E amplifier developments are a load-pull harmonic controlled Class-E amplifier presented in [22]. With an operational frequency of 900 MHz, a commercial bipolar transistor, the MRF557, is used. The measured PAE is 79% with collector efficiency of 91% and output power of 1.5 W. Finally, an 850 MHz lumped component Class-E amplifier using a newly developed tunable inductor has been demonstrated. An input power of 0.6 W yields 4.9 W of output power and 75% drain efficiency 75%. The switching element is an LDMOS transistor [23].

1.4 Class-E Amplifiers Developed at Caltech

This section profiles the activities of our research group at Caltech in the development of Class-E high-efficiency power amplifiers. The descriptions below are categorized by the frequency bands in which this work has been done.

1.4.1 HF-Band

Our development of Class-E amplifiers commenced five years ago within the High Frequency band (3–30 MHz) and continues today. Joyce Wong [24] built a 7 MHz, 300-W, Class-E amplifier using a water-cooled International Rectifier (IR) IRF840 MOSFET. A drain efficiency of 89% was achieved. Meng-Chen Yu [25] developed a modified Class-E amplifier configuration using paralleled power MOSFETs to attain an output power of 500 W. With water-cooled International Rectifier IRF740 MOSFETs, the amplifier reached a drain efficiency of 87% at 13.56 MHz. Eileen Lau and Kai-Wai Chiu [8] developed 300 W and 500 W air-cooled amplifiers for amateur radio communications. Both amplifiers operate on the 40-meter (7-MHz) band and have drain efficiencies in the 90% range. Transistors used are the International Rectifier IRFP440 and IRFP450, respectively. Each amplifier is driven by a QRP transceiver, the NorCal 40A, for modified for greater power output. Figure 1.7 depicts the amateur communications work.

Fig. 1.7. Caltech Class-E amplifier profiled in amateur radio literature.

John Davis developed Class-E amplifiers for industrial applications operating at 13.56 MHz. The first of which is a 200 W water-cooled unit that uses an International Rectifier IRFP440 power MOSFET. With a drive level of 10 W, the amplifier achieves a drain efficiency of 91% and an overall efficiency of 87% [26]. Next, higher power is attained with a 400-W amplifier that uses a faster switching device, the International Rectifier IRFP450LC. This is an air-cooled amplifier which uses a drive power of 12 W to attain drain and overall efficiencies of 86 and 84% respectively [27]. In both amplifiers, all harmonics are more than 40 dB below the carrier.

Finally, another Class-E amplifier has been developed for a higher operational frequency in the HF amateur radio band. This is a 10 MHz (30-meters), 200-W, amplifier by Teo Der-Stepanians. The unit incorporates an International Rectifier IRFP440 and requires only 3 to 8 W of drive power for reliable, efficient operation. A modified NorCal40A transceiver is the driver. Drain efficiency is 87% and with a corresponding overall efficiency of 85% [16].

1.4.2 VHF-Band

Prof. Herbert Zirath of Chalmers University, Sweden, developed a 144-MHz Class-E amplifier using the Motorola MRF183 MOSFET [28]. With the newly developed Silicon LDMOS device, a record high output power of 54 W with an efficiency of 70% is obtained at this frequency. Input power of 5 W with bias voltage of 20 V is needed to attain these results. The amplifier is shown in Figure 1.8. Central to this development was the use of efficient device models, simulation tools, and the invention of a novel high-Q inductor for the output series resonance network. This inductor allows for low losses in the output network and simultaneously provides a wide tuning range for maximum output power or maximum efficiency optimization. The inductor is comprised of a copper ribbon 5 mm above the ground plane and is tuned by inserting a piece of conductor

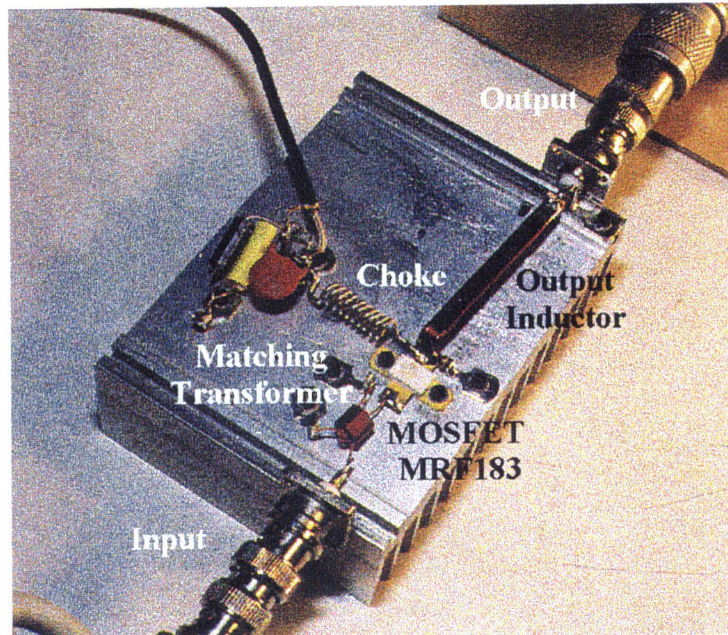

Fig. 1.8. 144 MHz amplifier with the copper ribbon inductor on the output.

between the ribbon and the ground plane.

Currently under development in collaboration with NASA's Jet Propulsion Laboratory (JPL) is a 50-MHz Class-E amplifier with a 3-dB bandwidth of 10 MHz. The device in use is the Motorola MRF183 and preliminary performance results are as follows: Input Power = 0 dBm, Output Power = 30 W, Drain Efficiency = 90%, DC Input = 15 V at 2.2 A. Figure 1.9 shows the initial development of the amplifier.

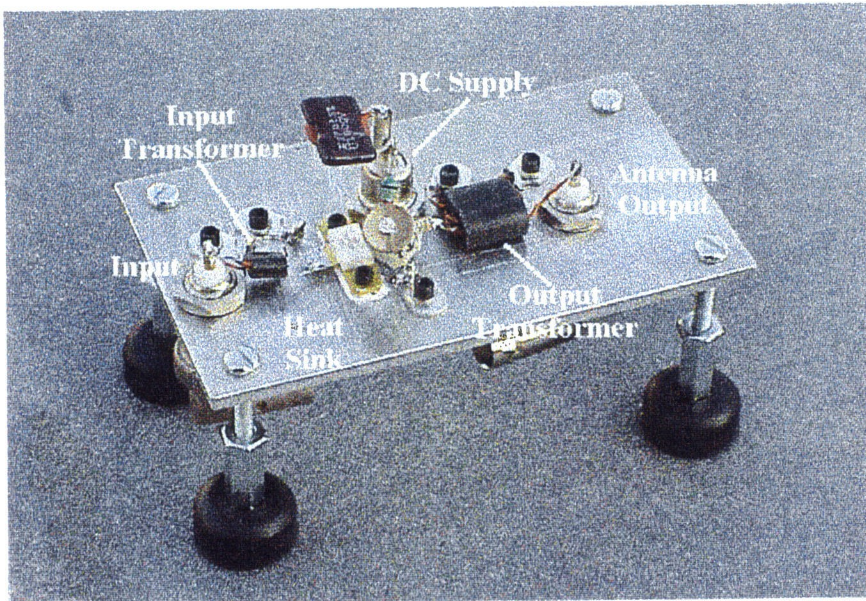

Fig. 1.9. Caltech/JPL 50-MHz amplifier.

1.4.3 UHF-Band

Another Class-E amplifier based on the Motorola MRF183 is one with an operational frequency of 440 MHz. Designed and developed by Shijie Li [29], an output power of 16 W with drain efficiency of 77% and 70% PAE result.

1.4.4 X- and Ka-Band

Shijie Li's Class-E work continued with two X-band amplifiers. The first one uses a Fujitsu FHZ35X HEMT and achieves an output power of 30 mW, drain efficiency of 80% and PAE of 64%. The second incorporates the Fujitsu FLR056 MESFET and delivers an output power of 190 mW, drain efficiency of 72% and PAE of 56% [29]. Both amplifiers use transmission lines for the output load network and input matching.

In the early stages of development are X- and Ka-band high efficiency amplifiers by Ichiro Aoki. This X-band design, done in collaboration with JPL and

Rockwell Science Center, uses a pHEMT as its active device. Presently this amplifier yields an output power of 17.6 dBm, drain efficiency of 75% and PAE of 67%. The DC input is 3 V at 25.6 mA and RF input power is 8 dBm. Figure 1.10 shows the actual circuit layout of the amplifier and a closeup view of the transistor.

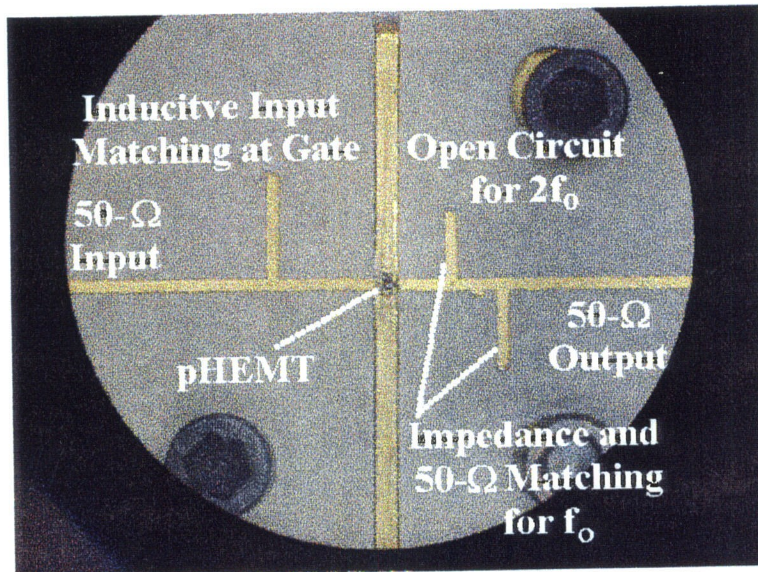

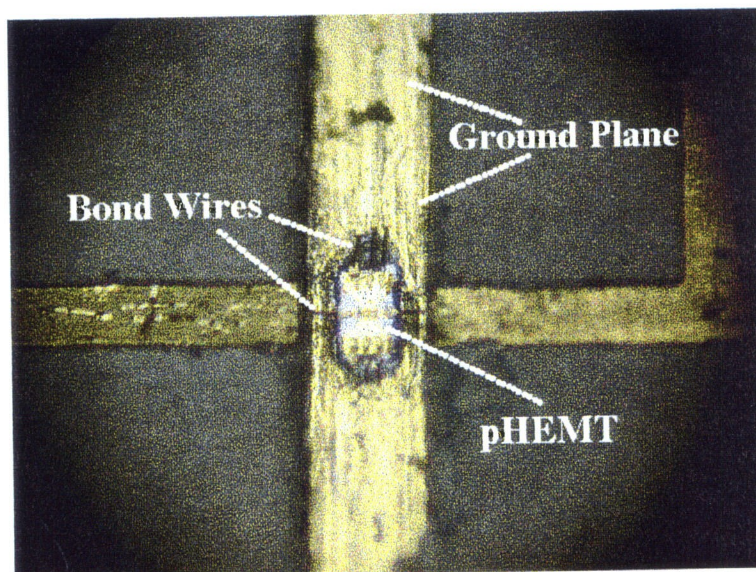

Fig. 1.10. The X-band (8.5 GHz) Class-E amplifier.

1.5. Organization of the Thesis

In Chapter 2, a 200-W, 13.56-MHz Class-E amplifier for industrial applications is designed, developed, and constructed. This HF-band amplifier uses sine-wave drive and incorporates the low-cost International Rectifier IRFP440 Power MOSFET as a switch. While this enhancement mode device is intended for use in switching power supplies, we have found that it works well at RF. To insure the transistor is off when not driven, a transformer is used at the gate-source terminals to set the DC bias to zero volts. This is far below the threshold voltage of 4 V. Water cooling is used in this development to facilitate removal of heat from the active device. Extensive measurements are done not only to measure the amplifier's components but to also accurately characterize the RF output power. Experimental data of this circuit is compared with PSpice simulation results. The transistor is modeled as a switch with a linear capacitor and a nonlinear dependent voltage source to model the square-root behavior of the drain-source capacitance. The simulation accurately predicts the voltage waveforms, efficiency, and harmonic levels. A drive level of 10 W yields a drain efficiency of 91% and an overall efficiency of 87%. All harmonic levels are more than 40 dB below the carrier.

Chapter 3 discusses the design and construction of a 400-W, 13.56-MHz Class-E amplifier. A low-charge power MOSFET, the International Rectifier IRFP450LC, is used as the switch. This is a new feature that improves the switching speed of the device and allows for reduced gate drive requirements. While a gate-transformer is again used to set the DC bias to zero volts, it also serves to match impedances of the gate and drive circuit. Additionally, a capacitor in parallel with a variable inductor is added to tune out the inductive reactance of the gate. A more accurate power measurement system is employed that uses digital power meters accompanied by directional power sensors. Experimental data is again compared with a PSpice simulation employing the same

model topology used in the 200-W simulation. Particular attention is paid to the simulated RF harmonic spectrum and its comparison to the experimental data. Parasitic components are added to the model so that the theory predicts the experimental harmonic observations. Whereas the 200-W amplifier was constructed using a "homemade" circuit board, the 400-W version is built on a circuit board designed using a PCB layout package. A drive level of 12 W is used to attain a drain efficiency of 86% and an overall efficiency of 84%. All harmonics are more than 40 dB below the carrier.

The focus of Chapter 4 is on a Class-E amplifier thermal management study. With the potential of obtaining higher output power from these highly efficient amplifiers, a component's ability to handle high temperatures due to excessive power dissipation is paramount. The thermal investigation conducted in Chapter 3 involved using experimental measurements to determine thermal resistances of the active component and PSpice results to calculate their respective thermal rise, dissipated power, and junction temperature. This process can be viewed as an indirect approach in determining component temperatures. However, in Chapter 4, direct measurement of component and junction temperatures is done by using Infrared (IR) Thermographic Imaging or Thermography. The key instrument in this process is an IR camera capable of taking thermal images of the components while the amplifier is operational. The imaged temperatures and calculated power dissipations show good agreement with the Chapter 3 results. A 400-W, 14.025-MHz Class-E amplifier is used in this study and operated under continuous and intermittent conditions. While all components are imaged, further study is conducted on the load network capacitors as they get really hot under continuous operating conditions. The effect of replacing the load network capacitor values with their parallel and series equivalents on thermal stress is examined.

Chapter 5 discusses directions for future work in Class-E power amplifiers.

References

[1] H. Krauss, C. Bostian, and F. Raab, *Solid State Radio Engineering*, John Wiley and Sons, New York, 1980.

[2] G.D. Ewing, "High-Efficiency Radio-Frequency Power Amplifiers," Ph.D. Thesis, Oregon State University, June 1964.

[3] N.O. Sokal and A.D. Sokal, " Class E - A New Class of High-Efficiency Tuned Single-Ended Switching Power Amplifiers," *IEEE Journal of Solid-State Circuits*, vol. SC-10, no. 3, pp. 168-176, June 1975.

[4] N.O. Sokal and A.D. Sokal, "High Efficiency Tuned Switching Power Amplifier," U.S. Patent 3 919 656, November 11, 1975.

[5] L.R. Kahn, "Single-Sideband Transmission by Envelope Elimination and Restoration," *Proc. IRE*, vol. 40, pp. 803–806, July 1952.

[6] M. Johansson and L. Sundstrom, "Linearisation of RF Multicarrier amplifiers using Cartesian Feedback," *IEE Electronics Letters*, vol. 30, no. 14, pp. 1110–1112, July 7, 1994.

[7] F.H. Raab and D.J. Rupp, "High Efficiency single-sideband HF/VHF transmitter based upon envelope elimination and restoration," *Proc. Sixth Int. Conf. HF Radio Systems and Techniques (HF'94)*, pp. 21–25, July 4–7, 1994.

[8] E. Lau, K.-W. Chiu, J. Qin, J.F. Davis, K. Potter, D.B. Rutledge, "High-Efficiency, Class-E Power Amplifiers," *Part 1, QST*, pp. 39–42, May 1997; *Part 2, QST*, pp. 39–42, June 1997.

[9] L. Hobson, "High Power Class-E Amplifier for High Frequency Induction Heating Applications," *IEE Electronics Letters*, vol. 24, no. 14, pp. 886–888, July 7, 1988.

[10] J. Ebert and M. Kazimierczuk, "Class E High-Efficiency Tuned Power Oscillator," *IEEE Journal of Solid-State Circuits*, vol. SC-16, no. 2, pp. 62–66, April 1981.

[11] E.W. Bryerton, W.A. Shiroma, and Z.B. Popović, "A 5-GHz High-Efficiency

Class-E Oscillator," *IEEE Microwave and Guided Wave Letters*, vol. 6, no. 12, pp. 441–443, December 1996.

[12] R.E. Zulinski and J.W. Steadman, "Performance Evaluation of Class E Frequency Multipliers," *IEEE Transactions on Circuits and Systems*, vol. CAS-33, no. 3, pp. 343–346, March 1986.

[13] R.E. Zulinski and J.W. Steadman, "Idealized Operation of Class E Frequency Multipliers," *IEEE Transactions on Circuits and Systems*, vol. CAS-33, no. 12, pp. 1209–1218, December 1986.

[14] D.B. Rutledge, *The Electronics of Radio*, Cambridge University Press, New York, 1999.

[15] R. Boylestad and L. Nashelsky, "Power Amplifiers," in *Electronic Devices and Circuit Theory*, Prentice Hall, New Jersey, 1992, pp. 676–682.

[16] T. Der-Stepanians and D.B. Rutledge, "10-MHz Class-E Power Amplifiers," *Communications Quarterly*, pp. 31–38, Winter 1999.

[17] N.O. Sokal, "Class E High Efficiency Power Amplifiers, From HF to Microwave," *1998 IEEE MTT-S International Microwave Symposium Digest*, Baltimore, MD, pp. 1109–1112, June 1998.

[18] R. Frey, "500-W, Class E 27.12-MHz Amplifier Using A Single Plastic MOSFET," *Advanced Power Technology Application Note APT9903*, pp. 1–7, Advanced Power Technology, www.advancedpower.com/.

[19] T. Sowlati *et al.*, "Low Voltage, High Efficiency GaAs Class E Power Amplifiers for Wireless Transmitters," *IEEE Journal of Solid-State Circuits*, vol. 30, no. 10, pp. 1074–1080, October 1995.

[20] T. Sowlati *et al.*, "1.8-GHz Class E Power Amplifier for Wireless Communications," *IEE Electronics Letters*, pp. 1846–1848, September 26, 1996.

[21] T.B. Mader, "Quasi-Optical Class-E Power Amplifiers," Ph.D. Thesis, 1995, Univ. of Colorado, Boulder, CO.

[22] F.J. Ortega-González *et al.*, "High-Efficiency Load-Pull Harmonic Controlled

Class-E Power Amplifier," *IEEE Microwave and Guided Wave Letters*, vol. 8, no. 10, pp. 348–350, October 1998.

[23] L.Å. Bengtsson and H. Zirath, "An 850-MHz Lumped Class-E LDMOS Power Amplifier," to be published in *IEEE Microwave and Guided Wave Letters.*

[24] J. Wong, "A 300-W Solid-State Class-E Amplifier for Amateur Communications," Bachelor's Thesis, California Institute of Technology, Pasadena, CA, June 1995.

[25] M. Yu, "Radio Frequency Power Amplifier," Bachelor's Thesis, California Institute of Technology, Pasadena, CA, June 1995

[26] J.F. Davis and D.B. Rutledge, "Industrial Class-E Power Amplifiers with Low-Cost Power MOSFETs and Sine-Wave Drive," *Proc. RF Design '97 Conference and Expo*, Santa Clara, CA, pp. 283–297, July 1997.

[27] J.F Davis and D.B. Rutledge, "A Low-Cost Class-E Power Amplifier with Sine-Wave Drive," *1998 IEEE MTT-S Int. Microwave Symp. Dig. Vol. 2,* pp. 1113–1116, June 1998.

[28] H. Zirath and D.B. Rutledge, "An LDMOS VHF Class E Power Amplifier Using a High Q Novel Variable Inductor," *1999 IEEE MTT-S Int. Microwave Symp. Dig. Vol. 1,* pp. 367–370, June 1999.

[29] S. Li, "UHF and X-Band Class-E Amplifiers," Ph.D. Thesis, California Institute of Technology, Pasadena, CA, 1998.

Chapter 2

200-W, 13.56-MHz Class-E Amplifier

This chapter discusses the design, construction, and performance of a Class-E amplifier that incorporates low-cost power MOSFETs and uses sine-wave drive. The amplifier operates at 13.56 MHz, one of the frequency bands designated by the Federal Communications Commission for Industrial, Scientific, and Medical equipment (ISM). These non-licensed frequencies have been set aside for the operation of such equipment that would not interfere with radio communication services [1]. The amplifier uses the International Rectifier (IR) IRFP440 Power MOSFET, which costs only $4. This transistor is intended for use in switching power supplies, but we have found that it works well at higher radio frequencies (RF). The circuit is a further development of a 7-MHz amplifier intended for amateur radio communications [2]. The 13.56-MHz design is based on scaling of the component values of the 7-MHz design while maintaining the same impedance of the ringing network. Water cooling is used for this development to facilitate removal of heat from the transistor. Extensive measurements are done not only to measure the amplifier's components but to also accurately characterize the RF output power. Experimental data of this Class-E circuit is compared with PSpice simulation results. The model used in this simulation incorporates a simple switch model with square-root drain capacitance. It includes the actual measured component values and accurately predicts the amplifier's performance. The 200-W amplifier is built on a single-sided copper-clad board with the foil

pattern designed to optimize component placement and minimize RF coupling. A drive level of 10 W yields a drain efficiency of 91% and an overall efficiency of 87%. All harmonic levels are more than 40 dB below the carrier.

2.1 International Rectifier IRFP440 Power MOSFET

The acronym MOSFET stands for Metal-Oxide-Semiconductor Field-Effect Transistor. This is a unipolar device that depends on electron (n-channel) or hole (p-channel) conduction. The basic modes of operation can be defined in terms of either depletion (channel open or "ON") or enhancement (channel closed or "OFF"). Figure 2.1 shows the cross-section of an n-channel enhancement-mode MOSFET. In enhancement-mode operation, the region between the source and drain takes the configuration of two back-to-back series diodes. There is negligible current for zero gate voltage. However, applying a positive gate voltage above a threshold value results in an increase in the concentration of electrons to the semiconductor surface. An induced n-type region or channel is formed that can sustain measurable current flow between the source and the drain.

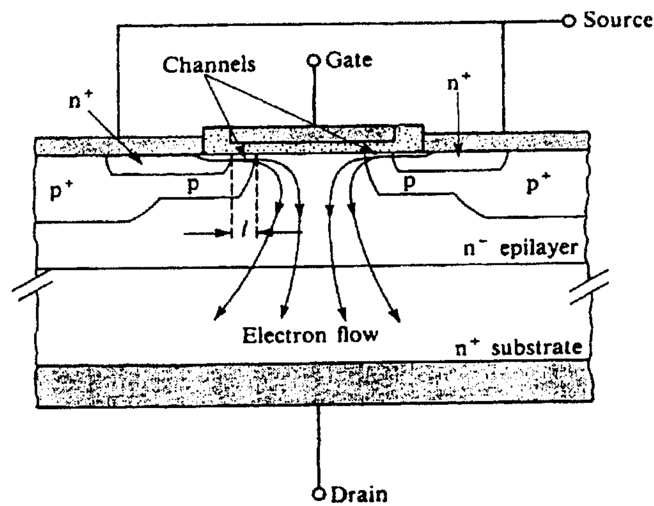

Fig. 2.1. The cross-section of an n-channel power VDMOS Field Effect Transistor [3].

There are several reasons n-channel enhancement-mode devices are used for the Class-E amplifier application. First, the conductivity is due to electrons, which generally have higher degree of mobility than holes. Thus, for given dimensions, the channel resistance is lower and the carrier transit time is shorter in an n-channel device. Second, as an enhancement-mode device, it draws negligible current and hence dissipates virtually no power in its OFF state [3]. Since gate bias is not essential, this makes the Class-E amplifier circuit simpler. When no RF input is applied, there is no DC current and no DC power dissipation.

The Vertical Double-diffused MOS (VDMOS) transistor is developed for high frequency and high power applications [4]. The VDMOS structure incorporates short channel lengths for fast switching speeds, low parasitic capacitances, and high breakdown voltage. The difference between a VDMOS and the conventional MOSFET is the existence of a lowly doped n-epilayer extending to the highly doped n-region that forms the drain. The double-diffusion process determines the channel length l and the resulting structure supports the drain voltage vertically in the n^--epilayer. The current flows laterally from the source through the channel parallel to the silicon surface and then turns through a right angle to flow vertically down through the drain epilayer to the substrate and the drain contact. The p-type "body" region in which the channel is formed when a sufficiently positive gate voltage is applied, and the n^+ source contact regions are diffused successively through the same window etched in the oxide layer [3]. The double-diffusion process makes it possible to attain extremely narrow channels with conventional fabrication techniques thus making it possible for the MOSFET to work at high frequencies. Operation frequencies up to 21 MHz have been attained using these types of MOSFETs.

The International Rectifier IRFP440 is an n-channel enhancement mode vertical D-MOSFET (VDMOS-FET) designed primarily for commercial-industrial applications. While not specifically identified in the IR application literature,

this device is well suited for use in switched-mode RF power amplifiers in the 3–30 MHz range. However, in using this or similar active component in Class-E amplifiers, there are certain parameters of key importance in its selection. The first of these, the Drain-to-Source Breakdown Voltage, V_{DSS}, must be large enough to handle the transient voltage at the drain that results when the MOSFET turns off. Losses in the transistor are typically the largest in the entire circuit, thus it is helpful to have a device whose Drain-Source On-State Resistance, $R_{DS(on)}$, is as low as possible when the junction temperature is at ambient. As the junction temperature rises so does the resistance and losses increase. Next, the device must be able to switch fast enough to handle the desired drive frequency. The switching speed is affected by the size of the gate charge, Q_g. The larger this number, the more work must be done to charge and discharge the input capacitance at the gate. This in turn decreases the switching speed. Finally, Gate-Source Voltage, V_{GS}, is important as it is the maximum value of voltage at which the oxide breakdown will occur. In the Class-E amplifier, the drive signal into the gate is measured by the amplitude of V_{GS} and must be monitored carefully as the amplifier is optimized for the best operation [5].

2.2 200–W Amplifier Design

The amplifier circuit is shown in Figure 2.2 [6]. The AC input passes through the isolation transformer and the full-wave rectifier. The rectified signal passes through the input filter, the 40-μH choke (RFC), and the bypass capacitor (Cb). The RF choke converts the 0 to 100-Vdc input from the power supply to a current source, and the bypass capacitor helps keep RF energy out of the power supply. The series inductor (Ls) and capacitor (Cs) form the resonant network that produces the rising and falling voltage waveform needed for the Class-E amplifier. Output power is determined by the supply voltage and the value of the series inductance (Ls). A supply voltage of 100 V gives an output power of

200 W. The tank circuit at the load (Ll and Cl) is a trap for the second harmonic. Without the trap, the second harmonic is at the −26-dB level. With the trap, all harmonics are more than 40 dB below the carrier. In addition, (Ll and Cl) transform the 50-Ω load to around 10 Ω, the appropriate range for a Class-E amplifier.

The impedance of the gate is small, only about 3 Ω and it is primarily resistive. The transformer (T) reduces the 50-Ω impedance of the drive circuit to about 2 Ω to match the low resistance of the gate. This gate transformer also sets the DC bias to zero volts and insures the transistor is "off" when it is not driven, as this is far below the threshold voltage of about 4 V.

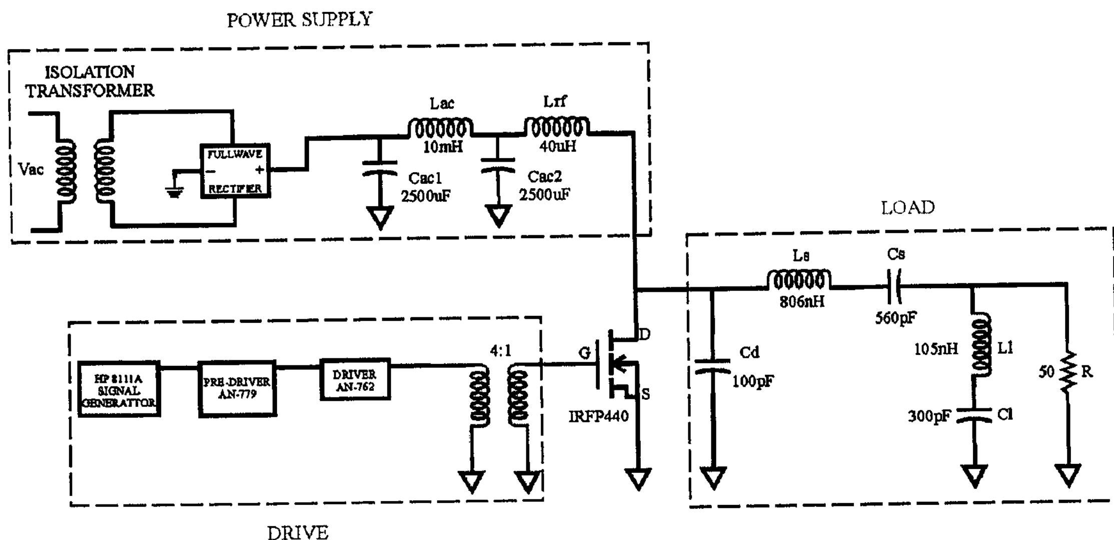

Fig. 2.2. 13.56-MHz Class-E amplifier circuit. The IRFP440 Power MOSFET acts as a switch that opens and closes at the RF frequency. The capacitors are all silver micas with a 1000-V rating.

This design of the 200-W amplifier is a further development of a 7-MHz amplifier intended for amateurs. To obtain the initial component values of the load network, scaling by a factor of 50% of the 7-MHz component values can be done as long as the impedance of the two networks remain the same. With

the shunt load resistance remaining at 50 Ω, the resulting values of R, L, and C produce the current and voltage waveforms needed for the Class-E amplifier. The quality factor of the load network, Q_L, is an important parameter of that affects the amplifier's operation. It affects the bandwidth of the amplifier, has a direct bearing on the efficiency, and influences the harmonic content of the power at the load. When Q is low, the output load network is easier to tune. If the Q is too low, large harmonic currents will flow through the load and additional filtering will be needed. For a high load network Q, the harmonic content through the load will be low but makes it harder to tune the output load network. The load Q for the 13.56-MHz amplifier is 5 and this yields a 3-dB bandwidth of 2.7 MHz.

2.3 Amplifier Construction

A photograph of the 200-W Class-E amplifier is shown in Figure 2.3. The circuit is made on a printed-circuit board made from insulating material, usually glass epoxy or phenolic, coated with conductive copper [7]. The area for the metal patterns (dashed lines) are drawn first on paper, colored black, and then reproduced on transparency film. The resulting dark patterns (the copier toner) on the transparency film are transferred to the copper surface by the heat of an iron. This "homemade" circuit board is then etched to remove all metal except the darkened traces.

Figure 2.4 shows the board design. To facilitate heat removal from the power MOSFET, the device is mounted to a water-cooled copper fixture with silicone grease used to provide good thermal contact between the two surfaces. A side-view photo of the MOSFET mounted on the heat sink is shown in Figure 2.5.

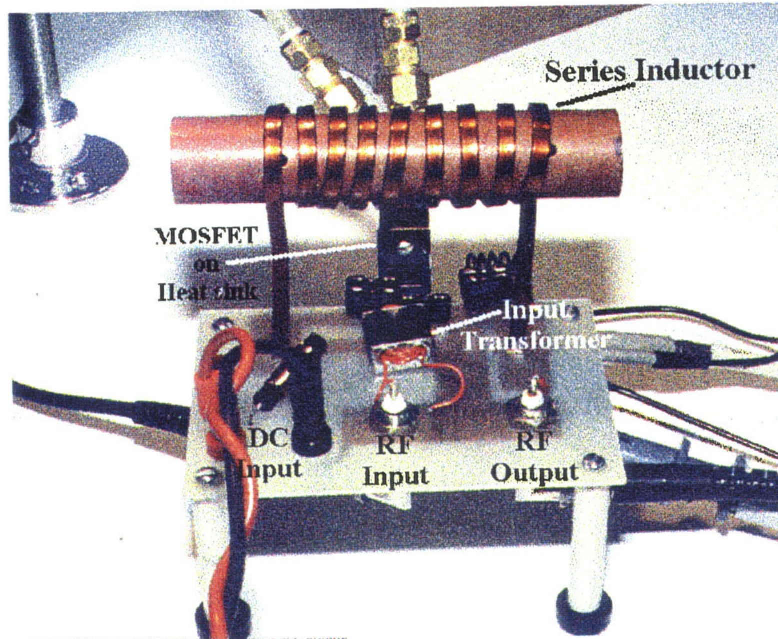

Fig. 2.3. The 13.56 MHz, 200-W Class-E amplifier.

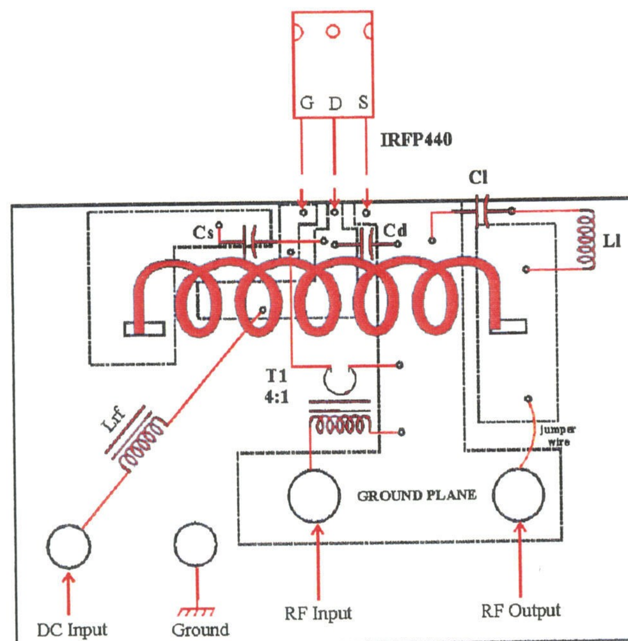

Fig. 2.4. Circuit board for 200 W amplifier.

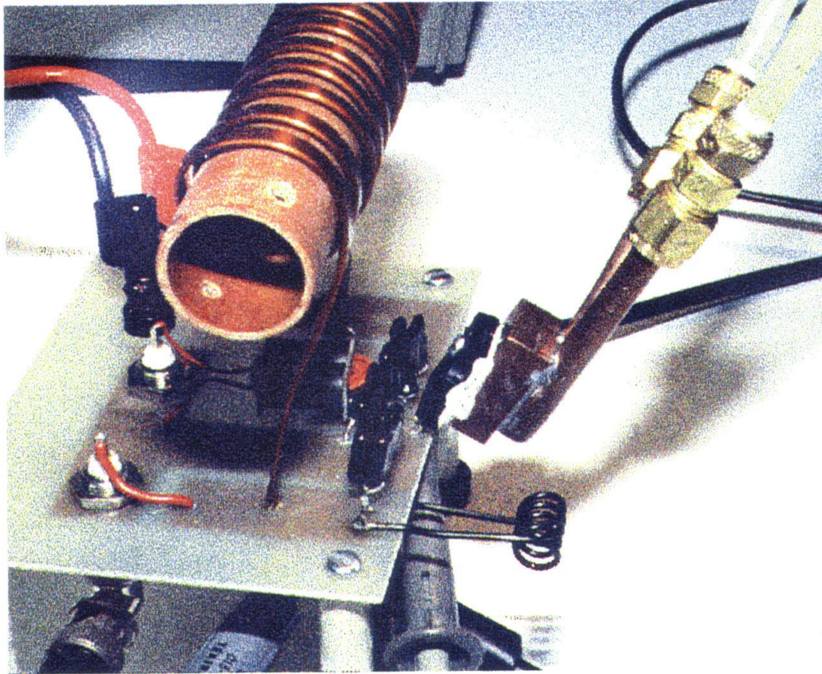

Fig. 2.5. The 13.56 MHz, 200-W Class-E amplifier, showing the arrangements for water cooling.

Components in the load network must withstand high power levels during operation. We use copper tape inductors that have a high Q (~ 300) and can take very high power levels without damage. For the capacitors, many different types have been tried polystyrene, polyethylene, 500-V mica, and polyethylene. However, they all failed. The arcing (internal due to dielectric breakdown) not only destroyed the capacitor but sometimes the transistor (due to external arcing). Currently, Cornell Dubilier 1000-V mica capacitors, with Q's of 500, are used with great success.

After initial testing of the amplifier, it was determined that the series capacitor (Cs) and the trap filter capacitor (Cl) were hot to the touch after turning off the amplifier. This is attributed to power dissipation related of the capacitor's equivalent parallel or leakage resistance. To alleviate this excess heating, the Q of these capacitances is increased by replacing the initial capacitance with two

capacitors in parallel yielding the same design value. The effect of the parallel combination is to decrease the equivalent series resistance.

2.4 Tuneup and Power Calibration

The measurement setup of the 200-W Class-E amplifier is shown below.

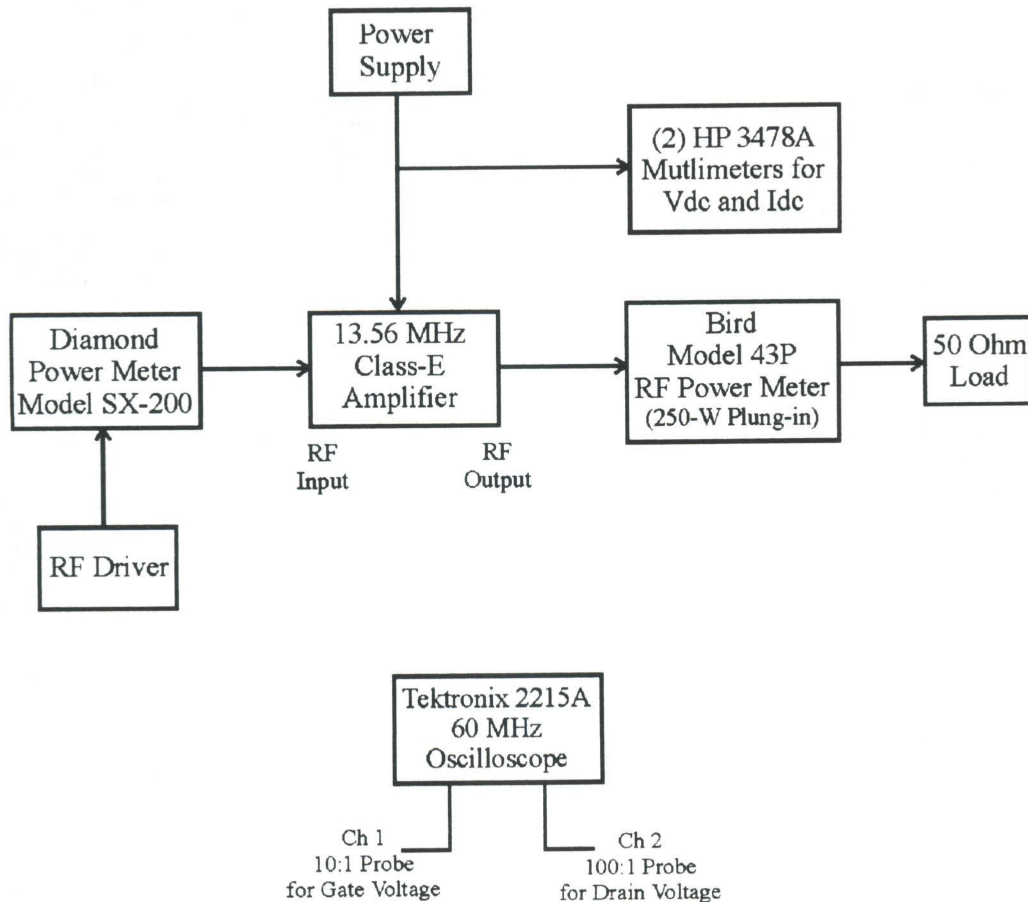

Fig. 2.6. The schematic diagram of the 200-W amplifier measurement setup.

The signal power at the gate is measured with a Diamond SX-200 power meter. It has a power handling capability of 200 W and can also measure the standing wave ratio. The output RF power is measured using a Bird "Thruline" power meter, model 43P. This meter has the feature of using exchangeable power elements that

correspond to both the frequency and power level being measured. This meter can also measure reflected power. Accuracy is critical when making efficient amplifiers, especially in the DC power measurements. Two Hewlett Packard 3478A, $5\frac{1}{2}$ digit, multimeters are used to measure voltage and current. It is estimated that the DC power is accurate to 1%. Since the performance of the meters is affected by RF fields, they must be bypassed by a capacitor on the input. The gate and drain voltage waveforms are viewed with a Tektronix 2215A, 60-MHz, oscilloscope. Channel 1, using a 10:1 probe, measures the gate voltage at the gate terminal of the MOSFET and channel 2, with a 100:1 probe attached, measures the voltage at the drain of the transistor.

When initially powering the amplifier, two adjustments are made. First the standing wave ratio (SWR) is checked with full RF input. If it cannot be brought down below 2:1, a turn is added or subtracted from the gate transformer. With a power meter and a 50-Ω dummy load on the RF output, the output power is set by stretching or squeezing (Ls). This, however, is done before the dc input voltage is applied. Stretching the coil reduces the inductance and increases the output power. However, the input power will also increase and lower the efficiency. Squeezing reduces the output power and usually increases the efficiency. Thus, Ls is adjusted to optimize the trade-off between output power and efficiency. It should be pointed out, that too much inductance can cause severe ringing in the gate and drain waveforms. To achieve RF output power of 200 W, heat removal from the MOSFET is facilitated by attaching it to a water-cooled, copper, heat sink instead of a conventional metal heat sink. The gate and drain waveforms are shown in Figure 2.7.

Class-E amplifiers have high efficiency and it is important to obtain accurate readings of the output power to calculate the circuit losses accurately. A Bird wattmeter with an accuracy of ±13 W was used to measure the output power. To improve this accuracy, the wattmeter was calibrated using a thermal method

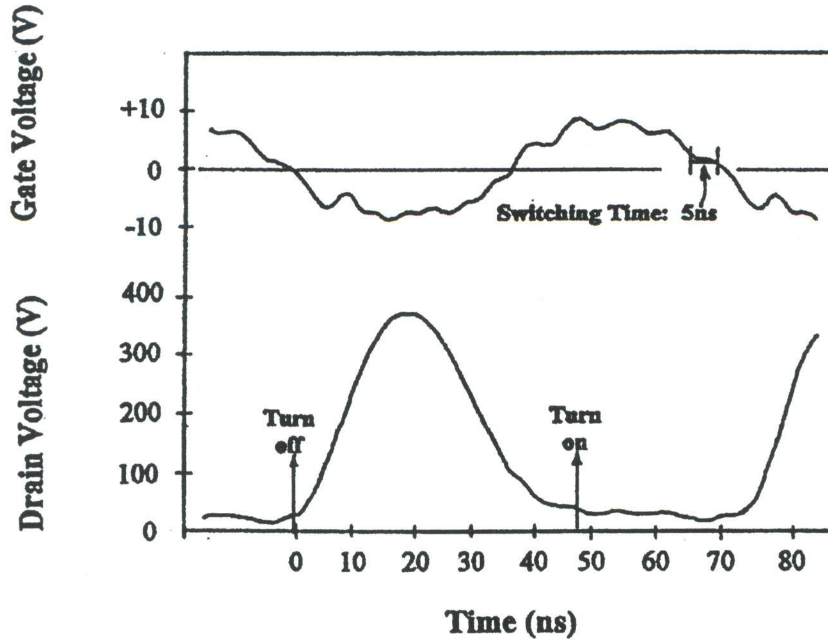

Fig. 2.7. Oscilloscope trace of the measured gate and drain voltage for the 200-W amplifier with 10-W drive. The DC supply is 100 V and the input SWR is 1.8:1. The peak voltage voltage is 9 V, and the peak drain voltage is 350 V, safely within the manufacturer's ratings of 20 V and 500 V.

developed by Joyce Wong [8].

The calibration procedure is as follows: a thermocouple is attached to the output end of the 50-Ω load. It is placed at this location to account for the delay in temperature rise between the input and output ends. Next, DC power is applied to the load at a level that is close to the RF power used for the amplifier: 175 W. The temperature is measured at every minute during a 30-minute "on" period and for another interval of 30-minutes when the power is turned off. We get a rising curve of temperature, with a peak that occurs a minute of two after the power is turned off. This peak is characteristic of the amount of power applied to the load and the time we applied it.

After letting the load cool back to room temperature, subsequent measure-

ments at 200 W_{dc} and 225 W_{dc} are made. Finally, the amplifier is run with a 200-W nominal reading on the Bird wattmeter. The thermocouple does not function when RF power is on, thus the temperature of the load is recorded starting at the 30th minute when the amplifier is turned off. Figure 2.8 shows a plot of thermal measurements where the load temperatures peaked at the 32nd minute.

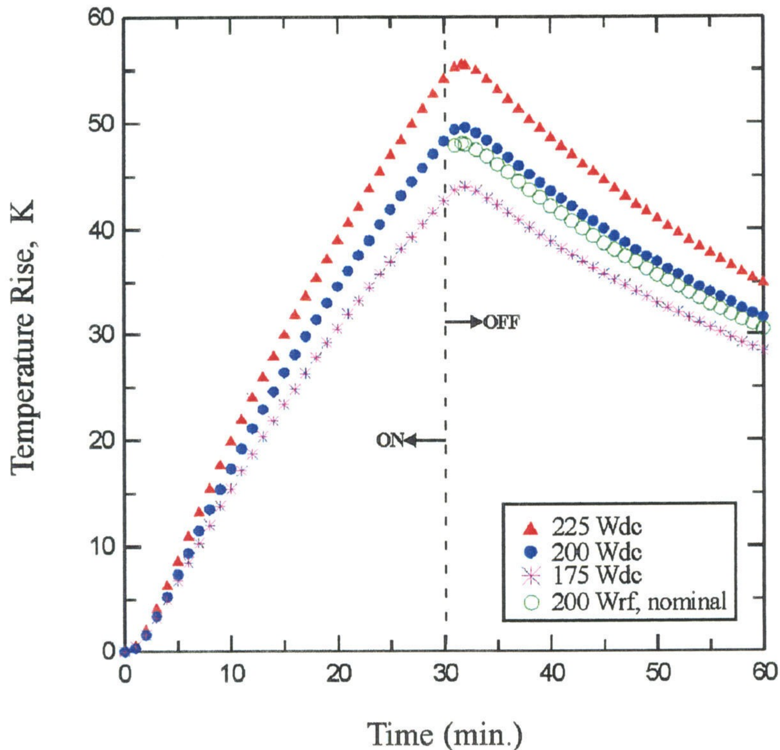

Fig. 2.8. Plot of load temperature vs. time.

Figure 2.9 is a plot of power versus the peak temperature values. By using the load temperature at the 200-W nominal RF power, we can interpolate to determine the actual RF wattmeter reading. From the plot, the wattmeter reads 3.4% too high. By subtracting this from the nominal RF power we get the correct load power of 193.5 W. To compensate for this overestimation, a 5-ft section of coaxial cable is added in front of the Bird meter. Adding this to the load power

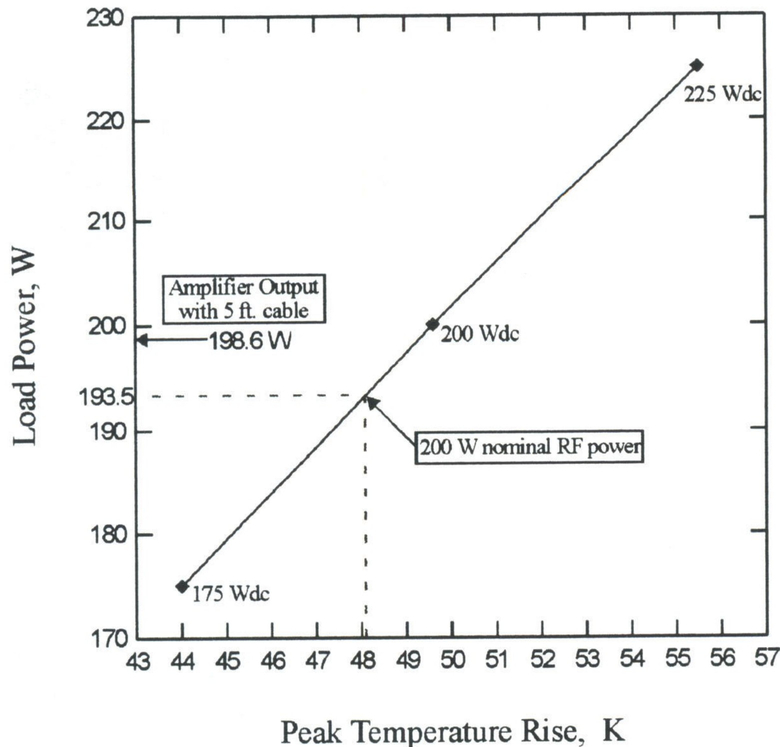

Fig. 2.9. Load power versus peak temperature rise of 50-Ω load.

results in the correct amplifier output power of 198.6 W.

2.5 Experimental Results

The waveforms for the gate and drain voltage for the switching transistor were shown in Figure 2.7. A sine wave signal to the gate is used as a means to deal with the gate reactance by resonating it. Note, however, that the gate curve is quite bumpy with ringing in the VHF range. This ringing is driven by the sudden turn-on and turn-off of the transistor which acts like the gong of a bell. A drive power of 10-W is chosen as it keeps the gate voltage well within the manufacturer's rating of ±20 V. The RF drive level is important as it must be powerful enough to switch the transistor on an off quickly and completely. If the

transistor is not reliably switched on and off, inefficient operation of the device results, leading to overheating and potential failure.

The efficiency of the 200-W amplifier as a function of drive power is examined in Figure 2.10. The drain efficiency is above 91% for input powers above 10 W. However, large drive levels increase the heat dissipated in the amplifier. To take this into account *overall efficiency* or ratio of the RF output power to the total input power (DC plus RF) is plotted. Overall Efficiency is a better indicator of how hot the transistor is going to get.

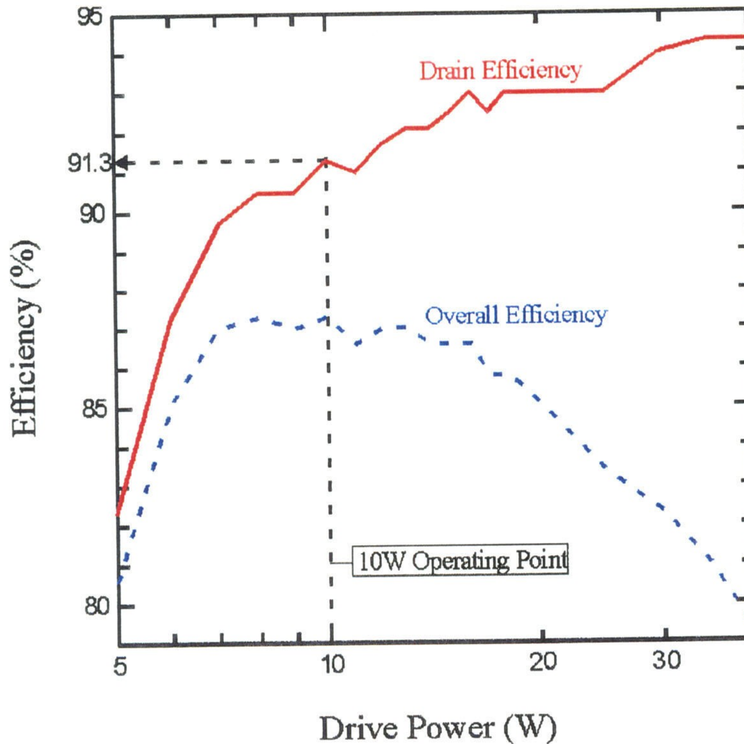

Fig. 2.10. Drain and overall efficiency versus drive power. A drive power below 15 W is recommended to minimize heat dissipation in the MOSFET.

Another performance measurement examines how the drain efficiency varies with output power. Figure 2.11 shows that high efficiency is maintained over a wide

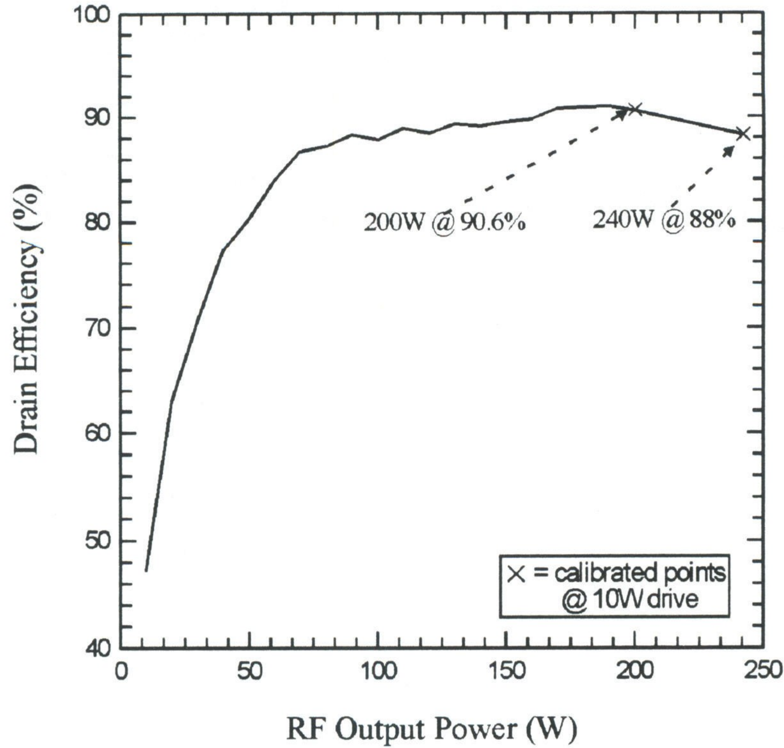

Fig. 2.11. Drain efficiency versus output power.

range of powers, 100 W to 250 W. Note the calibrated data points.

When the 13.56 MHz signal is transmitted, all higher harmonics are transmitted simultaneously, causing possible interference for users in the other frequency bands. As previously mentioned in section 2.2, this design of the Class-E circuit includes a trap for the second harmonic frequency, 27.12 MHz. Figure 2.12 shows the amplifier's output waveform spectrum. Without the tank circuit, the second harmonic is –26-dB below the fundamental but falls to –45-dB below the fundamental with the resonator in place.

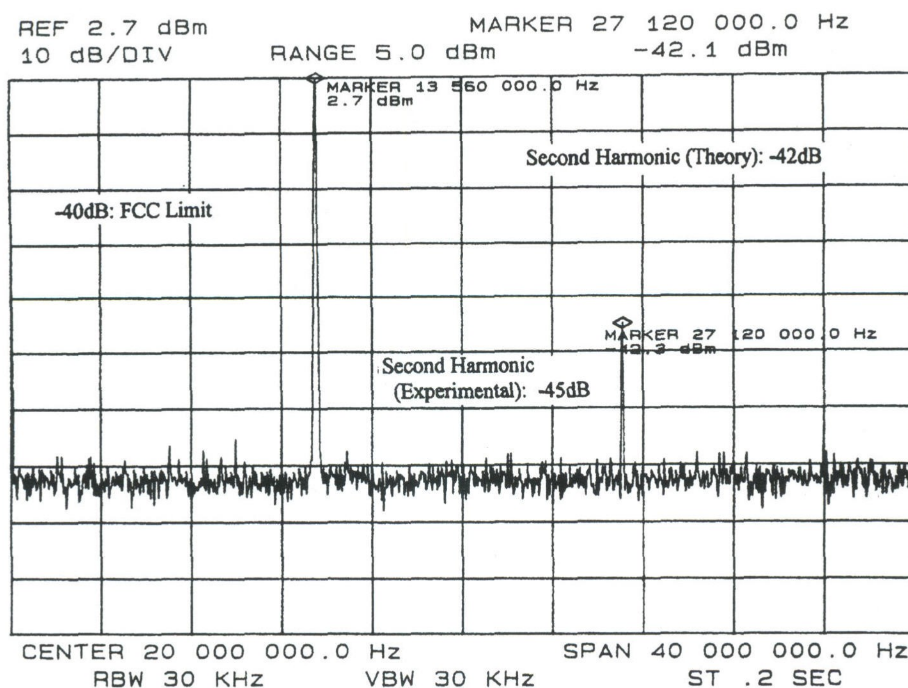

Fig. 2.12. The measured spectrum of the 13.56 MHz Class-E amplifier with the IRFP440 MOSFET.

One of the main concerns in the design of high-efficiency power amplifiers is power dissipation in the active device. The overall efficiency is an aid in setting the drive level to minimize this loss while still maintaining high power and efficiency. Central to this issue is the accurate determination of the transistor junction temperature. A series of measurements are undertaken to arrive at this result. The first of which is the effect the MOSFET's temperature has on its on-resistance, $R_{DS(on)}$. With the MOSFET attached to the water–cooled heat sink, the case temperature is measured with a thermocouple making contact to the exposed drain tab of the MOSFET. Thermal grease is used to insure good thermal contact at the drain tab and at the MOSFET–heat sink interface. Figure 2.13 depicts the measurement setup. The gate-source voltage, V_{GS}, is set to 10 V to make sure the device is in full enhancement. Next the water temperature

is varied, from 10°C to 40°C, to heat the heat sink–MOSFET combination and thus cause the on-resistance to change. Figure 2.14 shows how the resistance changed over this temperature range. Note that the curve is linear with a slope of 7.7m$\Omega/°C$. This slope will be used to find the thermal resistance of the MOSFET.

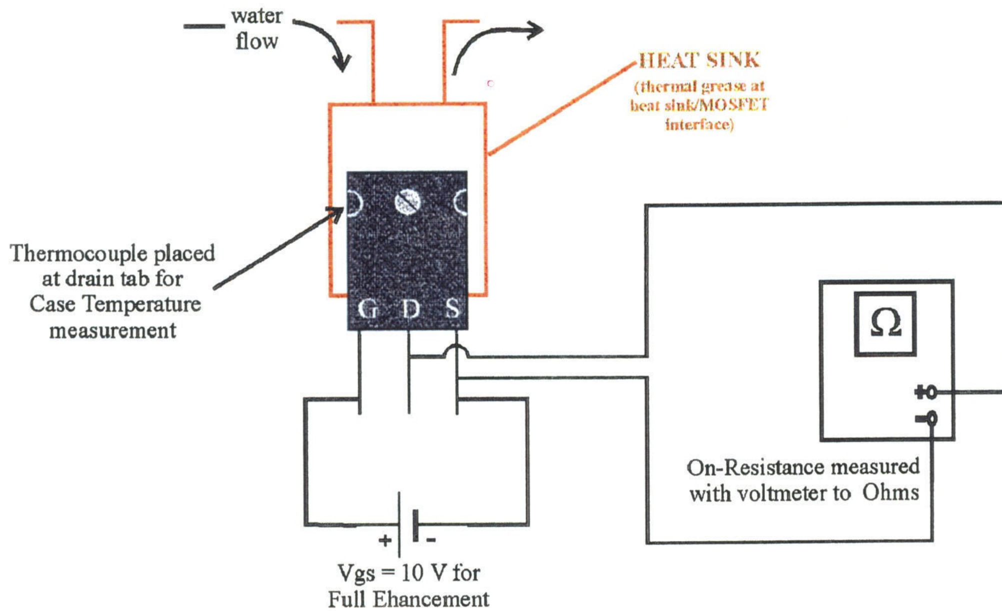

Fig. 2.13. Measurement set-up to determine relationship between MOSFET on-resistance and temperature.

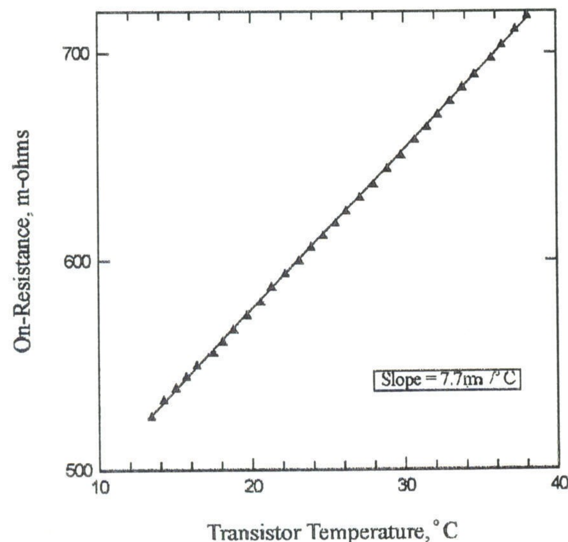

Fig. 2.14. Plot shows the linear relationship between the on-resistance and case temperature.

To determine the thermal resistance, a relationship between $R_{DS(on)}$ and input power to the device must be found. With the setup shown below, the same heat sink–MOSFET combination is used with the cooling water. Two sets of data are collected: one with the use of thermal compound at the heat sink–MOSFET interface and another using a polymer pad at the interface. This pad, made by the Bergquist Company, is specifically designed to isolate the high voltage of the drain from the heat sink. All measurements are done at a constant temperature, 22°C, as we want to measure the change in on-resistance power as power is dissipated in the MOSFET. The gate-source voltage, V_{GS}, is again set to 10 V so the device is fully turned-on (full-enhancement). Measurements are taken at input powers of 1 W, 2 W and 3 W. By monitoring the dc-voltage and current at each power level, the on-resistance can be calculated.

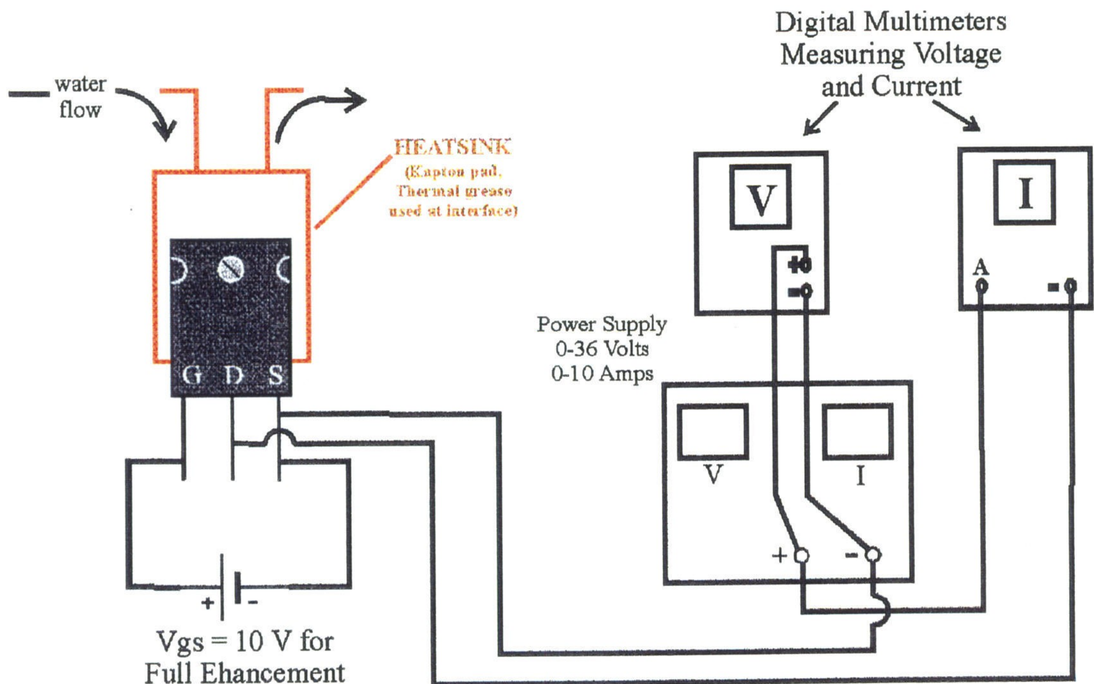

Fig. 2.15. Measurement setup of on-resistance versus input power.

The relationship between the temperature and the power is shown in Figure 2.16. It should be pointed out that the temperature change is inferred from the on-resistance measurement rather than a measured temperature change. The 7.7mΩ/°C from the previous measurement is used in its determination. The lower curve, the transistor with some thermal compound at the interface, yields a thermal resistance of 0.8K/W. For an air cooled heat sink, the thermal compound does not provide good isolation from 350-V drain voltage. The upper curve reveals that the use of the polymer pad will yield a higher thermal resistance of 1.5K/W. When either of these two numbers is multiplied by the power dissipated in the transistor, the change in the junction temperature above room temperature, 25°C, is determined.

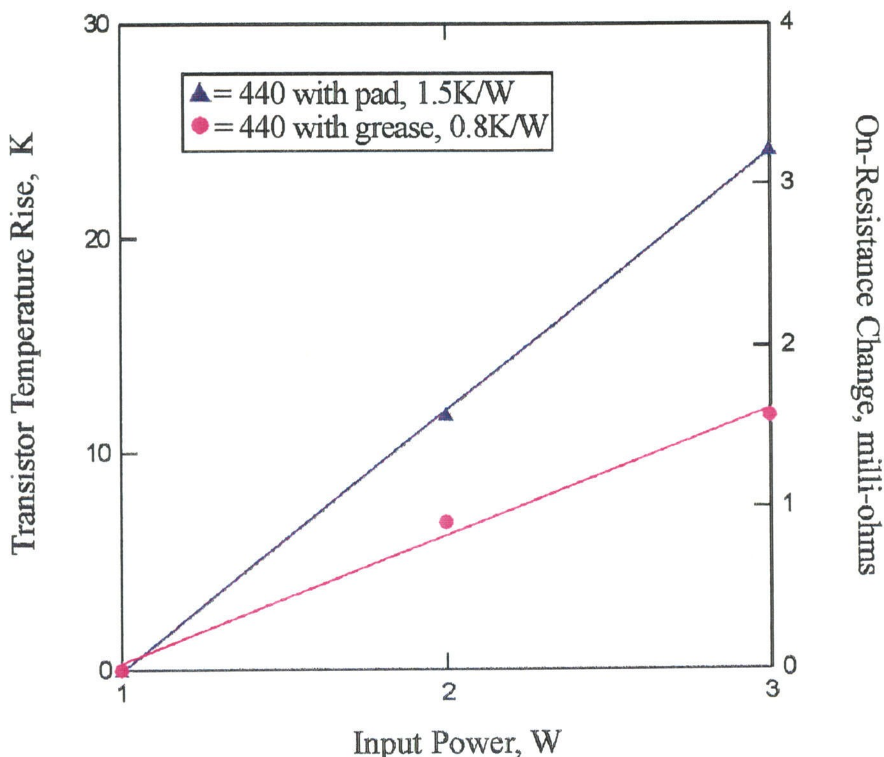

Fig. 2.16. Temperature of the IRFP440 (TO-247AC) vs. input power.

2.6 Class-E Amplifier Simulation Using PSpice

The schematic in Figure 2.17 represents the Class-E circuit implemented in PSpice [9]. All components in the model are measured using the Hewlett Packard HP 4194A Impedance Analyzer. The transistor is modeled as a switch with a linear capacitor (Ct) and a nonlinear dependent voltage source (Ect) to model the square-root behavior of the drain-source capacitance. The PSpice simulation netlist is shown in Figure 2.18. A plot of drain capacitance versus voltage for the IRFP440 MOSFET is depicted in Figure 2.19. The measured data fits well to a square root behavior of the drain-source capacitance.

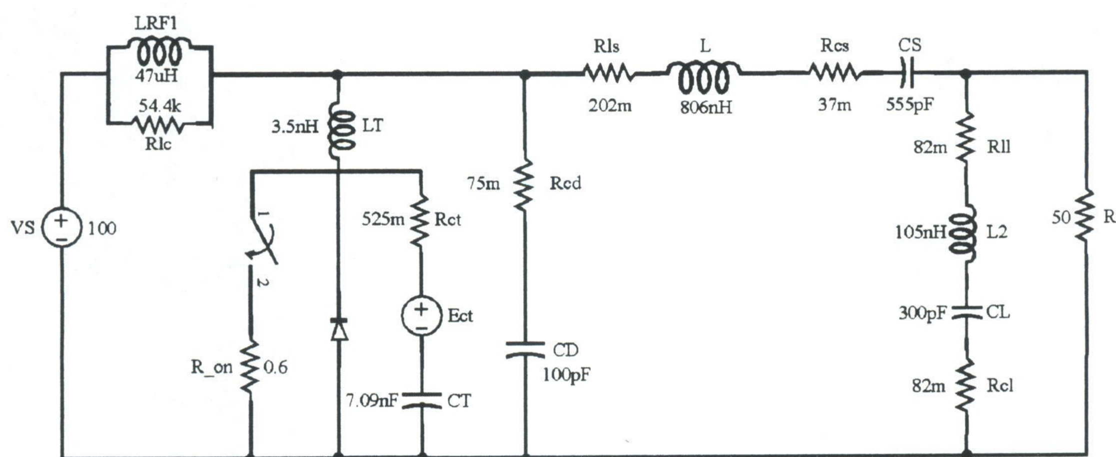

Fig. 2.17. 13.56 MHz Class-E SPICE model. All component values used in the model are measured.

A performance comparison between the actual data and the simulation is shown in Table 2.1. Note that the power prediction is close to the experimental result. The switch current and drain voltage waveforms resulting from the simulation are shown in Figure 2.20. For the switching current, we have not succeeded in making correct measurements and have modeled it. The switching time is estimated by examining the gate voltage curve on the oscilloscope. There is a plateau on the curve which seems to be about 5 ns. The measured drain

voltage is drawn on top of the simulated result for comparison.

```
VS     1  0  100V   ;  DC source voltage
VG1   12  0  PULSE (0V 1V 0NS 0NS 15NS 36NS 73.75NS)
RG1   12  0  1MEG   ;  high resistance for continuity
LRF1   1  2  47UH   ;  RF choke
Rlc    1  2  54.4K  ;  parasitic resistance parallel to RF choke
LT     2  3  3.5NH  ;  series inductance within transistor

*                          TRANSISTOR MODEL
Rct    3  4  525M   ;  series resistance of drain-source capacitance
CT     5  0  7.09NF ;  transistor drain-source capacitance
Ect    4  5  VALUE = {((V(5) + SQRT(V(5)*V(5)))/8)*V(5)*97.3}
D      0  3  DIODE  ;  body-diode internal to IRF440 MOSFET
.MODEL  DIODE  D

*                            LOAD NETWORK

Rcd    2 15    75M  ;  drain capacitor series resistance
LCD   15  6   13NH  ;  lead inductance of drain-source capacitor
CD     6  0   99PF  ;  drain capacitor
Rls    2  7   202M  ;  resistance of series inductance
L      7  8  806NH  ;  series inductance
Rcs    8  9    37M  ;  resistance of series capacitance
CS     9 10  555PF  ;  series capacitance
Rl1   10 13    82M  ;  resistance of series induct. in 2nd harm. res.
L2    13 11  105NH  ;  series inductance used for 2nd harm. resonator
CL    11 14  300PF  ;  capacitance parallel to the load
Rcl   14  0    82M  ;  series resist. of capacitance parallel to load
R     10  0    50   ;  load resistance

*                        SWITCH(TRANSISTOR) MODEL

S1     3  0  12  0  SW1   ;  model for the IRFP440
.MODEL SW1 VSWITCH (RON=.6 ROFF=1MEG)

*                          TRANSIENT ANALYSIS

.TRAN 500PS 10.4US 10US 500PS
.PROBE

.END
```

Fig. 2.18. 200-W Class-E amplifier PSpice netlist.

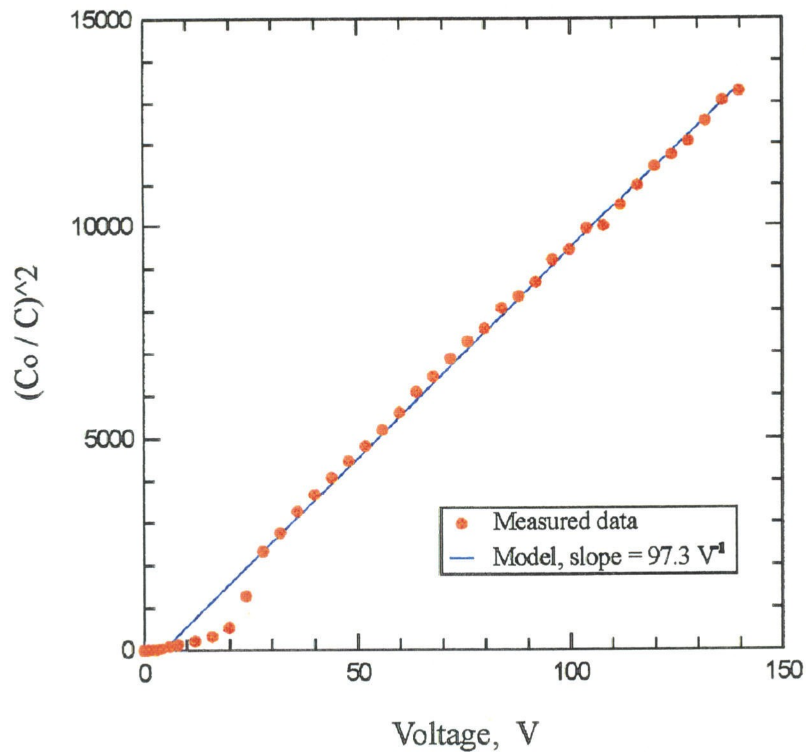

Fig. 2.19. Measured drain capacitance is in good agreement with theory.

Measurement	Experimental Results	SPICE Model
RF Output Power	200 W	203 W
DC Input Power	291 W	222 W
Drain Efficiency	91%	92%
Peak Drain Voltage	350 V	360 V

Table 2.1. Comparison of the experimental results and SPICE simulation of the 200 W Class-E amplifier with the IRFP440 MOSFET.

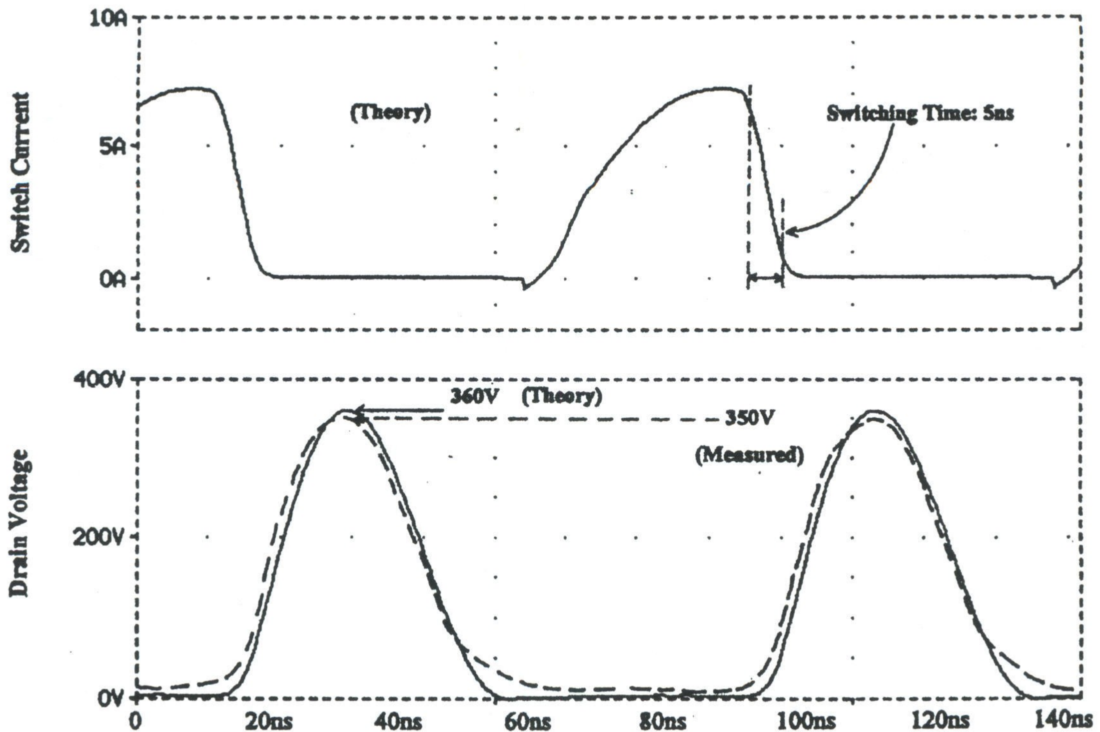

Fig. 2.20. Simulated switch current and voltage. The experimental switch voltage is also shown.

Another aspect of the PSpice simulation involved calculating the RF harmonic spectrum and comparing it with the experimental data. The results of this comparison are shown in Figure 2.21. The first few harmonics (1 through 7) do well in the prediction. However, there is a problem: strong harmonic components exist at 108 MHz and 230 MHz that are not predicted by the simulation. These spurious VHF signals are also seen on the oscilloscope as depicted in Figure 2.22.

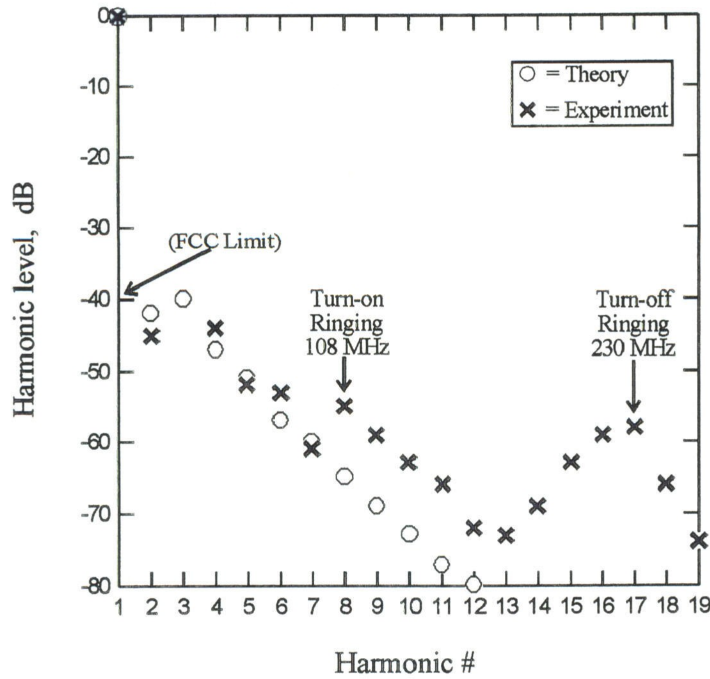

Fig. 2.21. Initial RF output spectrum.

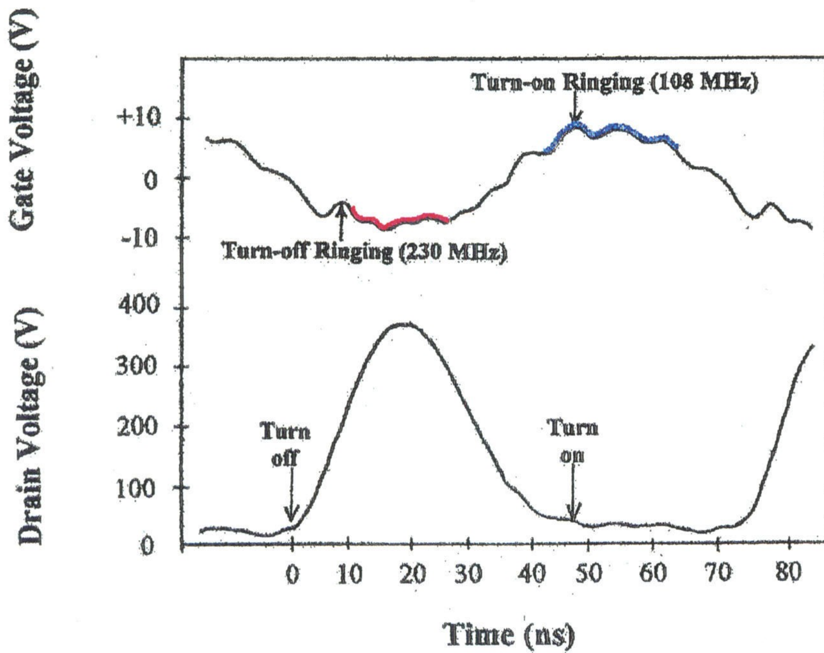

Fig. 2.22. VHF harmonics are seen by examining the gate voltage waveform.

If we examine at the positive cycle of the gate waveform, the transistor is turning on and the bumps are further apart indicating a lower frequency component. On the negative portion of the cycle, the transistor is turning off and the bumps are closer together indicating a higher frequency component. In order to predict both frequencies, one component was added to the model: the measured parasitic inductance (Lcd) of the drain capacitor (Cd). The revised PSpice schematic and the new spectrum are shown in Figure 2.23.

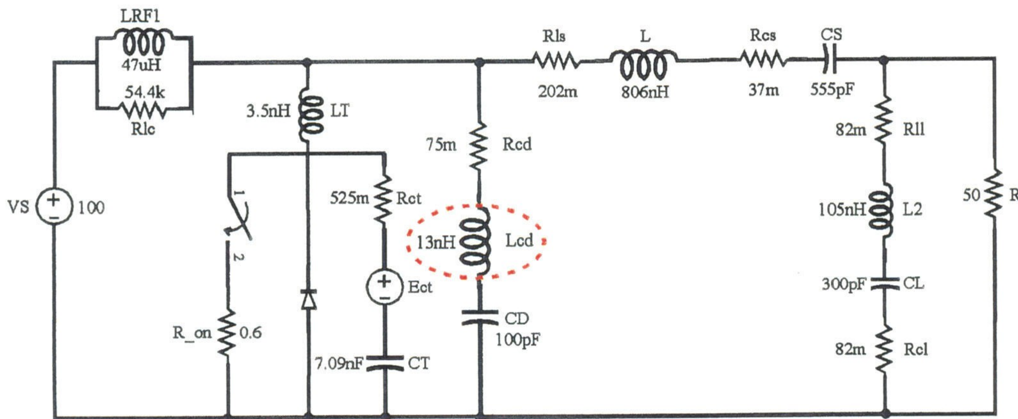

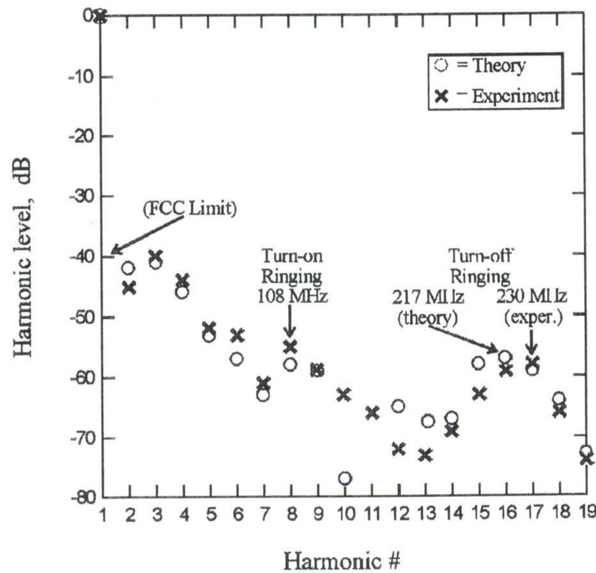

Fig. 2.23. The top figure highlights the inclusion of the parasitic inductance Lcd. This results in a more accurate harmonic prediction.

To further understand this VHF ringing, a simple model was developed. The top circuit in Figure 2.24 shows the ideal switch in parallel with the internal inductance and capacitance of the drain and the external drain capacitance with its parasitic inductance. At turn-on, the internal capacitance is shorted out leaving an increased total capacitance which results in a reduced resonant frequency of 108 MHz. When the switch is turned-off, the internal capacitance is in series reducing the total capacitance and increasing the resonant frequency to 230 MHz.

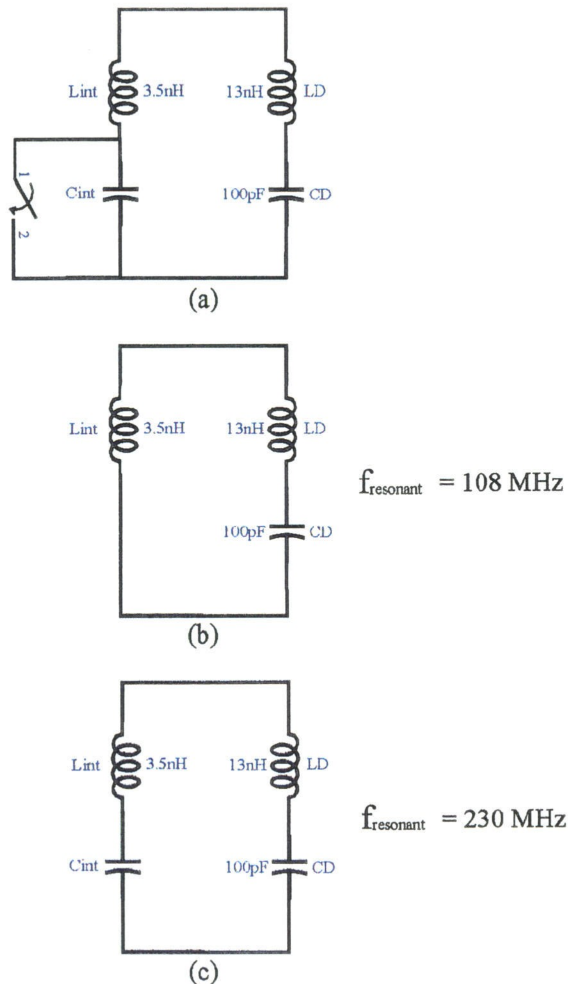

Fig. 2.24. (a) VHF ringing seen in the spectrum is modeled with a switch, the intrinsic inductor and capacitance of the drain and the external drain capacitance with its parasitic inductance. (b) Ringing circuit when MOSFET is on and (c) off.

The final PSpice simulation involves the calculation of component losses. Knowing where the losses occur in the circuit will aid in determining which elements get hot and ultimately fail. The table below shows these results.

Component	Calculated Losses and Temperature Rise
Capacitors: Cd	0.2 W / 13°C
Cs (pair)	0.6 W / 19.5°C, single
Cl (pair)	0.9 W / 30°C, single
Total Capacitor Loss	1.7 W

Inductors: Lc	0.3 W
Ls	3.1 W
Ll	0.9 W
Total Inductor Loss	4.3 W

Transistor: Off-Resistance	0.6 W
On-Resistance	7.8 W
Turn-off Loss	4.1 W
Drive Power	10.0 W
Total Transistor Loss	22.5 W

Table 2.2. Calculated component losses. Measured resistances are used in the simulation. The calculated maximum temperature rise in the capacitors is 30°C.

Associated with the loss calculations of the capacitors is the determination of their maximum temperature rise. The manufacturer, Cornell Dubilier [10], gives a formula for calculating the temperature rise, T, as

$$T = \frac{69P}{A} \tag{2.1}$$

where P = the power dissipation and A = the case area in square inches. The mica capacitors are in the CDV19 package with area of 1.07 square inches. Table 2.2 shows the calculated capacitor temperature. The manufacturer's rating for these capacitors is 125°C. The above results indicate that the drain, series, and load capacitors are not driven too hard. By taking T_{Cl} as the maximum temperature rise, the thermal resistance R_T is determined by dividing 30°C by the one-half the power lost in the Cl pair. Thus R_T = 67°C/W.

2.7. Conclusion

In this chapter, it has been shown that inexpensive power MOSFETs can be used to make industrial RF power amplifiers. Using the IRFP440 and 10 W of drive power, 200 W of output power is obtained with a drain efficiency of 91%. Water cooling was necessary for this development to aid in heat removal from the transistor. Based on measurements of the thermal resistance of the transistor, the junction temperature of the MOSFET is determined to be 40°C. From an operational standpoint, this means the transistor junction is cool. Manufacturers typically run their devices at 100°C. A performance summary table is shown below.

Measurement	Result
V_{ac}	87 V
V_{dc}	100 V
I_{dc}	2.2 A
Calculated $I_{D_{rms}}$ (manufacturer's limit: 8.8 A)	5.1 A
Drain Efficiency	91%
Calculated Transistor Loss	22.5 W
Calculated Junction Temperature (0.8 K/W, 22°C sink)	40°C
Calculated Inductor and Capacitor Loss	6 W
Gate Drive (VSWR 1.8:1)	10 W
Harmonics (3rd)	41 dB

Table 2.3. 200-W Class-E amplifier operation results.

References

[1] Federal Communications Commission regulations for Industrial, Scientific, and Medical equipment (Part 18) is located at the National Archives website: www.access.gpo.gov/cgi-bin/cfrassemble.cgi?title=199847.

[2] E. Lau, K.-W. Chiu, J. Qin, J.F. Davis, K. Potter, and D.B. Rutledge, "High-Efficiency, Class-E Power Amplifiers," *Part 1, QST*, pp. 39–42, May 1997; *Part 2, QST*, pp. 39–42, June 1997.

[3] D.A. Grant and J. Gowar, "General Introduction," in *Power MOSFETS*, John Wiley and Sons, New York, 1989, pp. 4–14.

[4] E.S. Oxner, "Types of Power FETs," *Power FETs and Their Applications*, Prentice Hall, New Jersey, 1982, pp. 45–47.

[5] D.A. Grant and J. Gowar, "Appendix 7, A Power MOSFET Data Sheet," in *Power MOSFETS*, John Wiley and Sons, New York, 1989, pp. 467–482.

[6] J.F. Davis and D.B. Rutledge, "Industrial Class-E Power Amplifiers with Low-Cost Power MOSFETs and Sine-Wave Drive," *Proc. RF Design '97 Conference and Expo*, Santa Clara, CA, pp. 283–297, July 1997.

[7] E. Hare, B. Hale, I. White, and C. Adams, "Circuit Construction," *The ARRL Handbook, 1998*, The American Radio Relay League, Connecticut, 1997, p. 25.12.

[8] J. Wong, "A 300-W Solid-State Class-E Amplifier for Amateur Communications," Bachelor's Thesis, California Institute of Technology, Pasadena, CA, 1995.

[9] "MicroSim PSpice version 5.2," MicroSim Corporation, 16275 Laguna Canyon Road, Irvine, CA 92618, U.S.A.

[10] Cornell Dubilier Data Sheet on "Snubber Mikes – The mica capacitor for snubbers and resonant power supplies."

Chapter 3

A 400-W, 13.56-MHz Air-Cooled Class-E Amplifier

The high efficiency of the Class-E amplifier makes it possible to produce high output power because the dissipated power is minimized. A 500-W Class-E push-pull amplifier was demonstrated by Davis *et al.* that yielded an efficiency of 92% at 1.7 MHz [1]. Sokal *et al.* later demonstrated a 27-MHz Class-E power amplifier that delivered 24 W at 92% efficiency using a single IRF520 MOSFET [2]. In the previous chapter, a 200-W, 13.56-MHz, water-cooled amplifier is profiled with an attained efficiency of 91%. In this chapter, we discuss the design, construction, and performance of a 400-W, single-ended, Class-E power amplifier for 13.56-MHz industrial, scientific, and medical applications [3]. The amplifier uses International Rectifier's new low-charge MOSFET, the IRFP450LC. This low-charge feature improves the switching speed of the device and allows for reduced gate drive requirements. The device comes in the TO-247 plastic package and costs $8 in quantities of 100.

To understand the behavior of the amplifier's performance, extensive measurements are done to characterize the components and the RF output power. A more accurate power measurement system is employed that uses digital power meters accompanied by directional power sensors. Experimental data is again compared with a PSpice simulation employing the same model topology as in the 200-W simulation. The 400-W amplifier is built on a single-sided printed circuit board (PCB), designed using the PCB layout software from Protel Technology.

Again, the layout took into consideration optimum component placement to minimize RF coupling. A drive level of 12 W is used to attain a drain efficiency of 86% and an overall efficiency of 84%. All harmonics are more than 40 dB below the carrier.

3.1 400-W Amplifier Design

The design of this higher-power amplifier has its origins in the water-cooled version discussed in Chapter 2. One significant change is in the active device. The IRFP450LC is similar to the IRFP440 but differs in that it can handle higher drain current, 14A (rms), and has a lower drain source resistance, $R_{DS(on)}$, of 0.4 Ω. When more power is the objective in power amplifier design, drain current needs to increase to get more power out at the same frequency. A lower drain source resistance means one of the dissipation mechanisms in the device is much less and translates to cooler operation. Lower gate charge, delineated by the "LC," allows for reduced gate drive and faster switching. Another significant improvement is higher gate-to-source voltage which allots more room for drive power variation if we desire more output power. Determination of the initial component values is based on the 200-W amplifier in Figure 3.1.

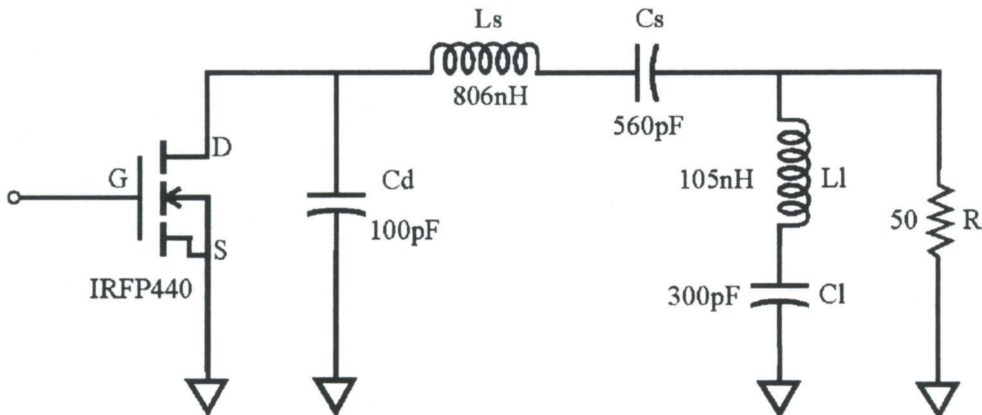

Fig. 3.1. The 400-W amplifier load circuit parameters are scaled from this 200-W design.

In the pursuit of greater RF power at 13.56 MHz, more current is needed at the load and this means a low impedance load circuit is required. This translates to more capacitance, less inductance, and less resistance in this network. Current can be scaled as long as we don't exceed the drain current of the MOSFET. The same rationale holds if we hold the DC voltage constant and only increase the DC current. The scaling factor, determined by dividing the rms current of the IRFP450LC by that of the IRFP440, is 1.6. The new series inductance, capacitance and drain capacitance values are found by either multiplying or dividing the corresponding component values from the 200-W by this number. The results are as follows: L′s = 504 nH, C′s = 896 pF, C′d = 160 pF.

To determine the resistance in the load network and the component values for the second harmonic resonator, several network transformations are performed. The parallel combination of the second harmonic resonator and the 50-Ω load, in Figure 3.2, is examined first.

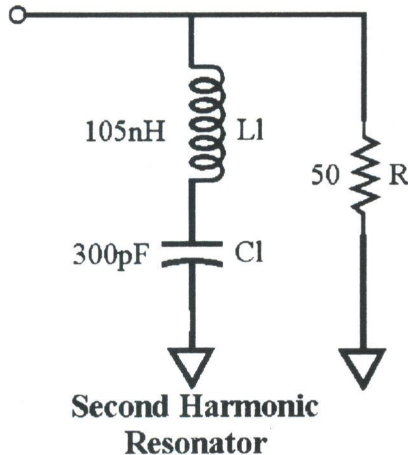

Fig. 3.2. Impedance transformation network of the 200-W amplifier.

In general, you want to transform the shunt L-C combination shown above into the result shown in Figure 3.3. This can be further clarified in the subsequent derivation. Let $f_o = 13.56$ MHz.

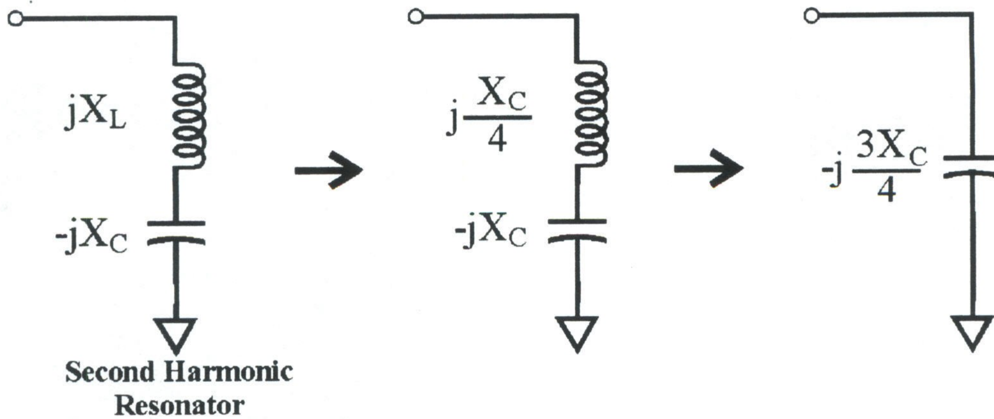

Fig. 3.3. Impedance transformation network of the 200-W amplifier.

$$X_L = X_C, \text{at } 2f_o \tag{3.1}$$

$$2(2\pi f_o L) = \frac{1}{2(2\pi f_o C)} \tag{3.2}$$

$$2X_L = \frac{1}{2}X_C \tag{3.3}$$

$$X_L = \frac{1}{4}X_C \tag{3.4}$$

With the value of X_C determined to be 39.1 Ω, $\frac{3}{4}X_C = 29.3$ Ω. This result forms the basis of a shunt R-C network shown in Figure 3.4. Another impedance converts the shunt network to its series R-C equivalent.

Since the series-parallel transformation is used frequently, let's define the general equations. Assume the two circuits are equivalent at a specified frequency. The quality factors for the parallel circuit and series circuit are defined as

$$Q_P = \frac{R_P}{X_P}, \tag{3.5}$$

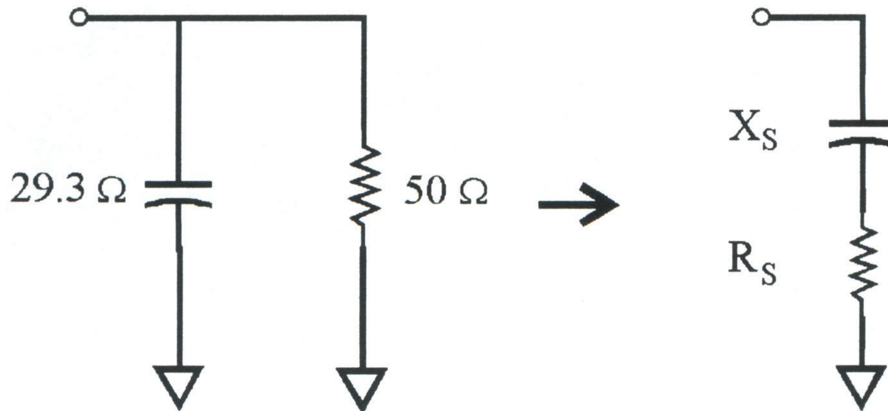

Fig. 3.4. Series-parallel impedance transformations are extensively used in the 400-W Class-E design.

and

$$Q_S = \frac{X_S}{R_S}. \tag{3.6}$$

By equating impedances, it can be shown that

$$R_S = \frac{R_P}{Q_P^2 + 1} \tag{3.7}$$

and

$$X_S = \frac{X_P Q_P^2}{Q_P^2 + 1} \tag{3.8}$$

for the parallel-to-series conversion. For the subsequent series-to-parallel conversions, the following two equations will prove useful.

$$X_P = \frac{R_P}{Q_P}, \tag{3.9}$$

$$Q_P = \sqrt{\frac{R_P}{R_S} - 1}. \tag{3.10}$$

With this foundation in place, calculated results for X_S and R_S are 21.8 Ω and 12.8 Ω respectively. Since the IRFP440 drain current is 63% of the IRFP450LC drain current, the "scaled" series resistance, R'_S, for the 400-W amplifier can be found. This new resistance is 63% of 12.8 Ω or 8.1 Ω.

Using equations (3.9) and (3.10), the remaining portion of the 400-W output circuit is found by using a series-to-parallel transformation. The circuit configuration is shown in Figure 3.5. The values of X_P and Q are 22 Ω and 2.3 respectively.

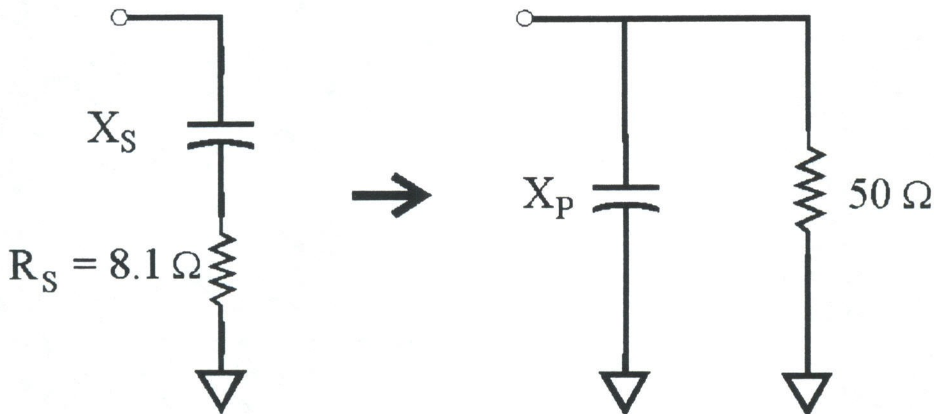

Fig. 3.5. Circuit transformation used to find the remaining components of the 400-W load network.

Referring to the Figure 3.3, we work backwards, starting at the capacitor, with the goal of determining the reactance values for the second harmonic resonator. The 22 Ω is equated to the capacitor's reactance of 3/4 X_C. Thus, $X_C =$ 29.3Ω. The inductive reactance, X_L, is 7.3Ω or 25% of X_C. The inductance and capacitance values for the second harmonic resonator are calculated from their respective reactance formulas. Figure 3.6 shows the reactances and component values of the resonator.

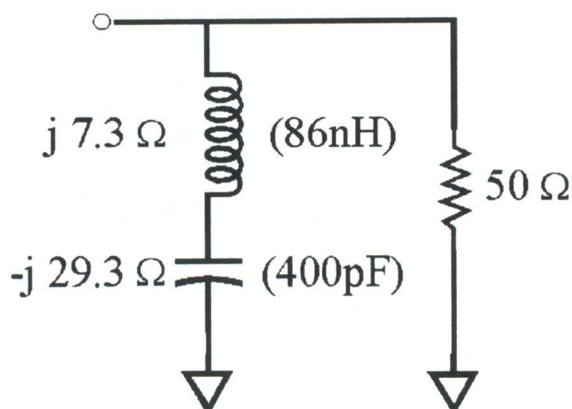

Fig. 3.6. The completed shunt portion of the 400-W amplifier load network.

In choosing components to fit the design results, the closet standard capacitor values are used in the circuit. The inductors are hand wound and depend on the gauge of wire used and the diameter of the coil form chosen. The completed 400-W Class-E design is below.

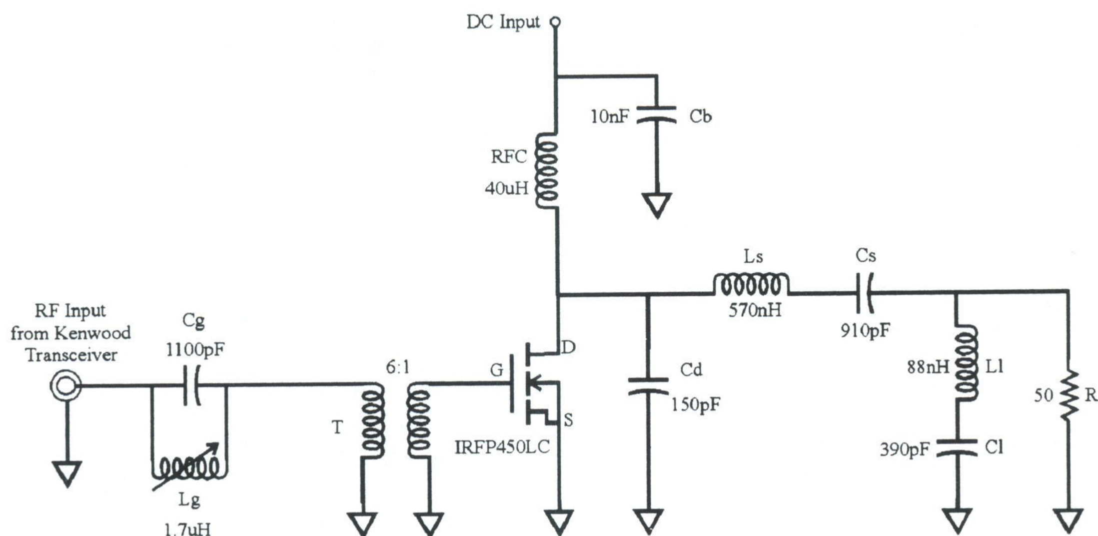

Fig. 3.7. 13.56-MHz, 400-W Class-E amplifier design. The new low-charge power MOSFET acts as the switch.

The transformer (T) is used to step up the gate resistance to the 50-Ω impedance

of the drive circuit. This gate transformer also sets the DC bias to zero volts and insures the transistor is off when it is not driven, as this is far below the threshold voltage of 4 V. Finally, capacitor (Cg) in parallel with the variable inductor (Lg) is used in tuning out the inductive reactance of the gate. The reason we use a capacitor is that the gate is already inductive since we are past the resonance of the bond wires of the intrinsic gate capacitance. A variable inductor is shunted with the capacitor to make it variable.

3.2 Amplifier Construction

Figure 3.8 shows the 400-W amplifier with its mesh cover removed. The transistor is mounted on a 4.1″×3.0″×1.4″ heat sink with dimensions with 1-inch fins using a 6-32 bolt and nut. The transistor generates most of the heat in the amplifier, so it must have good thermal contact to the heat sink. Because the transistor's case reaches high voltages and dissipates most of the heat (about 12% of the DC power), sufficient electrical isolation from and thermal contact to the heat sink is essential. We use a Kapton pad manufactured by Bergquist that has a thermal resistance of 0.2 K/W and a breakdown voltage of 6 kV. This assembly is depicted in Figure 3.9.

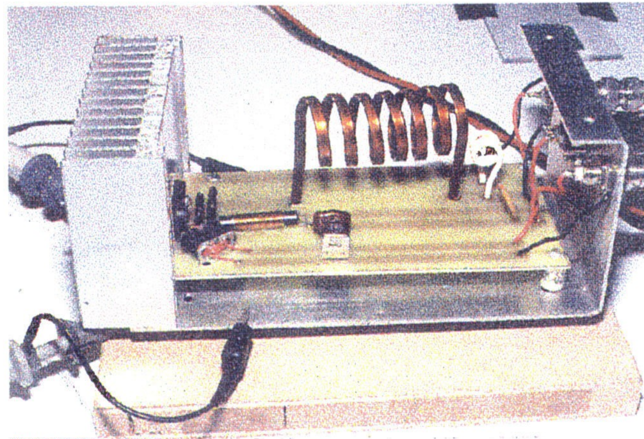

Fig. 3.8. Photograph of the 400-W amplifier with cover removed.

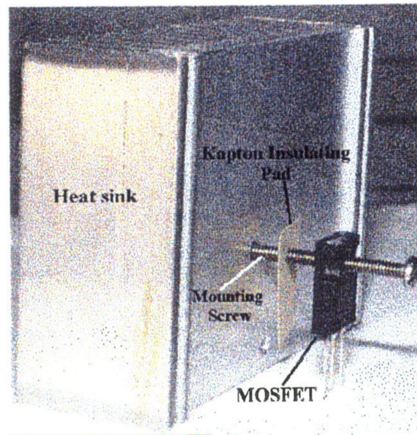

Fig. 3.9. Heat sink-Kapton pad-MOSFET assembly.

The heat sink surface must be free of burrs and the transistor should lie flat on the surface with minimal stress on the leads. A torque screwdriver is used to mount the transistor to the heat sink as International Rectifier recommends a mounting torque of 10 inch-pounds. The heat sink baseplate is an aluminum "L" bracket bent from 0.050-inch-thick aluminum sheet. A U-shaped mesh enclosure cover is made from 0.052-inch-thick aluminum.

The circuit is built on a printed circuit board designed using a PCB layout package from Protel Technology. A copy of the design is shown in Figure 3.10. To avoid bad ringing in the waveforms, the three main sections of the amplifier (DC power, input drive, and output) are kept separate with individual ground strips. Good electrical contact is needed between the MOSFET's source lead and the heat sink. A 6-32 bolt and nut, with washer spacers, are used so that the source lead does not bend. The photograph in Figure 3.11 displays this arrangement. To monitor the gate and drain voltage waveforms, scope probe pigtails are soldered to the MOSFET's gate and drain leads through holes in the baseplate. Rubber grommets in the holes prevent the pigtails from shorting to the chassis [4].

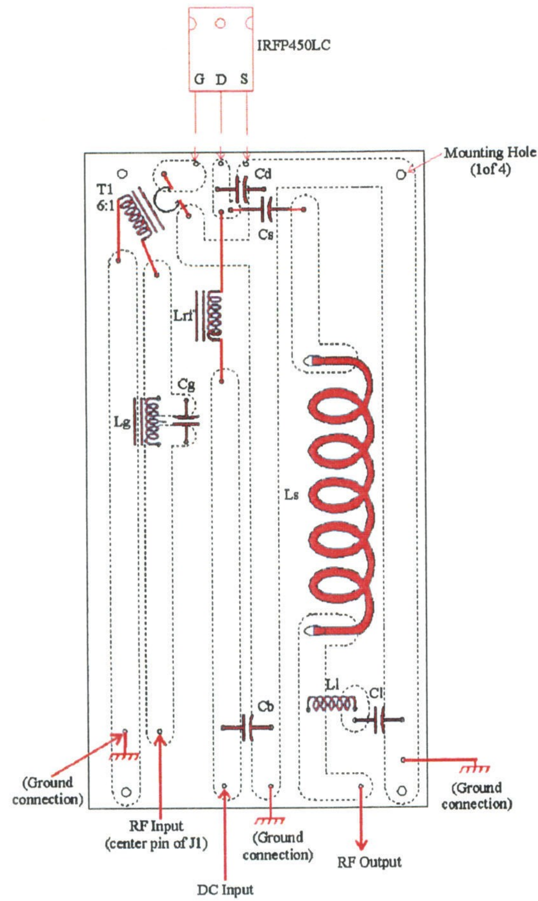

Fig. 3.10. Circuit board and component layout diagram.

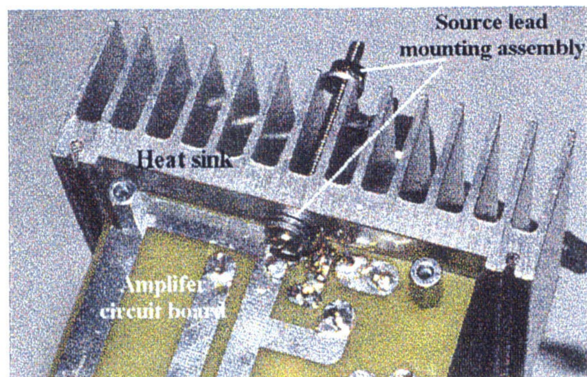

Fig. 3.11. To achieve electrical contact to ground, the MOSFET source lead is bolted to the heat sink.

The copper tape series (Ls) inductor and 18-ga wire inductor for the second harmonic trap are made by winding the wire on pipe and drill-bit forms.

3.3 Tuneup and Power Calibration

The measurement setup of the 400-W Class-E amplifier is shown below.

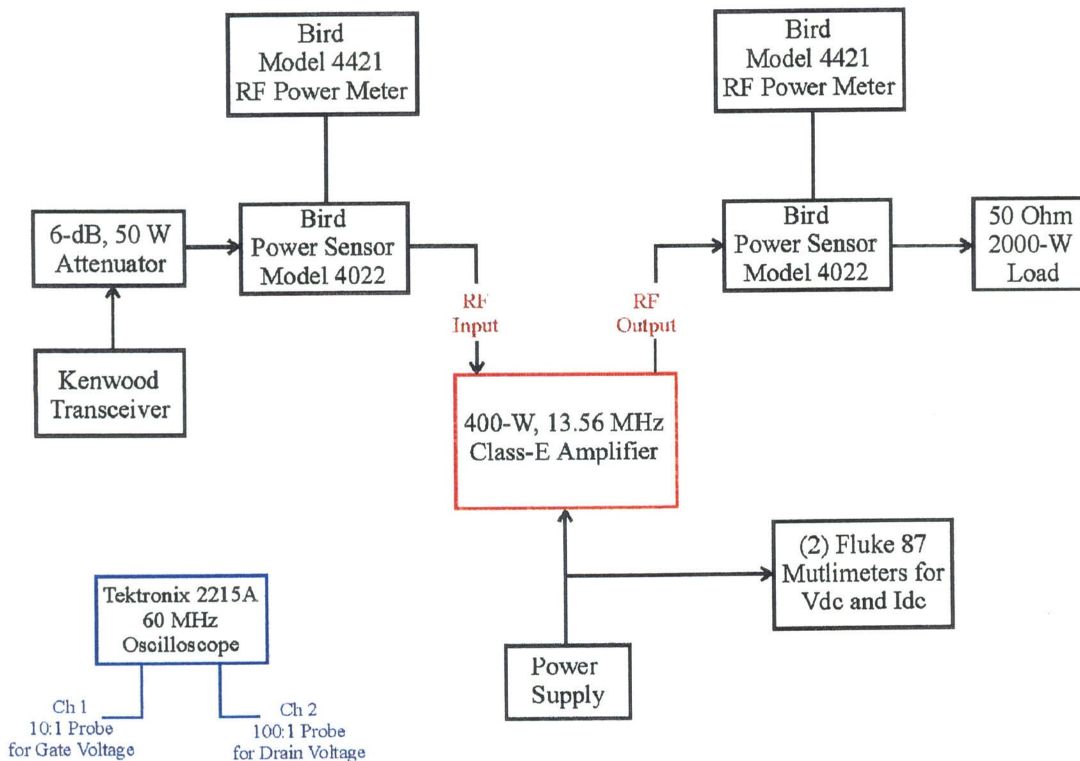

Fig. 3.12. The schematic diagram of the 400-W amplifier measurement setup.

RF input and output power levels are determined using digital power meters made by Bird Electronics. These meters are used in conjunction with RF directional "Thruline" power sensors. Each sensor can handle up to 1200 W of CW power and can simultaneously measure forward and reflected power in 50-Ω coaxial transmission systems. A Kenwood HF transceiver is used as the RF driver to the amplifier. To protect the transceiver from the amplifier's reflected power dur-

ing measurements, a 6 dB attenuator is connected to the Kenwood's RF output connector. A 2-kW oil-filled dummy load receives the 400 W of output power. These key components are shown in Figure 3.13. The remaining components of the measurement setup are exactly the same as described in section 2.4 of Chapter 2.

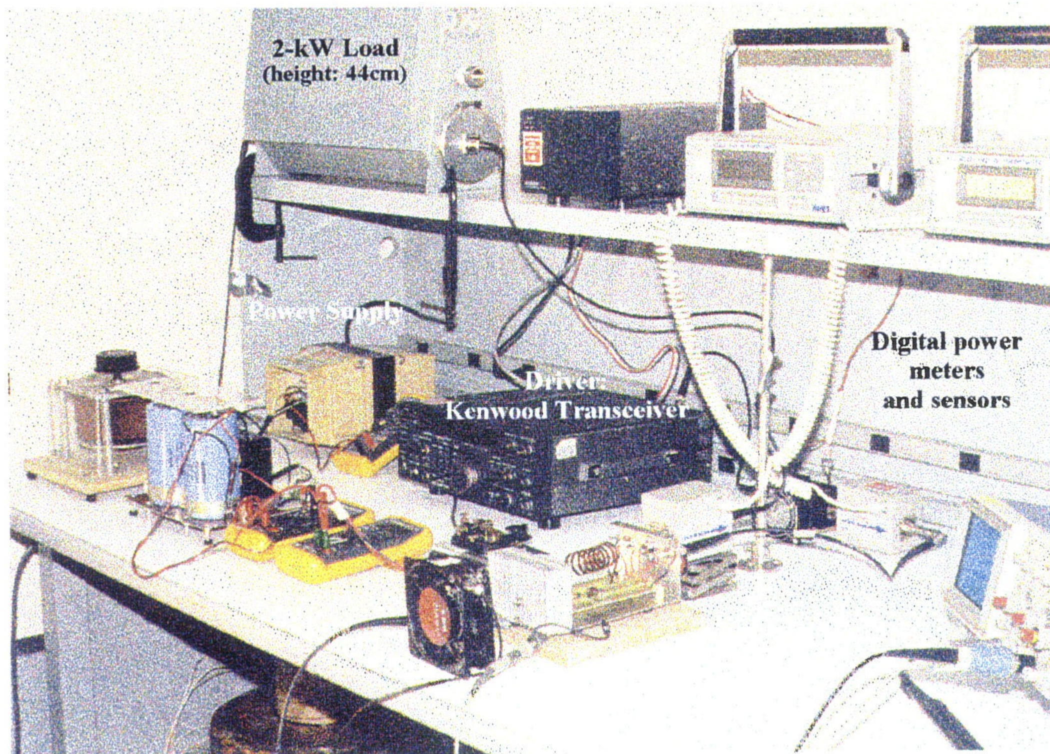

Fig. 3.13. Measurement setup for the 400-W amplifier.

When initially powering the 400-W, air-cooled amplifier, two amplifier coil adjustments are made. First, the standing wave ratio (SWR) is checked with the mesh cover on. Using a plastic tuning tool, the variable inductor, (Lg), is adjusted for minimum SWR with full RF input. If the SWR cannot be brought below 2:1, a turn is added or subtracted from the input transformer (T). With a power meter and a 50-Ω dummy load on the RF output, the output power is set by stretching

or squeezing (Ls) with the cover removed. This, however, is done before the DC input voltage is applied. It should be pointed out that the mesh cover plays an integral role in the adjustment of this series inductance. The cover, when bolted to the chassis, has the effect of reducing the series inductance which results in a noticeable increase in the DC current and a reduction in DC voltage. This translates to a decrease in efficiency. Therefore, to optimize the trade-off between output power and efficiency, the procedure entails making inductor adjustments, bolting the cover in place, and then powering up the amplifier. Stretching the coil reduces the inductance squeezing, reduces the output power, and usually increases the efficiency. Heat removal from the MOSFET is facilitated by blowing cooling air on the fins of the metal heat sink. The gate and drain waveforms are shown in Figure 3.14.

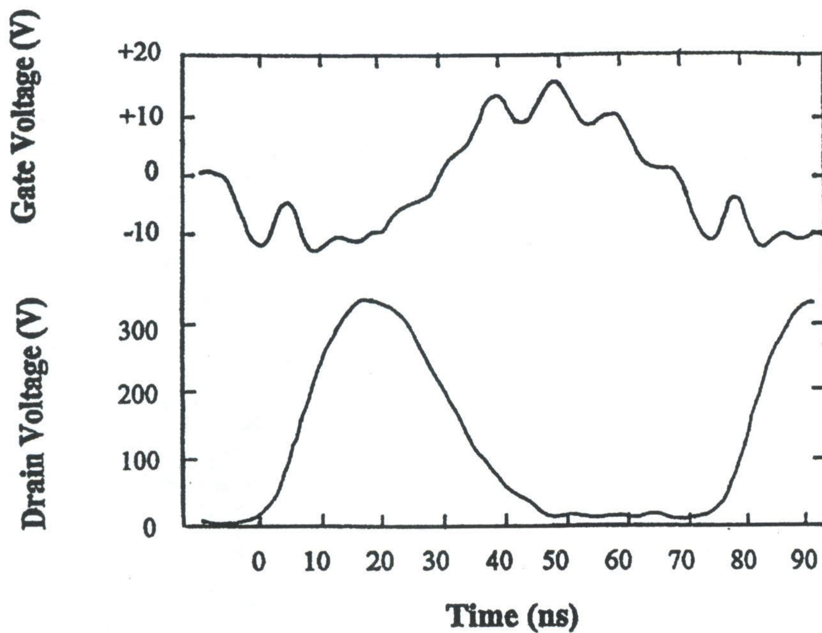

Fig. 3.14. Oscilloscope trace of the measured gate and drain voltage for the 400-W amplifier with 12-W drive. The DC supply is 120 V and the input SWR is 1.6:1. The peak voltage voltage is 14 V, and the peak drain voltage is 350 V, safely within the manufacturer's ratings of 30 V and 500 V.

With high efficiency being a major benefit of the Class-E design, accurate readings of the output power are important. The accuracy of the digital Bird wattmeters is specified by the manufacturer as ±3%, but we have improved this to an accuracy of ±0.5% by using the thermal calibration procedure, described in Chapter 2, on a 2-kW load.

3.4 Experimental Results

In the waveforms for the gate and drain voltage shown above, sine wave drive is again the preferred signal as a means of resonating the gate reactance. The gate curve is again quite bumpy with ringing in the VHF range. We can't see ringing on the drain (output) voltage because the voltage scale is much larger than the scale used for the gate (input) voltage. The ringing is coupled back from the output to the input via the Miller capacitance and source inductance as these are common to the input and output. This coupling is stronger at higher frequencies back to the gate. A drain efficiency of 86% is attained for input powers above 10 W. Higher efficiency is possible by increasing the drive power, but this means the MOSFET must dissipate more energy. Figure 3.15 shows the effect increased drive power has on efficiency for the 400-W amplifier.

Calculation of overall efficiency helps establish a range of drive levels over which heating in the MOSFET can be controlled and decent drain efficiency can be maintained. Input powers between 10–18 W yield an overall efficiency of 81%. For high gain/high efficiency amplfiers, overall efficiency is similar to power-added-efficiency (PAE), which is more common in the microwave community. Without benefit of water-cooling, it is interesting to see how drain efficiency varies with output power. The orange curve in Figure 3.16 shows that high efficiency is maintained over a wide range of powers, 100 W to 400 W, with a constant drive power of 12 W. Dissipated power is the result of adding the RF and DC input powers and subtracting the RF output power from the result. The blue

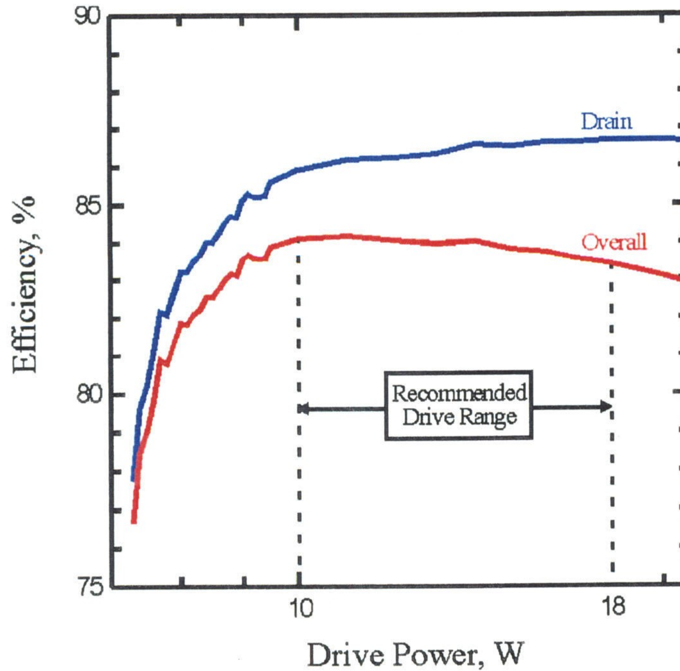

Fig. 3.15. Drain and overall efficiency versus drive power.

curve shows that as the RF output increases, dissipated power increases. This indicates stress on the transistor. However, reducing the output power below 100 W causes efficiency to drop along with the dissipated power. This is different in the Class-A type amplifier where the dissipated power increases as you reduce the output power.

Class-E amplifiers are known to generate harmonics at the switching frequency, but the second is seen to have the largest amplitude not only at the HF frequencies but also in the VHF and UHF bands [5,6]. As previously mentioned, the design of the 400-W amplifier incorporates a filter tuned to the second harmonic. With the resonator in place, the second harmonic falls to –54-dB below the fundamental as shown in Figure 3.17.

The next series of measurements are concerned with understanding power dissipation in the MOSFET, especially since the device is now attached to an air-cooled heat sink. Even with the drive level set to maximize the overall efficiency

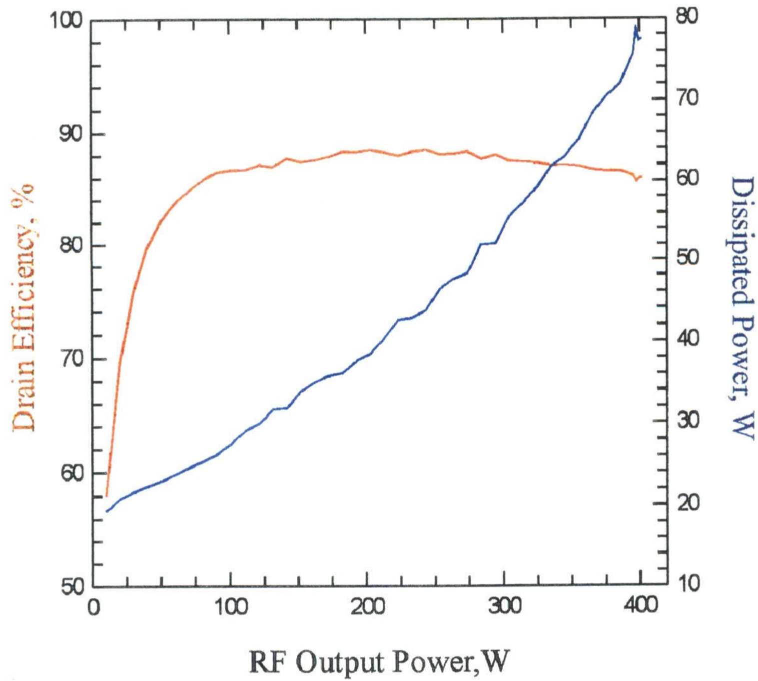

Fig. 3.16. Drain efficiency versus output power.

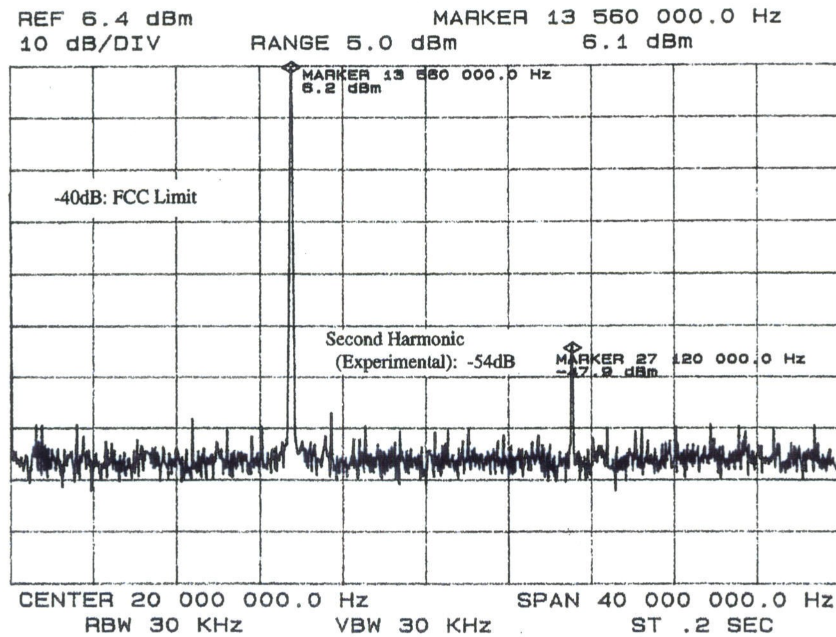

Fig. 3.17. The measured spectrum of the 13.56 MHz Class-E amplifier with the IRFP450LC MOSFET.

while minimizing loss, determination of the transistor junction temperature is an important result. On-resistance of the MOSFET is directly affected by the device temperature. As power dissipated by the device increases, $R_{DS(on)}$ elevates. The procedure outlined in section 2.5 and Figure 2.13 is again followed, with the results shown in the graph below. Note that the curve is linear with a slope of 4.7mΩ/°K. This slope is helpful in finding the IFRP450LC's thermal resistance.

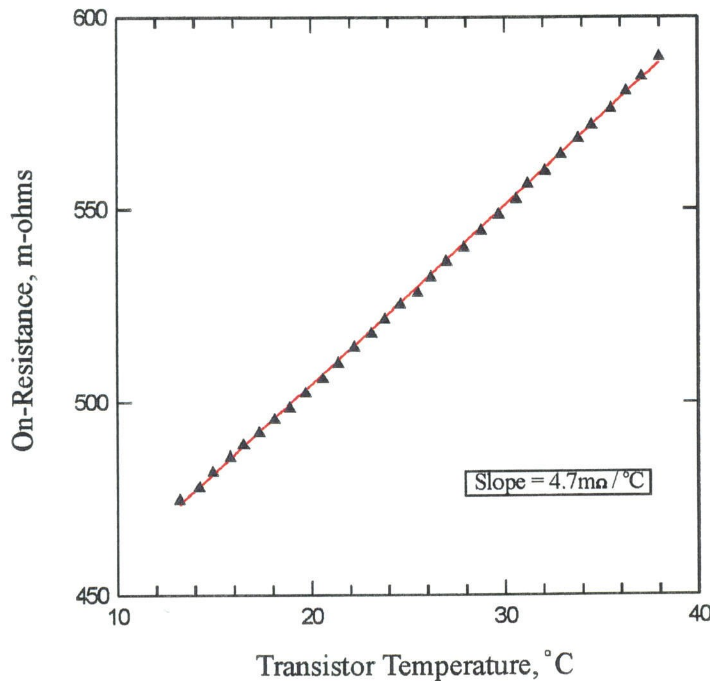

Fig. 3.18. Plot shows the linear relationship between the on-resistance and case temperature.

To determine the junction temperature, we measure the MOSFET's thermal resistance. The results that follow were obtained by Kai-Wai Chiu for a 7-MHz Class-E amplifier using a IRFP450 MOSFET [7]. Figure 3.19 shows the measurement setup. Procedurally, the gate-source voltage is set to 10 V so the device is in full-enhancement. A thermometer is placed between the fins of the heat sink and the temperature rise is recorded. A constant 10 mW of DC power is applied to the drain and the on-resistance, $R_{DS(on)}$, is calculated from the

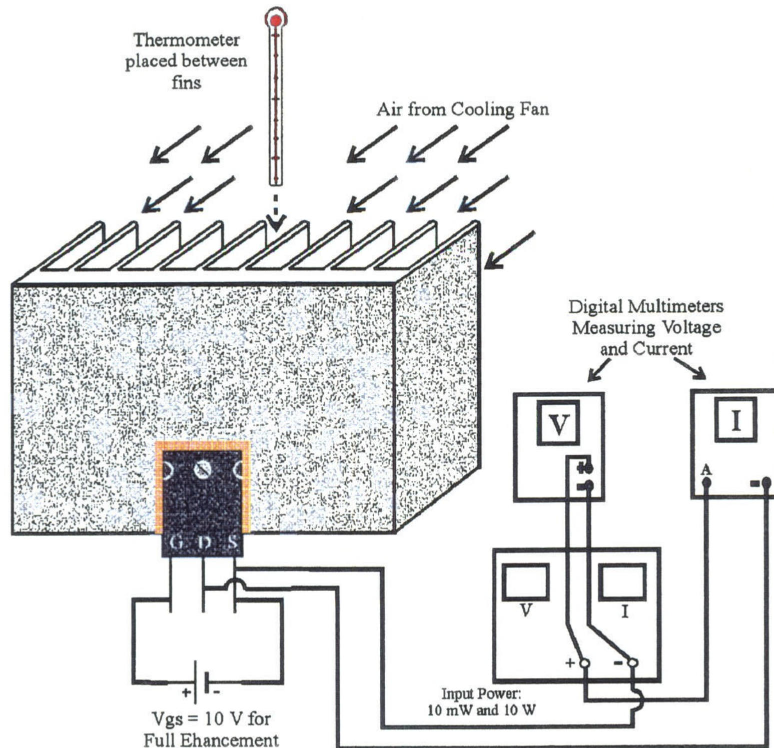

Fig. 3.19. Thermal resistance measurement setup.

voltage and current measurements. This is done to obtain a baseline value for the resistance at ambient temperature using a power level that would not appreciably raise $R_{DS(on)}$. Next, power at the drain is changed to 10 W DC and the drain voltage and current are recorded every minute until no resistance change is noted. The equation for heat sink thermal resistance in K/W is below with ambient temperature taken as 26°C:

$$HeatsinkThermalResistance = \frac{T_{heatsink} - T_{ambient}}{10\,W} \quad (3.11)$$

The thermal resistance of the MOSFET junction is calculated as follows:

$$J_{TR} = \frac{R_{DS(on)} - R_{DS(on,ambient)}}{10\,W}(\frac{K}{4.7m\Omega}) \quad (3.12)$$

Plots of the heat sink and transistor junction temperature rise with and without the cooling fan are shown in Figures 3.20 and 3.21. To explain these curves, we use a thermal model shown in Figure 3.22.

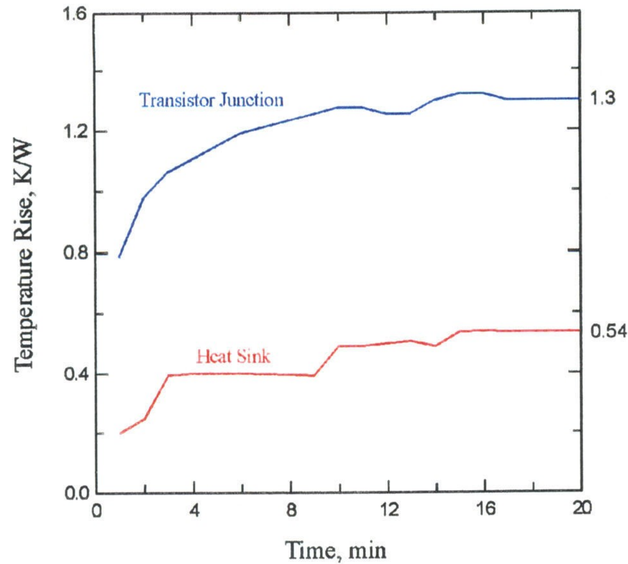

Fig. 3.20. Temperature rise for 1 Watt of power dissipation when fan is used.

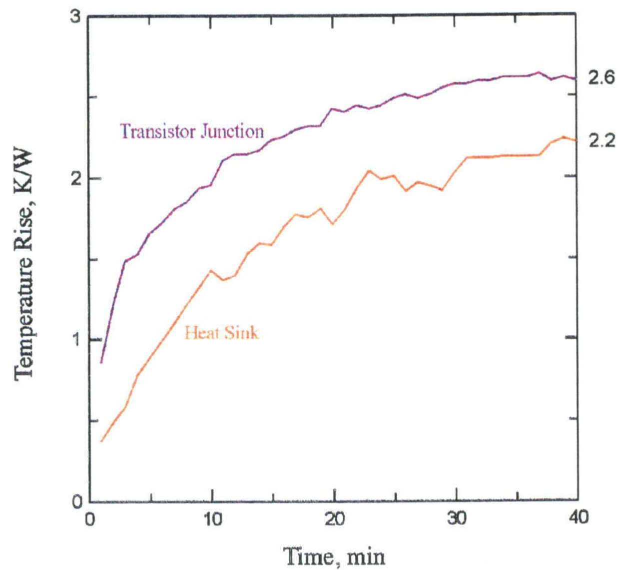

Fig. 3.21. Temperature rise for 1 Watt of power dissipation without cooling fan.

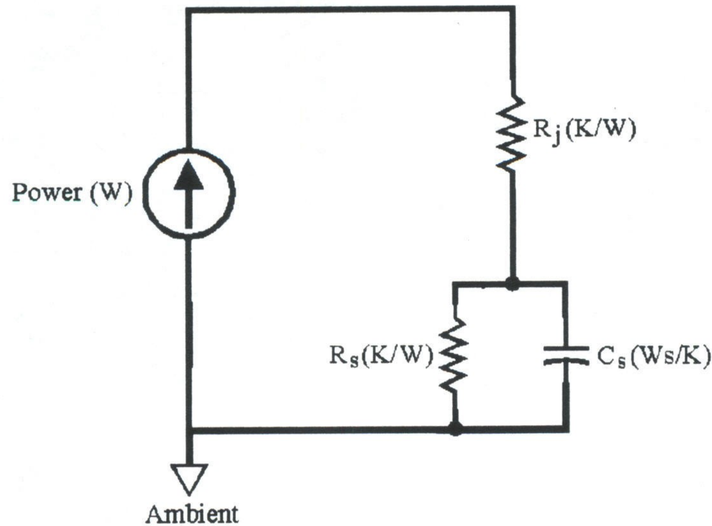

Fig. 3.22. Thermal model of the IRFP450 with heat sink attached.

R_j is the transistor junction-case-pad thermal resistance, R_s is the heat sink thermal resistance and C_s is the heat sink capacitance. The power input to the thermal circuit is modeled as a current source and the temperature rise as the voltage. When a fan is used outside the heat sink, R_s is small and we will neglect it; the final temperature of 1.3 K/W corresponds to R_j. When the fan is removed, a final temperature rise is seen to give an additional increase of 1.3 K/W. Furthermore, the curve is seen to have an exponential shape with a time constant of 14.4 minutes and yields a C_s of 24.8 Ws/K. These results show that operation of the transistor below 80°C means we can operate the amplifier continuously with a fan dissipating 62 W (80.3) from the transistor. Without a fan, the dissipation will be 31 W (80.6). Note the close correlation between the heat sink temperature and the transistor junction temperature.

3.5 Amplifier Simulation

The PSpice model for the 400-W amplifier is shown in Figure 3.23. In the

simulation, all the components are actual measured values. As in the 200-W simulation, the transistor is modeled as a switch with a linear capacitor (Ct) and a nonlinear dependent voltage source (Ect) to model the square-root behavior of the drain-source capacitance. Prediction of the observed ringing frequencies require additional inductors and capacitors to be added. The PSpice netlist is shown in Figure 3.24. A plot of the drain capacitance versus voltage for the IRFP450LC is depicted in Figure 3.25. Again, the measured data fits well to a square root behavior of the drain-source capacitance.

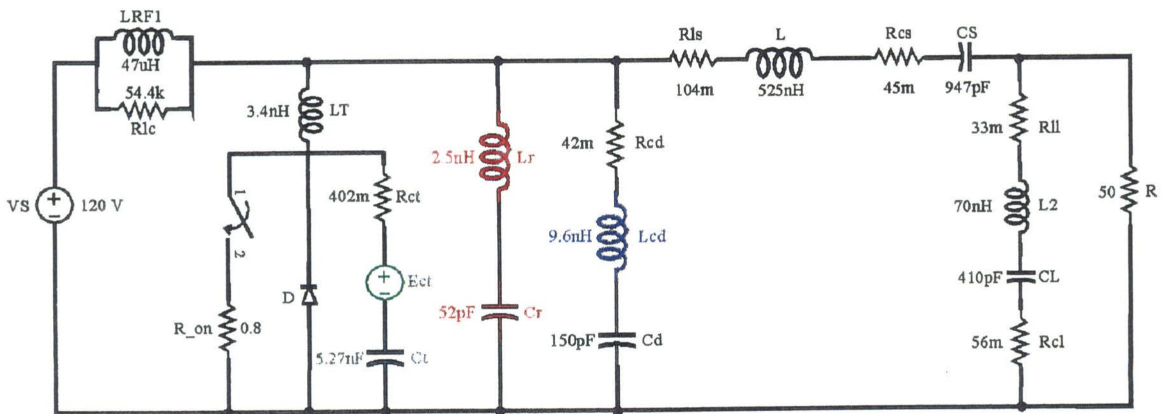

Fig. 3.23. Circuit model on which computer simulation is based.

The drain voltage waveform resulting from the simulation is shown in Figure 3.26 with the measured drain voltage on top for comparison. A performance comparison between the actual data and the simulation is shown in Table 3.1. Note that the power prediction is close to the experimental result.

```
*                    SINGLE-ENDED 13.56MHz CLASS-E POWER AMPLIFIER

VS     1   0   120V    ;   DC source voltage
VG1   12   0   PULSE (0V 1V 0NS 0NS 17NS 28NS 73.75NS)
RG1   12   0   1MEG    ;   high resistance for continuity
LRF1   1   2   47UH    ;   RF choke
Rlc    1   2   54.4K   ;   parasitic resistance parallel to RF choke
LT     2   3   3.4NH   ;   series inductance within transistor

*                                   TRANSISTOR MODEL
Rct    3   4   402M    ;   series resistance of drain-source capacitance
CT     5   0   5.27NF  ;   transistor drain-source capacitance
Ect    4   5   VALUE = {((V(5) + SQRT(V(5)*V(5)))/8)*V(5)*10.32}
D      0   3   DIODE   ;   body-diode internal to IRFP450LC MOSFET
.MODEL  DIODE  D

*                                     LOAD NETWORK

Rcd     2 15    42M     ;   drain capacitor series resistance
LCD    15  6    9.6NH   ;   lead inductance of drain-source capacitor
CD      6  0    150PF   ;   drain capacitor
Lr      2 16    2.5NH   ;   induct.in series with heatsink/pad/MOSFET cap.
Cr     16  0    52PF    ;   heatsink/pad/MOSFET capacitance
Rls     2  7    104M    ;   resistance of series inductance
L       7  8   534NH    ;   series inductance
Rcs     8  9    45M     ;   resistance of series capacitance
CS      9 10   947PF    ;   series capacitance
Rl1    10 13    33M     ;   resistance of series induct. in 2nd harm. res.
L2     13 11   80NH     ;   series inductance used for 2nd harm. resonator
CL     11 14   410PF    ;   capacitance parallel to the load
Rcl    14  0    56M     ;   series resist. of capacitance parallel to load
R      10  0    50      ;   load resistance

*                               SWITCH(TRANSISTOR) MODEL

S1     3   0   12   0   SW1    ;   model for the IRFP450LC
.MODEL SW1 VSWITCH (RON=.8 ROFF=1MEG)

*                                  TRANSIENT ANALYSIS

.TRAN 500PS 10.4US 10US 500PS
.PROBE

.END
```

Fig. 3.24. 400-W Class-E amplifier PSpice netlist.

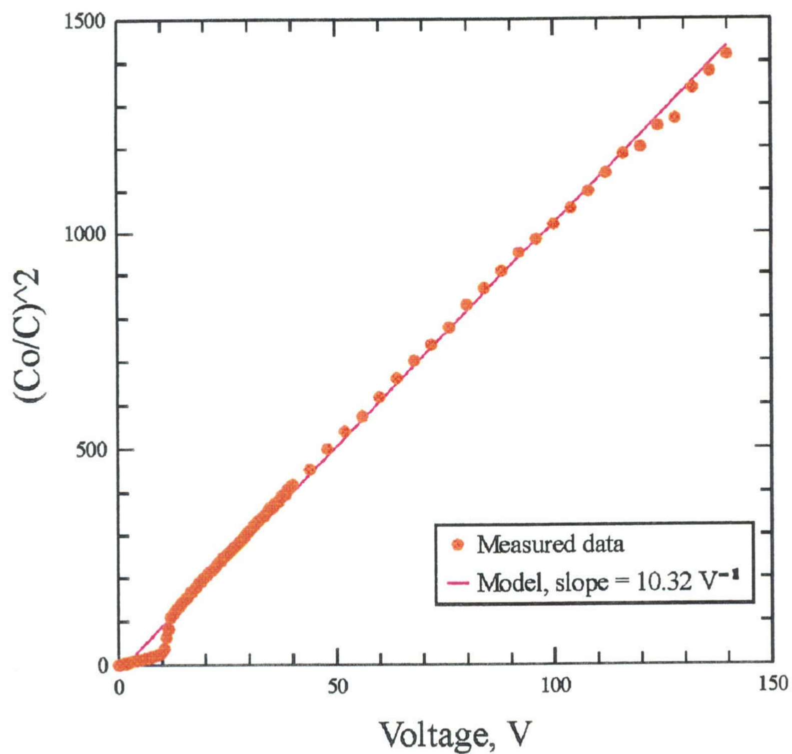

Fig. 3.25. 400-W Theory vs. experiment for the drain-source capacitance.

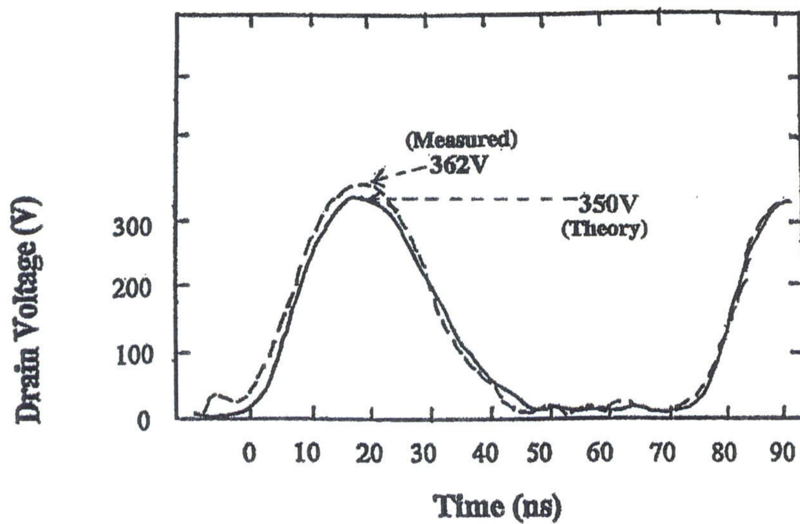

Fig. 3.26. Simulated and experimental drain voltage.

Measurement	Experimental Results	SPICE Model
RF Output Power	400 W	405 W
DC Input Power	468 W	463 W
Drain Efficiency	86%	87%
Peak Drain Voltage	350 V	362 V

Table 3.1. Comparison of the experimental results and SPICE simulation of the 200 W Class-E amplifier with the IRFP440 MOSFET.

The predicted output power spectrum and its comparisons with actual data is shown in Figure 3.27. To simulate the spectrum, it is important to include the parasitic inductance (Lcd) of the drain capacitor (Cd) and the parasitic capacitance (Cr) due to the heat sink, insulating pad, and MOSFET assembly.

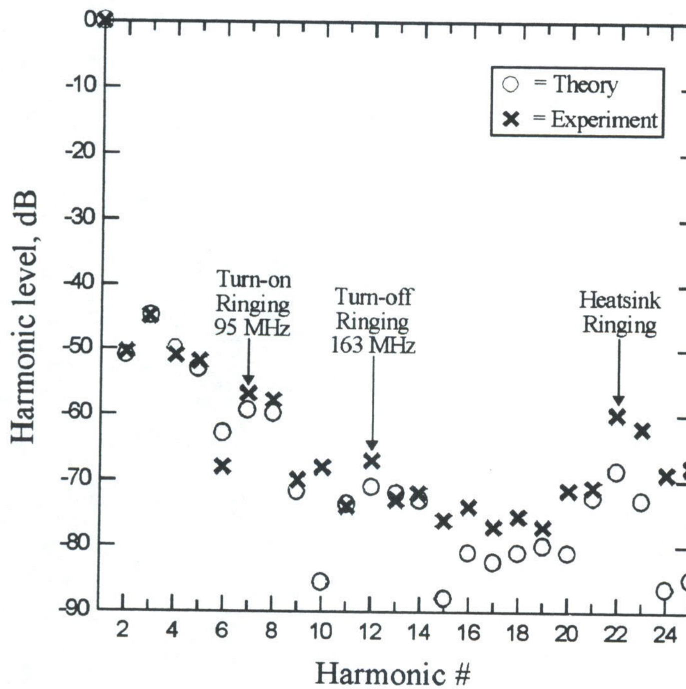

Fig. 3.27. RF output spectrum.

The sum of the inductances (LT) and (Lr) along with (Cr) predicts the resonating frequency at the 22nd harmonic or 298 MHz. Without these additions to the model, the theory predicts much lower harmonics than is observed experimentally. As in the previous amplifier design, some of the VHF harmonics are low enough in frequency to be observed on the oscilloscope. If we examine gate waveform in Figure 3.28, the spacing between the bumps on the positive and negative cycles are directly related to the on and off switching of the MOSFET. Close spacing is associated with high frequency ringing and the wider spacing, low frequency ringing.

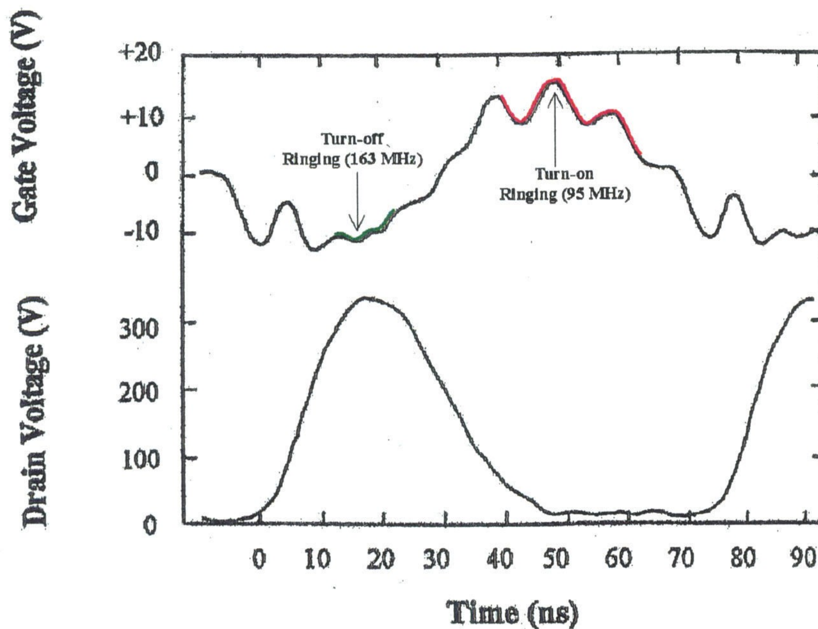

Fig. 3.28. VHF harmonics are seen by examining the gate voltage waveform.

The simple circuit model described in Chapter 2 for the VHF ringing is still applicable here. See Figure 3.29. Note that even though the intrinsic drain capacitance is nonlinear, its effect reduces the total capacitance in the circuit, resulting in a higher resonant frequency.

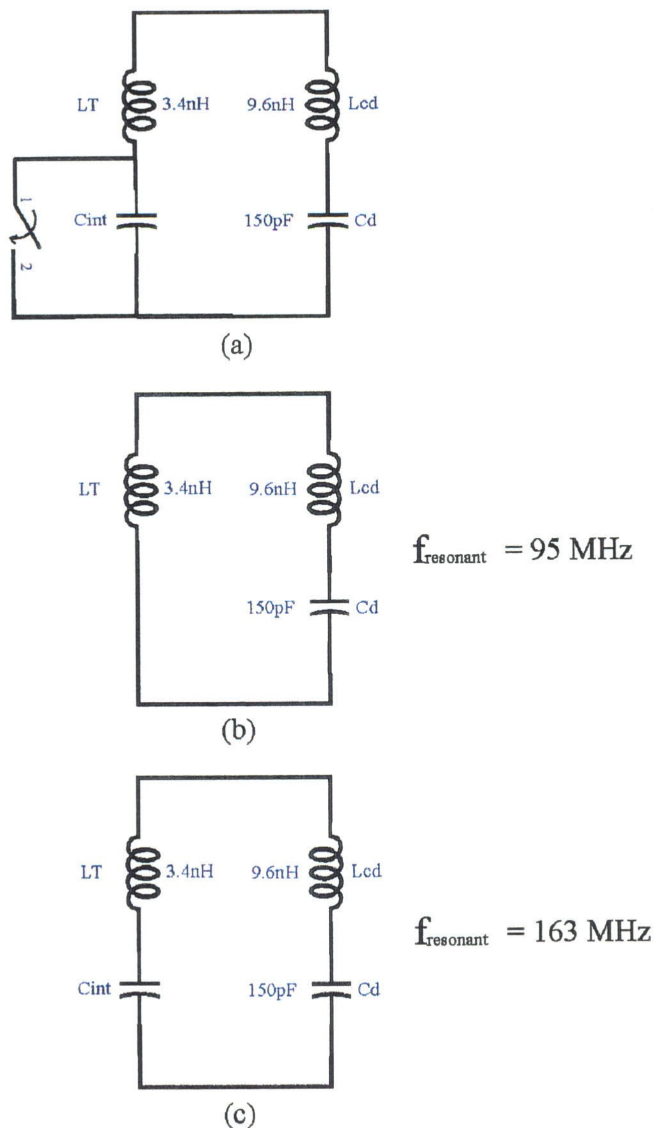

Fig. 3.29. (a) The VHF ringing seen in the spectrum is modeled with a switch, the internal inductor and capacitance of the drain and the external drain capacitance and its parasitic inductance. Ringing circuit when transistor is on (b) and off (c). The resonant frequency is higher when the transistor is off because of the series drain capacitance.

The UHF ringing mentioned earlier is attributed to the capacitance formed by the heat sink-insulating pad-MOSFET combination and the inductances of the source lead and its grounding screw. The capacitance is measured using a L-C-R

meter while the inductance used in the PSpice simulation ia a fitted parameter. To analytically deduce the 298 MHz resonant frequency, the total inductance of (LT) and (Lr) is used. Below is a picture showing how the equivalent circuit is determined.

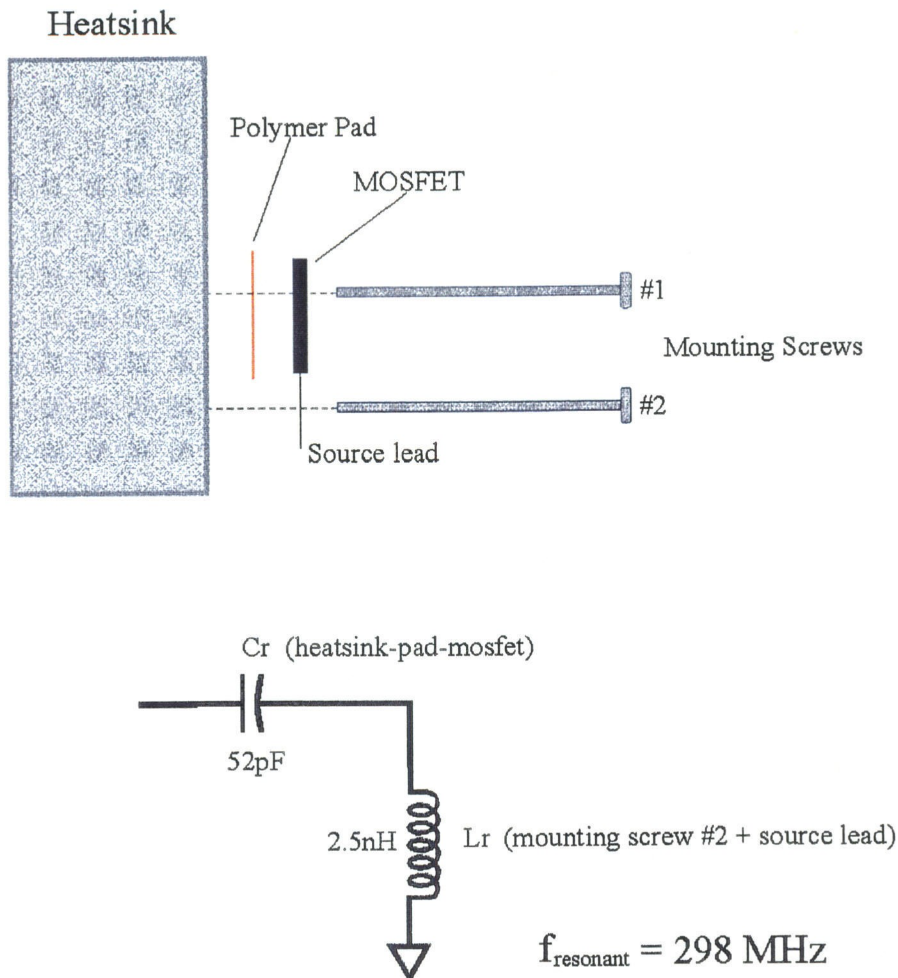

Fig. 3.30. UHF harmonics are prevalent in the RF spectrum but their effect on amplifier performance is minimal.

The final simulation involves component loss calculation. This uses the measured values of the resistances for the inductances and capacitors. Table 3.2 shows the results.

Component	Calculated Losses and Temperature Rise
Capacitors: Cd	0.2 W / 14°C
Cs	2.3 W / 124°C
Cl	2.4 W / 147°C
Total Capacitor Loss	4.9 W

Inductors: Lc	0.3 W
Ls	5.3 W
Ll	1.4 W
Total Inductor Loss	7.0 W

Transistor: Off-Resistance	2.0 W
On-Resistance	30.3 W
Turn-off Loss	12.4 W
Drive Power	12.0 W
Total Transistor Loss	56.7 W

Table 3.2. Calculated component losses. Measured resistances are used in the simulation. Total power loss amounts to about 69 W or 17% of the output power.

A calculation that directly results from the power loss calculations of the capacitors is that of their maximum temperature rise. Equation (2.1) is again used to determine these values. The various mica capacitors used come in different packages with areas of 1.07, 1.29, and 1.13 square inches. The calculated temperature rises are shown in Table 3.2.

The manufacturer's maximum rating for these capacitors is up to 125°C. The above results indicate that the drain capacitor is not driven hard but the series and load capacitors have reached and exceeded their rating. Taking ΔT_{Cl} as the maximum temperature rise, the thermal resistance, R_T, is determined by dividing 147°C by the power lost in Cl. Thus $R_T = 61°C/W$.

3.6. Conclusion

In this chapter, a HF Class-E amplifier that delivers 400 W of continuous power has been presented. This design employs the low-charge power MOSFET, IRFP450LC, which has lower on-resistance and improved switching speed. Sinewave drive aids in resonating the gate reactance of the MOSFET and with the transformer, sets the DC bias to zero volts. A drive power of 12 W was used to attain a drain and overall efficiency of 86% and 84%, respectively. Since this is an air-cooled design, the the MOSFET is operating at a much higher temperature, estimated to be 99°C. Table 3.3 profiles the performance of the 400-W amplifier.

Measurement	Result
V_{ac}	107 V
V_{dc}	120 V
I_{dc}	3.9 A
Calculated $I_{D_{rms}}$ (manufacturer's limit: 14 A)	10 A
Drain Efficiency	86%
Calculated Transistor Loss	57 W
Calculated Junction Temperature (1.3 K/W, 25°C ambient) (manufacturer's limit 150°C)	99°C
Calculated Inductor and Capacitor Loss	12 W
Gate Drive (VSWR 1.6:1)	12 W
Harmonics (3rd)	44 dB

Table 3.3. 400-W Class-E amplifier operation results.

References

[1] C. Davis and W. Via, "Designing a Practical 500 Watt Class-E RF Amplifier," *Proc. RF Technology Expo,* Anaheim, CA, pp. 17–26, March 1990.

[2] N.O. Sokal and K.-L. Chu, "Class-E Power Amplifier Delivers 24 W at 27 MHz, at 89–92% Efficiency, Using One Transistor Costing $0.85," *Proc. RF Expo East,* Tampa, FL, pp. 118–127, October 1993.

[3] J.F Davis and D.B. Rutledge, "A Low-Cost Class-E Power Amplifier with Sine-Wave Drive," *1998 IEEE MTT-S Int. Microwave Symp. Dig. Vol. 2,* pp. 1113–1116, June 1998.

[4] E. Lau, K.-W. Chiu, J. Qin, J.F. Davis, K. Potter, and D.B. Rutledge, "High-Efficiency, Class-E Power Amplifiers," *Part 1, QST*, pp. 39–42, May 1997; *Part 2, QST*, pp. 39–42, June 1997.

[5] H. Zirath and D.B. Rutledge, "An LDMOS VHF Class E Power Amplifier Using a High Q Novel Variable Inductor," *1999 IEEE MTT-S Int. Microwave Symp. Dig. Vol. 1,* pp. 367–370, June 1999.

[6] S. Li, "UHF and X-Band Class-E Amplifiers," Ph.D. Thesis, California Institute of Technology, Pasadena, CA, 1998.

[7] Kai Wai E. Chiu, "A 500-W 7 MHz RTTY Radio Communications System," Bachelor's Thesis, California Institute of Technology, Pasadena, CA, 1997.

Chapter 4

Class-E Amplifier Thermal Study

In the development of RF power amplifiers, thermal management is becoming increasingly important as output power levels increase. Even with high efficiencies attained by Class-E amplifiers, the ability of its key components (transistors, inductors and capacitors) to handle thermal stresses resulting from high output power levels is a concern. Excessive power dissipation generates high temperatures. The work in this chapter is a continuation of the thermal investigations discussed in the previous chapter. Chapter 3 profiled an indirect method to determine component temperatures. Operational temperatures for the MOSFET, capacitors, and inductors were calculated in PSpice in addition to their respective power losses. It was seen from these calculations that the capacitors are thermally stressed and the MOSFET junction temperature hovers at the temperature recommended by most manufacturers. To arrive at this junction temperature, measurement techniques were devised to extract the on- and thermal resistance. In this work, component and junction temperature data is obtained by a direct measurement technique, Infrared (IR) Thermographic Imaging or Thermography. All experimentation is performed using a 400-W, 14.025-MHz Class-E amplifier operated under two conditions: (1) continuous operation with full drive power of 13 Watts and cooling fan at the rear of the heat sink fins and (2) intermittent operation at a 50% duty cycle with no external cooling applied. Though all amplifier components are imaged, those of interest are the capaci-

tors and MOSFET. As previously mentioned, high Q inductors employed in the circuit can withstand high power levels without damage. However, a toroidal inductor used at amplifier's RF input exhibited temperatures as high as 122°C. This might be alleviated by using a larger core size and will be examined at another time. Confidence in the accuracy of these IR measurements is gained by the close agreement between the IR data and the previously calculated results.

4.1 Infrared Thermography

4.1.1 Modes of Heat Transfer

There are three methods by which heat flows from one object to another: conduction, convection, and radiation. In conduction, thermal energy is transferred from molecule to molecule in a solid, heating up each adjacent area in the material [1]. In other words, a temperature gradient exists in the body and energy is transferred from a region of high-temperature to one of low-temperature. The rate of conductive heat transfer is directly proportional to the thermal conductivity of the material [2]. Convection, however, results in a more rapid dissipation of thermal energy because heat is transferred by the movement of a heated cooling agent such as water or air [3]. The third cooling scheme, radiation, is electromagnetic radiation emitted by a body as a result of its temperature and travels directly to its point of absorption at the speed of light [4]. Thermal radiation wavelengths, shown in Figure 4.1, range from the longest infrared rays through the visible light spectrum to the shortest ultraviolet rays [5]. The temperature of the emitting surface controls the intensity and distribution of radiant energy within this spectral range. Total radiant energy emitted by a surface is proportional to the fourth power of its absolute temperature [6]. Most of this emission falls within the infrared or "beyond red" portion of the spectrum and is not visible to the human eye.

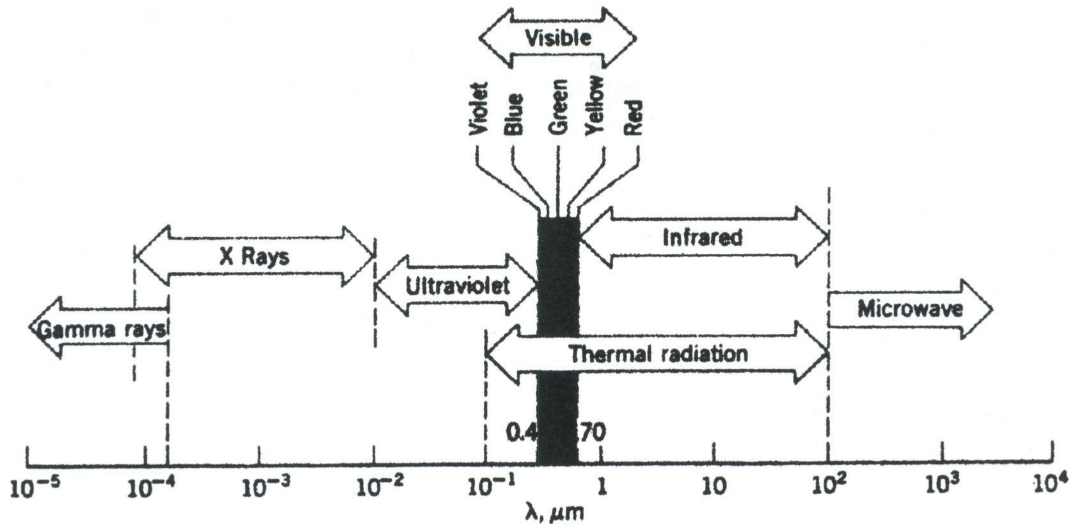

Fig. 4.1. Electromagnetic spectrum [5].

4.1.2 Emissivity and Blackbodies

Electromagnetic radiation is emitted by all materials above absolute zero. For most solid objects, which are opaque to the human eye, part of the IR energy striking the object's surface will be absorbed and part will be reflected. Of the energy absorbed, a portion will be re-emitted and the rest reflected internally. This also applies to objects transparent to the eye, such as glass, but additionally, some of the IR energy will pass through the object. This phenomena is referred to as the emissivity of the material [1]. Emissivity is the ratio of the radiated power of a body to the radiated power of a blackbody at the same temperature [4]. Before proceeding, a brief explanation of the term blackbody is necessary.

When describing the radiation characteristics of real surfaces, it is useful to introduce the concept of a blackbody. The is an ideal surface having the following properties: 1) absorbs all incident radiation, regardless of wavelength and direction, 2) for a prescribed temperature and wavelength, no surface can

emit more energy than a blackbody, and 3) radiation emitted by a blackbody is not only a function of wavelength and temperature, but also of direction (i.e., the blackbody is a diffuse emitter). As the perfect absorber and emitter, a blackbody serves as the standard against which radiative properties of actual surfaces may be compared. Such a perfect radiator has a theoretical emissivity of 1.0. Although closely approximated by some surfaces, it is important to note that no surfaces have precisely the properties of a blackbody [5].

The closest approximation to a blackbody is an IR opaque cavity, shown in Figure 4.2, that is very large in comparison to the opening in its side. Multiple reflections of an incident ray of energy, on its blackened interior, results in a drastic reduction of the ray's energy. Practically none of the radiation entering the hole escapes [4]. The inner surface of such a structure would have an emissivity of 0.998 [1].

Highly polished surfaces will reflect a majority of incident IR energy. Thus, surface characteristics of a material have a direct influence on its emissivity. This

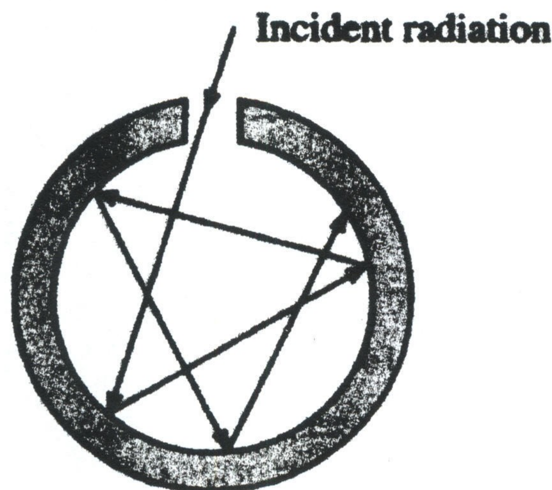

Fig. 4.2. The blackened interior of the enclosure approximates a blackbody.

becomes significant when attempting temperature measurement of low emissive, infrared opaque materials. For example, a highly polished piece of stainless steel will have a much lower emissivity than the same piece with a rough, machined surface because grooves in the rough material prevent much of the IR energy from being reflected [1]. Covering the surface with a high emissivity paint, like lamp-black, will enhance its ability to either absorb incident light or radiate thermal energy [6]. This will have a positive impact when doing thermal measurements.

4.1.3 Temperature Measurement

Thermography uses specially designed infrared video or still cameras to make images (called thermograms) that show surface heat variations [1]. One of the many applications of thermograms is in the detection of abnormally hot electrical connections or components in electrical systems. The standard against which radiative properties of actual surfaces are compared is the blackbody. The basic laws on which thermography is based are blackbody radiation laws. Spectral distribution of blackbody radiation is expressed by Planck's distribution law. This law describes the intensity of radiation emitted by the unit surface area into a fixed direction (solid angle) from the blackbody as a function of wavelength for a fixed temperature:

$$E(\lambda, T) = \frac{2\pi hc^2}{\lambda^5[\exp(hc/\lambda kT) - 1]} \tag{4.1}$$

where

$E(\lambda, T)$ = blackbody emissive power (W/m^2·μm)

h = Planck's constant (6.6256×10^{-34} W·sec^2)

k = Boltzmann's constant (1.3805×10^{-23} W·sec/K)

$$c = \text{speed of light in vacuum } (2.998 \times 10^8 \,\text{m/sec})$$

$$T = \text{absolute temperature (K)}$$

$$\lambda = \text{wavelength (m)}$$

Total radiant-heat energy emitted from a blackbody in all directions over all wavelengths is found by integrating (4.1) over all wavelengths:

$$E(T) = \int_0^\infty E(\lambda, T)\, d\lambda = \sigma T^4 \tag{4.2}$$

where

$$\sigma = \text{Stefan-Boltzmann's constant } (5.670 \times 10^{-8}\,\text{W/m}^2 \cdot \text{K}^4)\ [5].$$

By incorporating these principles, thermal infrared imagers translate energy transmitted at infrared wavelengths into data that can be processed into a visible light spectrum video display. Recall that visible light is dependent on a source of light (the sun or artificial) reflecting off an object to be received by our eyes. Since all objects above 0 K emit thermal infrared energy, the detector and lens combinations of thermal imagers can passively see all objects regardless of ambient light. Imagers commonly used in industrial and medical applications are the "radiometric" type and are designed to give actual temperature measurement of the scene along with a color video presentation [1].

4.2 Thermal Measurement Setup

Thermal measurements of the amplifier components are performed using the Inframetrics ThermaCam ^{TM} PM290 infrared imaging system. The ThermaCam incorporates a 256×256 platinum silicide focal plane array (FPA) detector with full-screen temperature measurement and analysis capabilities. This detector system requires cooling to cryogenic temperatures for peak performance. When the camera is initially turned on, a closed-cycle microcooler module inside the camera cools the detector to 77 K after 8 minutes. Data is stored on a removable solid-state Flash memory card that holds up to 10 MB of data. Images are displayed on a color LCD viewfinder and can be output as standard video. Figures 4.3 and 4.4 show the ThermaCam and main keypad [7].

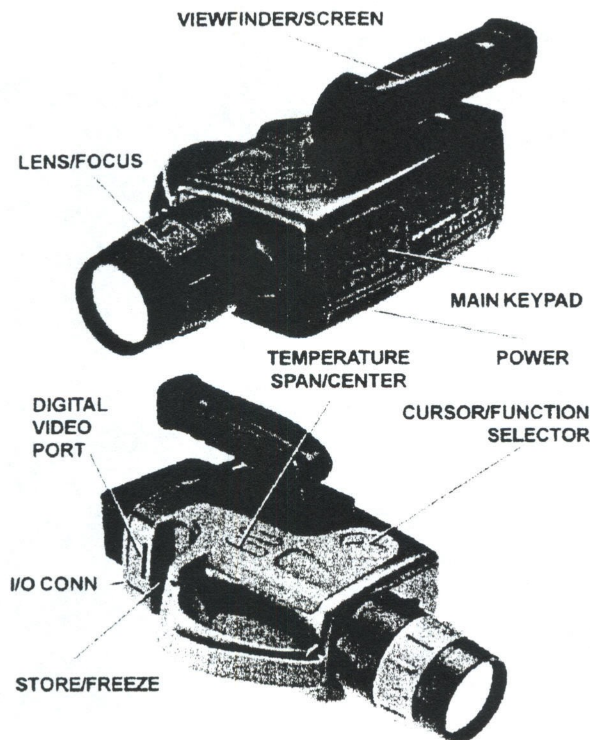

Fig. 4.3. Operating controls and indicators of the ThermaCam imaging system.

Fig. 4.4. All ThermaCam controls are situated on the main keypad.

Prior to taking thermal images, the ThermaCam is calibrated to the target (amplifier). First, permit the entire amplifier to reach thermal equilibrium (room temperature) with its surroundings. External background heating and reflections are minimized by covering all windows near the work area to block sunlight, dimming lights in the lab, and placing an enclosure made of microwave absorber (cones facing outward) around the amplifier, shown below.

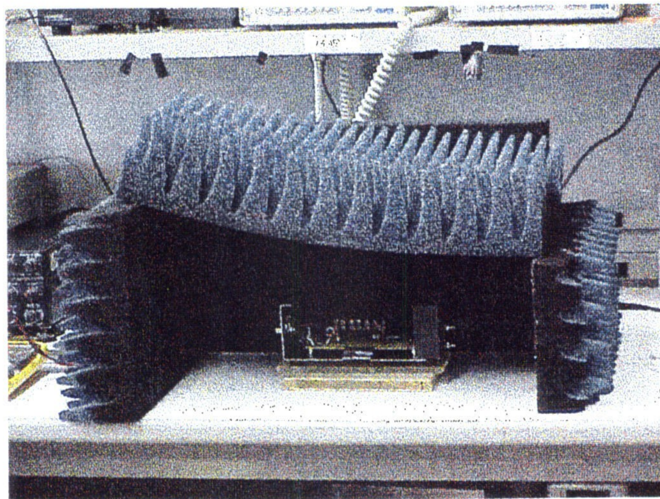

Fig. 4.5. Amplifier inside microwave absorber enclosure.

Next emissivities (ϵ) of the unknown targets are determined:

1) Place a target of known emissivity next to or on a target of unknown emissivity (Class-E amplifier). Black electrical tape, with a known emissivity of 0.95, is used as the measurement standard. Highly reflective surfaces such as the amplifier chassis, heat sink, and metal fittings are painted with a thin coating of flat black, heat resistant paint or covered with black electrical tape to minimize reflections and to give the surface an emissivity close to the tape. Figure 4.6 shows the amplifier prepared for thermal measurements. It should be pointed out that some black coatings contain metal flakes which give the painted surface an emissivity less than 0.95.

2) Set the camera in SPOT Mode to read temperature at a specific location on the image. Use the cursor buttons to move the crosshairs to the known target (black tape), set the emissivity to 0.95, and read the temperature in the view finder. Figure 4.7 depicts what the ThermaCam operator sees in SPOT mode.

3) Set the crosshairs on an unknown target and adjust the + and - ϵ key to match the temperature of the unknown target to that of the known target in step 2. Emissivity of the unknown is read in the epsilon window of the viewfinder [7]. A compilation of emissivities for each of the amplifier's major components is shown in Table 4.1. It should be noted that components with low emissivity (RF choke, series inductor, π-filter toroid) are partially covered with black electrical tape to enhance their thermal emission.

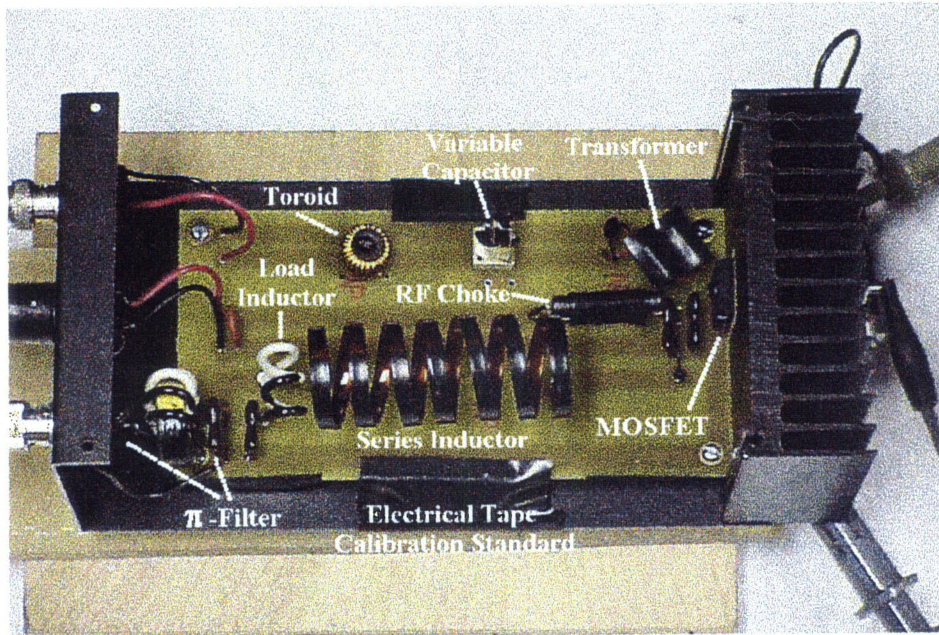

Fig. 4.6. Amplifier components are painted black or covered with black tape for thermograms.

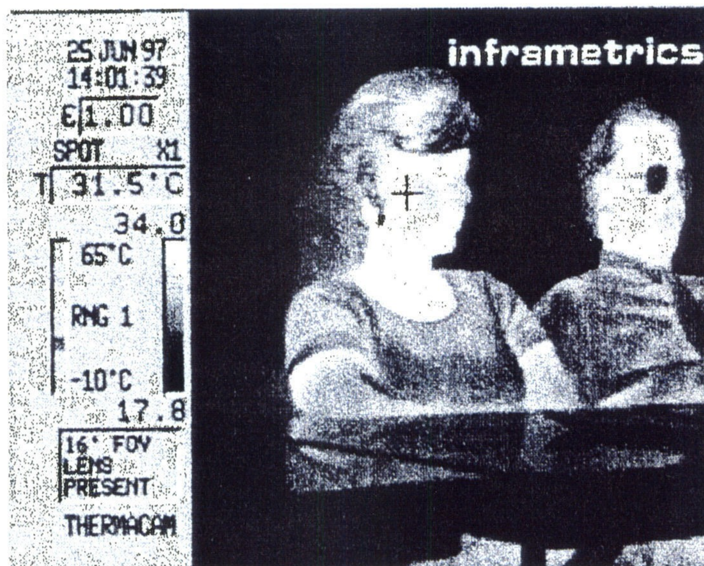

Fig. 4.7. ThermaCam in SPOT mode.

Component	Emissivity (ϵ)
MOSFET	0.95
C_d	0.91
C_s	0.91
RFC	0.95
L_s	0.95
L_l	0.95
C_l	0.91
$C_{\pi 1}$	0.91
L_π	0.94
$C_{\pi 2}$	0.91
Transformer	0.95
C_{var}	0.95
Toroid	0.95
Inverter Cap	0.95
Heat sink	0.95

Table 4.1. Emissivity calibration table. Temperature of the black tape (ambient) is 23.3°C with $\epsilon = 0.95$.

4.3 Experimental Results

As previously mentioned, component thermal measurements are taken using a 400-W Class-E amplifier operating at 14.025 MHz. This frequency is also part of the U.S. Amateur Radio operating band of 20 meters. Since 14.025 MHz is within the 3-dB bandwidth of the 13.56-MHz amplifier described in prior chapters, changes in component values are minimal. However, in order to improve

input matching to the gate and minimize spurious frequencies, circuitry has been changed to include a series inductor/variable capacitor combination and an inverter capacitor. At the output, a π-filter is inserted after the second harmonic trap to further reduce frequencies beyond the second harmonic. Modifications at the input and output employ toroidal inductors. The amplifier is operated under two scenarios: 1) continuous RF output (CW) with a cooling fan at the rear of the heat sink and 2) an automatically keyed, reduced duty cycle operation to mimic an amateur radio transmitter. No cooling fan is used for the keyed operation. Nominal amplifier operation parameters are: V_{DC} = 125 V, I_{DC} = 3.87 A, Input Power = 13.3 W, and SWR = 1.06.

In both situations the emissivities profiled in Table 4.1 are used and the mesh cover is removed to facilitate measurements. Static thermal images stored in the PCMCIA ImageBank memory card are analyzed using the TherMonitor ^{TM} software package sold by Inframetrics. This is a Windows program that displays the images using a wide range of pseudo-color palettes and incorporates a range of tools. Some of them include: Spot temperature tools to display the temperature at a pont in the image, Isotherm tools to color areas of the image lying in a defined temperature band, and Polygon tools to draw a region around the object so that the maximum, minimum and mean temperatures can be displayed [7]. Spot temperature and polygon tools are employed for examination of the recorded images.

4.3.1 CW Operation

Figure 4.8 shows the thermal measurement setup for CW operation. A cooling fan is placed approximately 3 inches behind the heat sink. After powering up the amplifier, the MOSFET is thermally imaged until it reaches a stabilized operating temperature. The following figures are thermograms of the 400-W amplifier components. Figure 4.14 is a schematic of the 14.025-MHz amplifier

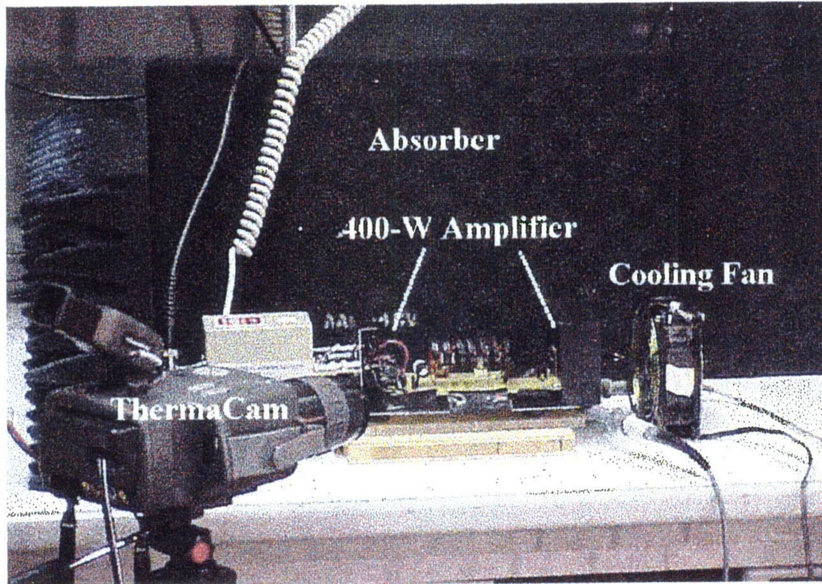

Fig. 4.8. Continuous RF output thermal measurement setup.

showing component temperature measurements.

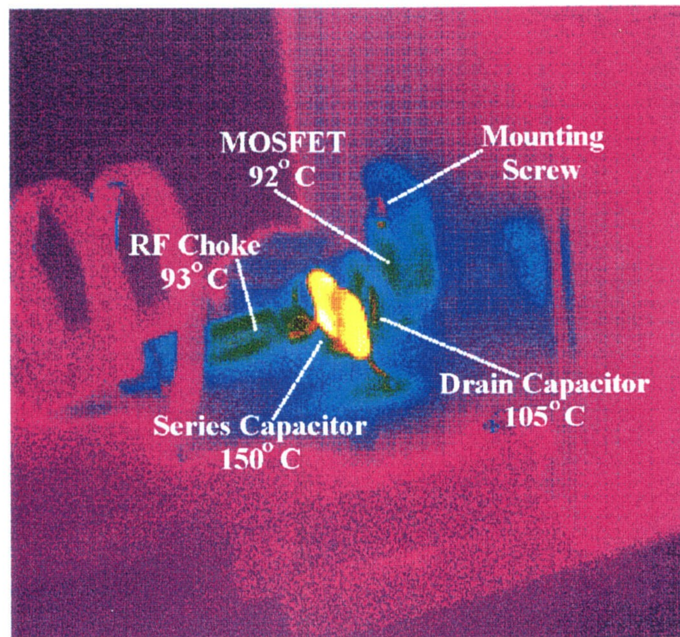

Fig. 4.9. The MOSFET thermogram reveals location of the integrated circuit die.

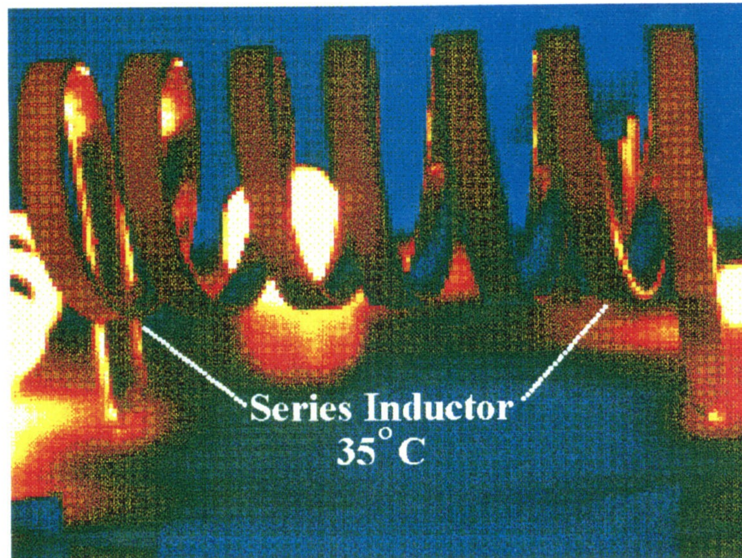

Fig. 4.10. Copper's conductivity in the series inductor has an impact on the resulting low temperature.

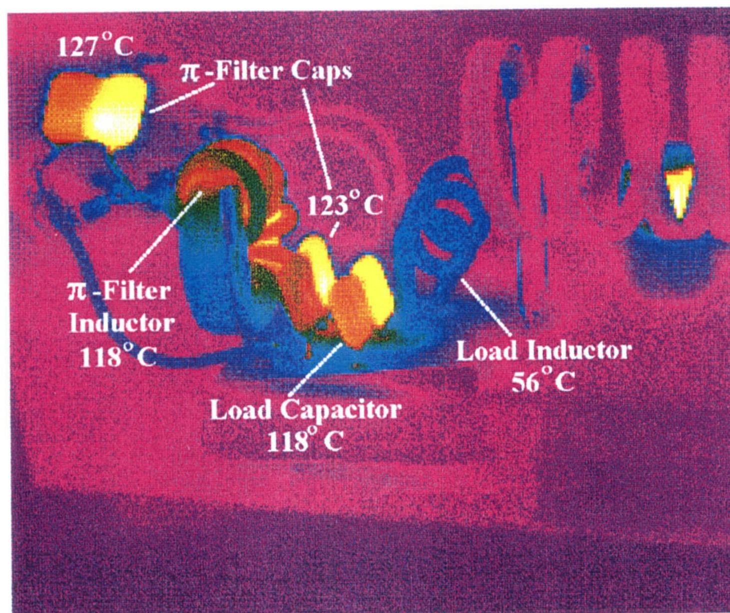

Fig. 4.11. Thermogram of second harmonic trap and π-filter.

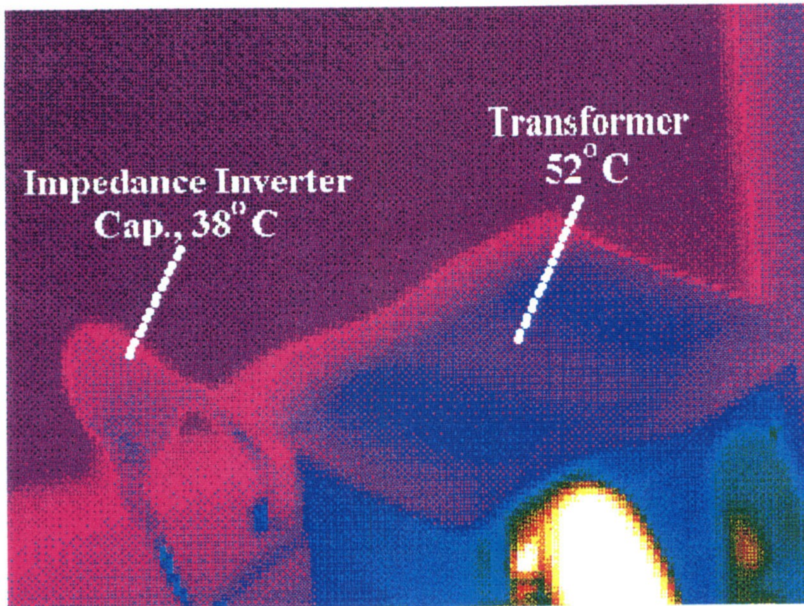

Fig. 4.12. With a drive power of 13 W, the transformer and inverting capacitor are relatively cool.

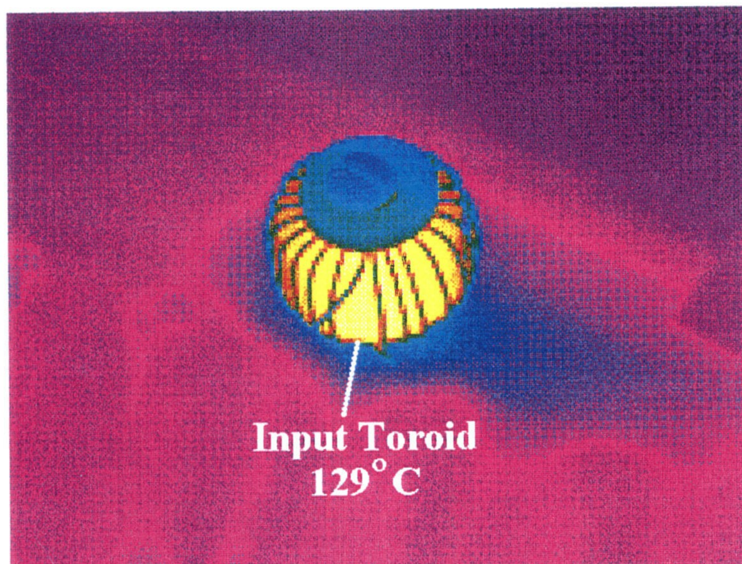

Fig. 4.13. The T51-6B toroid core gets quite hot. A larger diameter core will take its place.

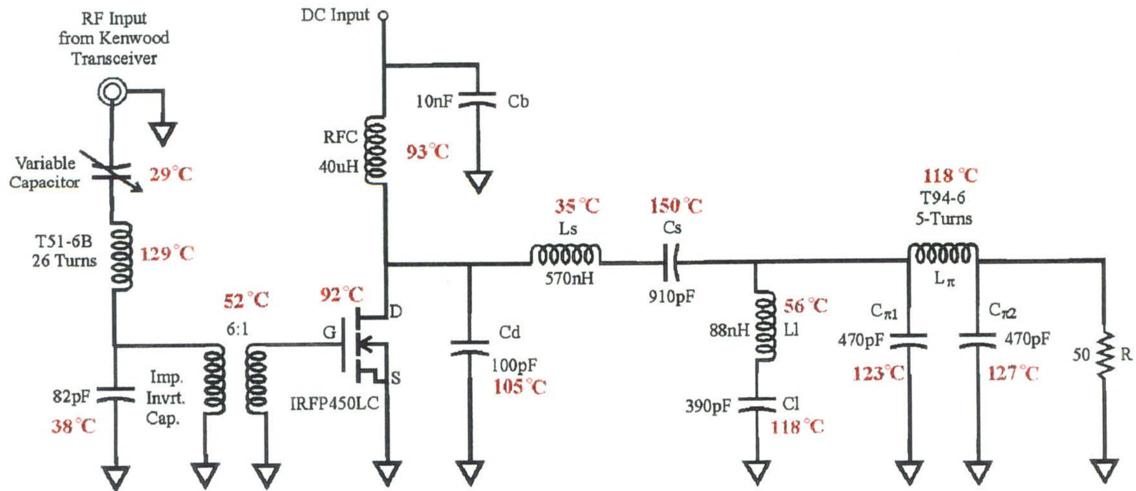

Fig. 4.14. Schematic diagram reflects component temperatures under CW operating conditions.

In examining the component temperatures, new power loss calculations are compared to the PSpice results in Chapter 3. For the MOSFET, power loss is determined by using the 1.3K/W thermal resistance from Chapter 3 and taking the temperature of the imaged region (92°C) as that of the junction. With an ambient temperature of 23.3°C, 53 W or 13% of the output power is lost in the transistor. This is close to the PSpice result of 57 W done previously. Note that manufacturers will run power MOSFETs at 100°C with a limit of 150°C. Other loss comparisons involving the capacitors are done by finding the maximum temperature rise above ambient and substituting this into equation (2.1), $T = 69P/A$, to calculate the power dissipated. The results are shown in Table 4.2. Not included in the table are the 470 pF π-filter capacitors. However, the temperature rise and dissipated power for $C_{\pi 1}$ and $C_{\pi 2}$ are 100°C/1.3 W and 104°C/1.4 W respectively. With a maximum temperature rating of 125°C, the series capacitor is thermally stressed enough to exceed this limit while the π-filter caps are not far from it.

Component	IR-based Losses, Temperature Rise, and Simulated Losses
Capacitors: Cd	1.3 W / 82°C / 0.2 W
Cs	2.4 W / 127°C / 2.3 W
Cl	1.5 W / 95°C / 2.4 W
Total Capacitor Loss	5.2 W vs. 4.9 W

Table 4.2. Load network capacitor losses compared. Ambient Temperature is 23.3°C.

4.3.2 Keyed Operation

In this set of measurements the amplifier is functionally set up to mimic a "keyed" transmitter as would be seen in an amateur radio communication set up [8]. With this intermittent operation, the components should have less opportunity to exhibit the thermal stresses experienced in the previous section. Thus, no cooling fan is used. The measurement setup is similar to that shown in Figure 4.8 with the exception of a HP 33120A function generator connected to the Kenwood transceiver to facilitate keying of the drive signal. This is shown below. The function generator settings are: 2.5-V_{pp}, 20-Hz square wave with a 50% duty cycle and 1.25-V_{DC} offset.

Fig. 4.15. A function generator with the driver delivers a keying signal to the amplifier.

Using the emissivities shown from Table 4.1, component temperatures are shown in the schematic below.

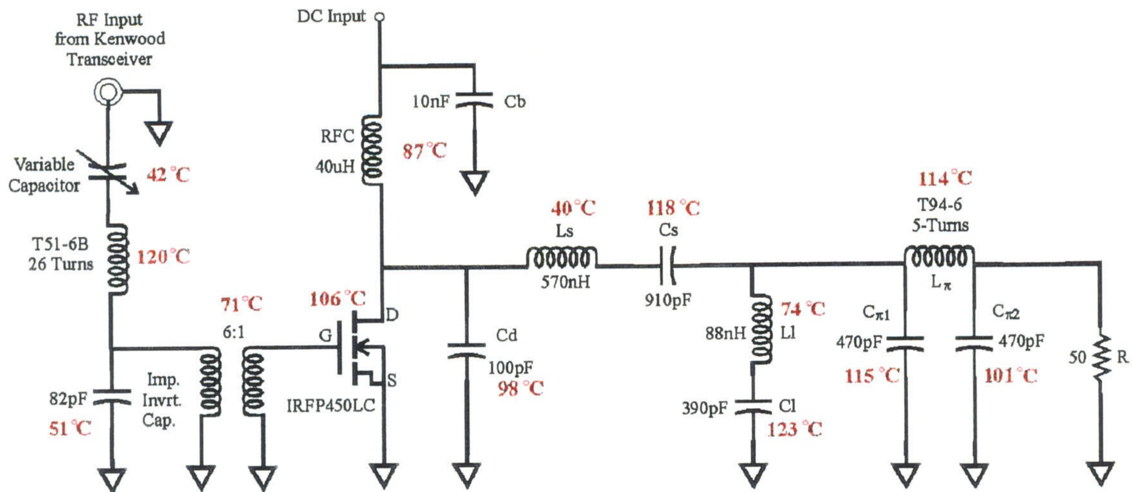

Fig. 4.16. Component temperatures of the keyed amplifier.

Thermograms from which this data is extracted are shown in the subsequent figures.

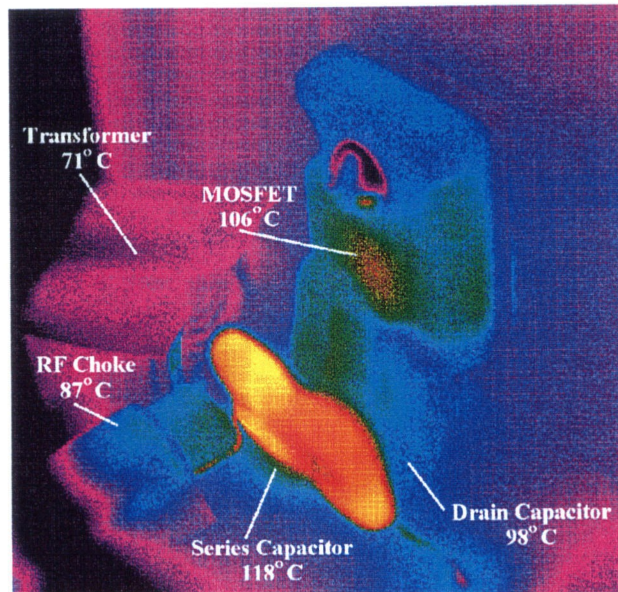

Fig. 4.17. Location of the MOSFET die is clearly revealed in the thermogram.

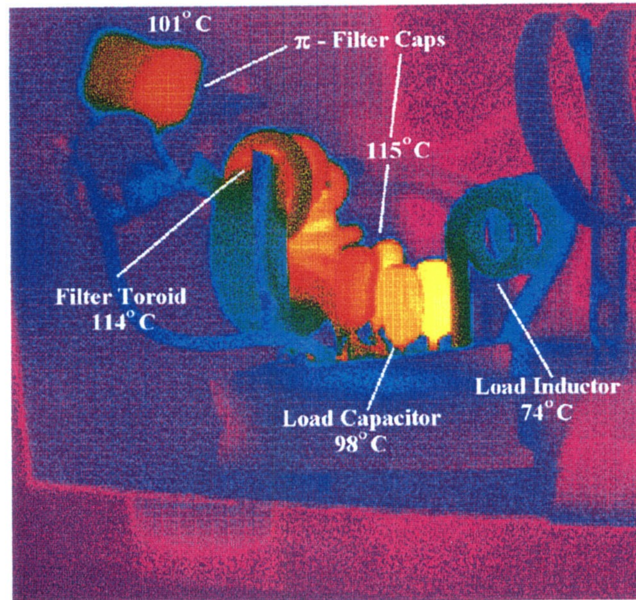

Fig. 4.18. Thermogram shows the π-filter and second harmonic trap components.

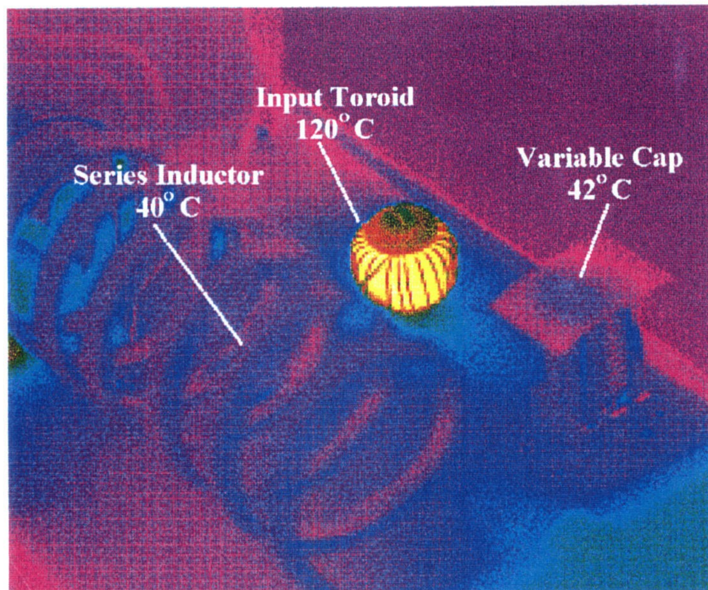

Fig. 4.19. Not shown is the inverter cap with measured temp. of 71°C.

Component	IR-based Losses and Temperature Rise
Capacitors: Cd	1.2 W / 75°C
Cs	1.8 W / 95°C
Cl	1.6 W / 100°C
$C\pi1$	1.2 W / 92°C
$C\pi2$	1.0 W / 78°C
Total Capacitor Loss	6.8 W

Table 4.3. Comparison of load network capacitor losses. Ambient temperature used is 23.3°C. Manufacturer's maximum rating is up to 125°C.

To determine the MOSFET junction temperature, a 2.6 K/W junction-case-pad thermal resistance from Chapter 3 is used. Power dissipation is found to be 32 W and corresponds to a temperature rise of 83°C. In Figure 4.17, the imaged temperature of 106°C corresponds to the MOSFET junction temperature and is well within device operational limits. Table 4.3 reflects the power dissipated in the load network capacitances. Note that the capacitors are well within thermal operating limits and results from the keyed-drive operation of the amplifier.

4.3.3 Capacitor Focus

While the keyed operation of the amplifier yielded more desirable thermal results, it is the continuous RF output mode that places more stress on the amplifier; particularly the capacitors. These stresses relate to either thermal management or peak voltage issues. To examine which of these stresses dominates, the amplifier is tested by replacing the original capacitor values in the load network first with their parallel equivalents and then series equivalents. A parallel combination has the effect of reducing the total component resistance and

subsequent heating effect. Since continuous operation also results in sustained high voltage levels across the component, the series combination should promote a reduction in the peak voltage across the components. While different capacitance values are combined to form parallel or series equivalents, it is important to know how each component is behaving thermally. At this frequency of operation, the losses in the capacitors are primarily ohmic and related to the internal series resistance. Also, power dissipation among the capacitors in series or parallel is disproportionate due to differences in their respective internal series resistance. The loss component for each capacitor is measured using the HP4194A impedance analyzer and will be used in conjunction with the imaged temperature to extract the power dissipated in a given capacitor. Additionally, case dimensions of each capacitor are used in this calculation. In the subsequent paragraphs, items examined for comparison are: 1) imaged temperature, 2) component temperature rise, 3) total power dissipated, and 4) component thermal stress as it relates to the manufacturer's thermal limit. Finally the thermal performance of Porcelain capacitors are examined for their potential use in high power Class-E amplifiers, performance. In doing theses measurements, the amplifier is operated under similar conditions as described in section 4.3.1 with a device temperature maintained at approximately 90°C.

Parallel Combination

The first set of measurements focuses on replacing capacitors in the load network with their parallel equivalents. Candidates for this are ones that are either close to or have exceeded the manufacturer's temperature limit: Cs, Cl and $C\pi 2$ shown in Figure 4.14. Since capacitors in the π-filter are identical, $C\pi 2$ is chosen for its ease of removal from the circuit. Each capacitor combination is thermally imaged under said operating conditions. Power dissipated in individual capacitors is determined by scaling the temperature rise of the combination. This

Component	Parallel Combination (pF)	Maximum Temperature Rise (new / previous)	Total Power Dissipation (new / previous)
Cs	680 / 220 (60°C) (39°C)	60°C / 127°C	1.3 W / 2.4 W
Cl	150 / 220 (3.4°C) (72°C)	72°C / 95°C	1.1 W / 1.5 W
$C\pi 2$	150 / 330 (9.0°C) (26°C)	26°C / 104°C	0.45 W / 1.4 W

Table 4.4. Parallel capacitor combination thermal results. Ambient temperature is 23.3°C.

is done by using the ratio of measured series resistances of the capacitors to find the percentage temperature rise associated with a given capacitor in the combination. For parallel combinations, higher temperature corresponds to a smaller resistance value. Power dissipation is calculated by solving for P in equation (2.1), $T = 69P/A$, where A is the case area in square inches. Results are shown in Table 4.4. In the second column, capacitance values are accompanied by their extracted temperatures.

From the table, it can be seen that using parallel equivalents not only results in lower operational temperatures, but the thermal stresses on individual capacitors is well below the manufacturer's maximum rating. With this combination, component Q is enhanced due to a smaller series resistance and this means cooler operation.

Component	Series Combination (pF)	Maximum Temperature Rise (new / previous)	Total Power Dissipation (new / previous)
Cs	2000 / 1500 (95°C) (84°C)	95°C / 127°C	2.8 W / 2.4 W
Cl	680 / 910 (99°C) (54°C)	99°C / 95°C	1.9 W / 1.5 W
Cπ2	1500 / 680 (40°C) (67°C)	67°C / 104°C	1.4 W / 1.4 W

Table 4.5. Series capacitor thermal results. Ambient temperature is 23.3°C. Manufacturer's maximum limit is up to 125°C.

SERIES COMBINATION

The next set of measurements is focused on replacing the same capacitors with their series equivalents. Measurements are taken under the same operational conditions. Power dissipation in each capacitor of the series combination is determined by again scaling the temperature rise of the combination. The ratio of series resistances is again used to determine the associated temperature rise of a given capacitor. However, for series combinations, higher temperature corresponds to the greater resistance. Power dissipation is calculated using the same procedure outlined for the parallel capacitances. Results are shown in Table 4.5. Capacitances in the second column are accompanied by their extracted temperatures.

In the table, it can be seen that using series equivalents results in higher operational temperatures. While peak voltages are distributed across the series combination, power dissipation is more prominent as seen by the temperature rise above ambient. The decrease in component Q is a result of a larger series resistance and this translates to hotter operation. If this capacitor combination

is used in the development of higher powered amplifiers, a shift in the operational temperature closer to the manufacturer's limit may result.

Porcelain Capacitors

While paralleling mica capacitors yielded good results in thermal performance, a single capacitor is needed with capabilities to handle higher thermal stresses as amplifier output powers increase. Porcelain capacitors, made by American Technical Ceramics (ATC), have low ESR and high Q characteristics that make them ideal for this kind of environment. These ATC 100E HF/VHF/UHF Low Loss Transmitter Porcelain Capacitors offer extremely high power handling per unit volume. The operating temperature is limited to 125°C by the manufacturer [9]. Component Q's at the 14.025-MHz operating frequency range from 600–1100. Again, capacitors Cs, Cl and $C\pi2$ are replaced with the closest ATC component values available. Amplifier operation is under the same conditions as before with MOSFET junction temperature maintained below 100°C. Prior to their installation into the circuit, leads of the ATC capacitors are changed from microstrip to wire, as shown in Figure 4.20, and the capacitor bodies covered with black electrical tape to facilitate the thermal imaging process. Figures 4.21 and 4.22 show the thermograms and respective component temperatures. Finally, Table 4.6 depicts a marked difference in temperature rise with the porcelain capacitors substituted for micas.

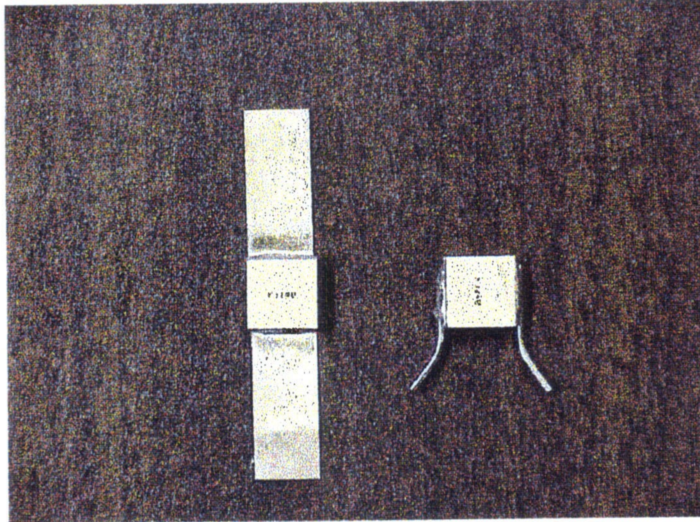

Fig. 4.20. Microstrip terminations on the ATC capacitor on the left are changed to wire to facilitate installation.

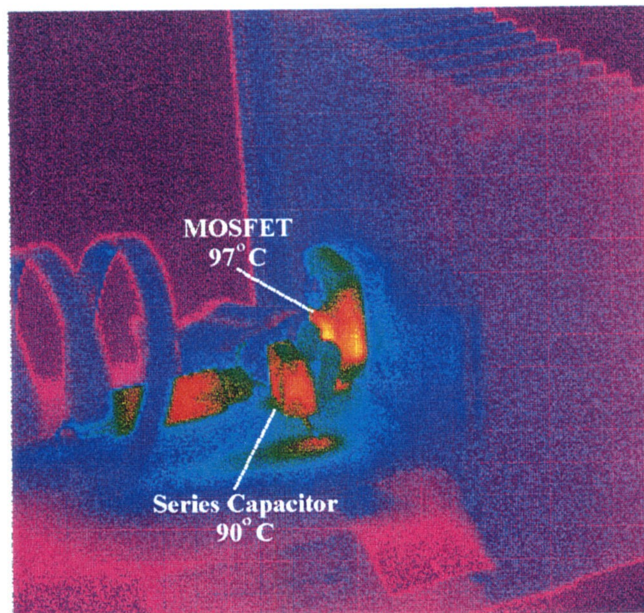

Fig. 4.21. At 400-W of output power, the ATC capacitor temperature rise is 67°C above ambient.

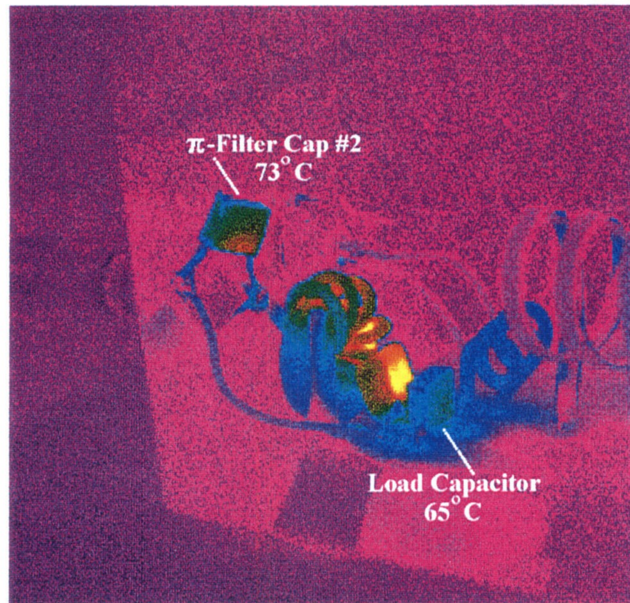

Fig. 4.22. ATC capacitors for the second harmonic trap and π-filter run cool.

From the table, low values of temperature rise indicate there is plenty of thermal margin for the ATC capacitors to be used in Class-E amplifiers at higher powers.

Component	Temperature Rise Porcelain / Mica
Capacitors: Cs	67°C / 127°C
Cl	42°C / 95°C
$C\pi 2$	50°C / 104°C

Table 4.6. Comparison of load network capacitor temperature rise. Ambient Temperature is 23°C.

4.4. Conclusion

In this chapter, a thermal study of high-power Class-E amplifiers has been presented. Its focus has been the examination of thermal stresses intrinsic to components vulnerable to failure. This study is facilitated by the use of an Infrared Thermal imaging camera to capture power losses radiated as infrared energy. Using a 400-W Class-E amplifier operating at 14.025 MHz, behavior under continuous-wave and pulsed operational modes are studied. In both cases, the MOSFET junction temperature remained within safe operational limits (in 100°C range). Capacitive components in the load network experienced high thermal dissipation. An additional study of the capacitors is made by replacing the load network capacitances with their series and parallel equivalents. Subsequent thermal measurements are carried out under the more stressful of the operating scenarios: continuous RF output with cooling fan. The parallel combinations produced lower operating temperatures due to reduced equivalent series resistance (ESR). Though paralleling produced the best results by reducing power dissipated, individual component temperatures can easily exceed the rated limit at higher output powers. To help alleviate this issue, a more robust capacitor in terms of higher Q and lower ESR is tried in the amplifier with excellent thermal results. ATC porcelain capacitors ran much cooler than the silver micas and would be ideal for use in higher power Class-E amplifiers.

References

[1] Sierra Pacific Innovations (SPI), Infrared Imaging Products. Infrared imaging reference library website: www.x20.org/library/thermal/infrared.htm.

[2] J.P. Holman, "Introduction," in *Heat Transfer*, McGraw-Hill, New York, 1997, pp. 2-3.

[3] F.P. Incropera and D.P. DeWitt, "Introduction," in *Fundamentals of Heat and Mass Transfer*, John Wiley and Sons, New York, 1985, p. 6.

[4] J.P. Holman, "Radiation Heat Transfer," in *Heat Transfer*, McGraw-Hill, New York, 1997, pp. 394, 404.

[5] F.P. Incropera and D.P. DeWitt, "Radiation Properties and Processes," in *Fundamentals of Heat and Mass Transfer*, John Wiley and Sons, New York, 1985, pp. 548–562.

[6] Encyclopedia Britannica Online website: http://search.eb.com/. Topics: Thermal Radiation and Blackbody.

[7] ThermaCam Operating Instructions by Inframetrics, Inc. 1998. Document 14882-000 RevA. Website: www.inframetrics.com.

[8] E. Lau, K.-W. Chiu, J. Qin, J.F. Davis, K. Potter, and D.B. Rutledge, "High-Efficiency, Class-E Power Amplifiers," *Part 1, QST*, pp. 39–42, May 1997; *Part 2, QST*, pp. 39–42, June 1997.

[9] American Technical Ceramics Corp., ATC Multilayer RF/Microwave Porcelain and Ceramic Data Sheets. Website: www.atceramics.com/.

Chapter 5

Suggestions for Future Work

The growth of the wireless communication industry has created a resurgence in RF research and development as there is a tremendous need for new technologies to fuel its growth. Today, many groups at research institutions and industrial firms are actively pursuing this technology development in conjunction with government agencies and industrial firms. While much is focused on the applications at microwave frequencies, there still remain many interesting issues to be addressed at lower frequencies. In fact, to provide a focal point for the developments of RF technologies, the IEEE Microwave Theory and Techniques Society formed a new technical committee (MTT-17) for HF, VHF, and UHF technology at the international symposium in Denver in 1997.

It has been shown in Chapter 3 that high output power in the hundreds of watts can be attained in a Class-E amplifier operating in the HF-Band using power MOSFETs. However, achieving this same power or greater at UHF in a solid-state amplifier is a challenge. At these power levels, vacuum tube technology dominates as it is well developed and still evolving, [1]. In fact, tubes are an integral part of today's broadcast transmitters. While solid-state device technology has not kept pace with these developments, new devices based on Silicon Carbide (SiC) and Gallium Nitride (GaN) materials may change this. The interest is to demonstrate a Class-E power module built around a SiC device. An amplifier operating at these power levels at UHF must not only be able to

function under the extreme temperature, but high voltage levels as well.

Power semiconductors based on Silicon Carbide (SiC) have shown the ability to function at very high temperatures, and this means higher output power is possible. SiC is a semiconductor material that can be used in radiation intense, high frequency, and high-temperature environments. While Silicon devices offer good performance at temperatures below 100°C, SiC devices can operate at temperatures in excess of 150°C [2]. It has been reported in [3] that SiC power MOSFETs are capable of operating over higher voltage, switching and temperature ranges than equivalently rated Silicon-based devices. Prototype SiC devices have been demonstrated in [4]. Here, a UHF SiC power module output 400 W, and an amplifier based on a SiC Static Induction Transistor (SIT) delivered 200 W. Devices are not commercially available as the crystal growth and fabrication techniques are still in the developing stages. However, Purdue University [5] and Cree Research [6] have produced SiC Power MOSFETS and Lateral Power MOSFETs for research purposes.

In order to properly design this high-power UHF Class-E module, extensive work needs to be done: device characterization measurements, use of this data to build a device model for simulation, circuit simulation, thermal modelling of the device. Development of passive components that comprise the external circuitry need to be thermally robust and this provides another avenue for study. To acquire higher power, power combining can be explored by combining modules in a configuration shown below [7]. The potential behind this development could give tube technology some serious competition for high-power UHF generation.

Lumped Element Combiner (Blodgett, *et al.*, "Power Combiner/Splitter," U.S. Patent 5,430,418, July 4, 1995)

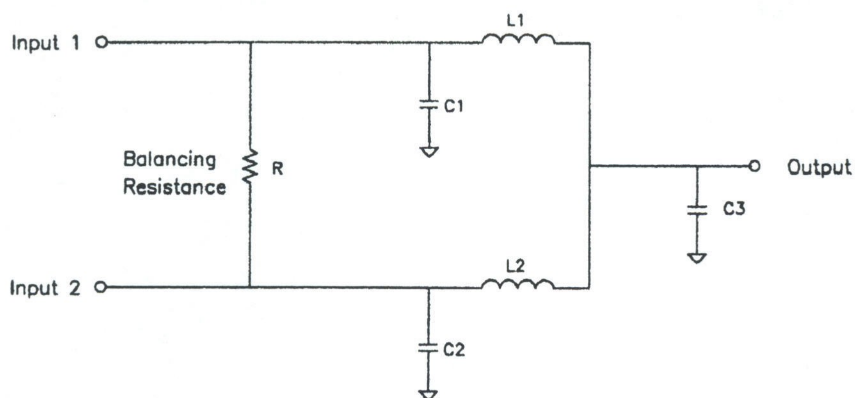

Proposed Combiner

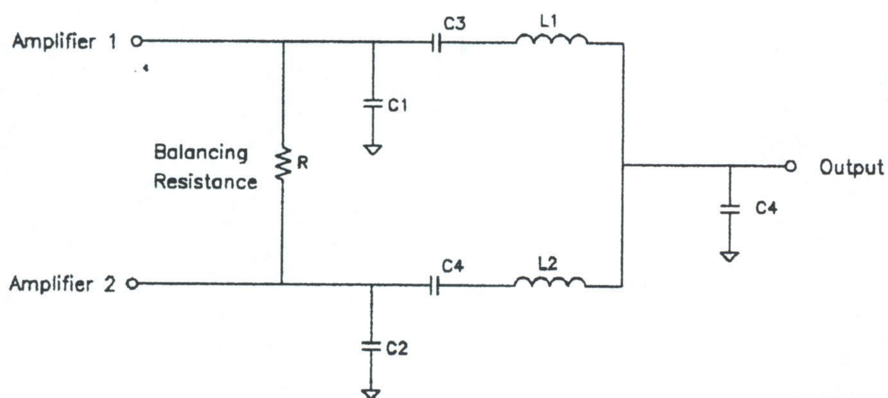

Fig. 5.1. Power combining scheme of two Class-E amplifiers.

References

[1] Acrodyne Industries, Inc., www.acrodyne.com.

[2] V.R. Garuda and M.K. Kazimierczuk, "High-Temperature Performance Characterization of Buck Converter Using SiC and Si Devices," *29th IEEE Power Electronics Specialists Conference*, May 17-22, 1998.

[3] M. Bhatnagar and B.J. Baliga, "Comparison of 6H-SiC, 3C-SiC, and Si for Power Devices," *IEEE Transactions on Electron Devices*, vol. 40, pp. 645–655, 1993

[4] A.W. Morse,*et al.*, "Recent Application of Silicon Carbide to High Power Microwave," *1997 IEEE MTT-S International Symposium Digest*, Denver, CO, pp. 53-56, June 1998.

[5] Purdue Univ. Wide Band Gap Research: www.ecn.purdue.edu/WBG/.

[6] Cree Research: www.cree.com/.

[7] J.R. Blodgett, "Power Combiner/Splitter," U.S. Patent 5 430 418, July 4, 1995.